Future changes in extreme rainfall events and circulation patterns over southern Africa

Izidine S. de Sousa Pinto

Thesis Presented for the Degree of

DOCTOR OF PHILOSOPHY

in the Department of Environmental & Geographical Science

Cape Town, December 2015

“After climbing a great hill, one only finds that there are many more hills to climb.”

Nelson Mandela (1918-2013)

Declaration

I declare that this thesis is my own work and has not been submitted in any form for another degree or diploma at any university or other institute of tertiary education. Information derived from the published and unpublished work of others has been acknowledged in the text and a list of references is given.

Signed by candidate .

(**Izidine S. de Sousa Pinto**)

Abstract

Changes in precipitation extremes are projected by many global climate models as a response to greenhouse gas increases, and such changes will have significant environmental and social impacts. These impacts are a function of exposure and vulnerability. Hence there is critical need to understand the nature of weather and climate extremes. Results from an ensemble of regional climate models from the Coordinated Regional Downscaling Experiment (CORDEX) project are used to investigate projected changes in extreme precipitation characteristics over southern Africa for the middle (2036-2065) and late century (2069-2098) under the representative concentration pathway 4.5 (RCP4.5) and 8.5 (RCP8.5). Two approaches are followed to identify and analyze extreme precipitation events. First, indices for extreme events, which capture moderate extreme events, are calculated on the basis of model data and are compared with indices from two observational gridded datasets at annual basis. The second approach is based on extreme value theory. Here, the Generalized Extreme Value distribution (GEV) is fitted to annual maxima precipitation by a L-moments method. The 20-year return values are analyzed for present and future climate conditions. The physical drivers of the projected change are evaluated by examining the models ability to simulate circulation patterns over the regions with the aid of Self-Organizing Maps (SOM).
The analysis used downscaled data from two Regional Climate Models (RCM) (COSMO-CLM and RCA4) driven by four General Circulation Models (GCM) (MPI-ESM-LR, HadGEM2-ES, CNRM-CM5, and EC-EARTH) forming an eight-member ensemble of climate projections for Africa. Data from evaluation runs, where the RCMs were forced by the ERA-Interim reanalysis were also used to establish bias in the models. Historical and evaluation results are evaluated against two observational datasets, namely the Tropical Rainfall Measuring Mission (TRMM 3B42 version 7) and Global Precipitation Climatology Project One-Degree Daily (GPCP 1DD Verion 1.2). The evaluation data show that the RCMs can adequately simulate the current extreme rainfall climate, however differences exist depending on which observed dataset is used for the evaluation. The synoptic circulation patterns are well simulated which indicates that the differences in precipitation extremes between the regional models and observations are related to model physics and parameterizations. As found in previous studies, the multi-model ensemble mean outperforms the individual RCMs. In an assessment of value the regional downscaling added to GCM results, positive added value was computed generally and found specifically to be a function on the type of metric used and geographical location. This added value over GCMs justify the additional computational effort of RCM simulation for the generation relevant climate information for regional application.

Regional climate models projections indicate that annual total precipitation will decrease while the maximum number of consecutive dry days increases. The decrease in annual total precipitation is primarily associated with increases in the frequency of high-pressure systems over the region and decreases in the occurrence of mid-latitude cyclones. Maximum 5-day precipitation amounts and 95th percentile of precipitation are also projected to increase significantly in the tropical and sub-tropical regions of southern Africa and decrease in the extra-tropical region. There are indications that rainfall intensity is likely to increase. This does not equate to an increase in total rainfall, but suggests that when it does rain, the intensity is likely to be greater. These changes are magnified under the RCP8.5 when compared with the RCP4.5 and are physically consistent with the circulation changes. Circulation changes include an increase in the occurrence of the oceanic high-pressure systems, a more dominant high-pressure circulation poleward of the continent and a decreased occurrence of patterns of continental lows and mid-latitude lows.

Aknowledgements

Foremost I would like to sincerely thank my supervisors, Dr. Chris Lennard, Dr. Mark Tadross and Prof. Bruce Hewitson for their encouragement, support and numerous helpful discussions from the beginning and completion of this project. The entire experience has been truly rewarding, as far as learning process is concerned.

This research was made possible through the financial support from the Applied Center for Climate and Earth Systems Science (ACCESS), Climate System Analysis Group (CSAG) and National Research Fund (NRF) of South Africa. I also would like to acknowledge the various institutions that provided data for this thesis.

I thank my office mates Brendan Argent, Huessen Endris, Steve Arowolo and Michael Kent for the friendly working environment, the interesting and fun conversations and the cheerful moments during all these years.

I would like to give thanks to my friends and family whose moral support has been instrumental in making this challenge less exhausting - mentally, physically and emotionally.

Contents

List of Figures

List of Tables

Acronyms

Notation	Description
AO	Atlantic Ocean
BC	boundary condition
CAB	Congo Air Boundary
CCAM	Conformal-Cubic Atmospheric Model
CDD	maximum number of consecutive dry days
CMIP5	Coupled Model Intercomparison Project Phase 5
CORDEX	CO-ordinated Regional Downscaling Experiment
CSIRO9	Commonwealth Scientific and Industrial Research Organization
DJF	December-February
EI	ERA-Interim
ENSO	El Niño-Southern Oscillation
EVT	extreme value theory
GCM	General Circulation Model

Notation	Description
GHG	green house gases
IO	Indian Ocean
ITCZ	Inter Tropical Convergence Zone
JJA	June-August
MC	Mozambique Channel
MME	multi-model ensemble
MSLP	mean sea-level pressure
N. E. Monsoon	north-eastern Monsoon
PRCPTOT	total wet-day precipitation
R10mm	heavy precipitation days
R95pTOT	very wet days
RCM	Regional Climate Model
Rx5day	maximum consecutive 5-day precipitation total
S. E. Trades	south-east trade winds
S. W. Monsoon	south-western Monsoon
SDII	simple daily intensity
SOM	Self-Organizing maps
SREX	Special report on Managing the Risks of Extreme Events and Disasters to Advance Climate Change Adaptation
SST	sea-surface temperature

Notation	Description
TTT	tropical-temperate trough
WMO	World Meteorological Organization

1 Introduction and Background

1.1 Introduction

Increases in atmospheric greenhouse gas concentrations are expected to result not only in changes in mean climate, but also to changes in circulation patterns and extreme weather events (Seneviratne et al., 2012; Rummukainen, 2012). Increased concentration of greenhouse gases have increased the ability of the atmosphere to hold moisture. According to the Clausius-Clapeyron relationship, for a degree increase in temperature the water holding capacity of the atmosphere increases by ∼7% (Willett et al., 2010). Increases in moisture can lead to an increase in the frequency and magnitude of extreme events (weather or climate) when other factors do not change (Seneviratne et al., 2012). Extreme weather events contribute to damaging impacts with important environmental and socio-economic consequences. The impacts from these events will depend on the nature and severity of the events (hazards), the geographical location (exposure) of the population and assets, social vulnerability, and how well the population is prepared to cope with the events (resilience) (Oppenheimer et al., 2014). The overlap of these three factors produce climate related disaster risk (Figure 1.1).

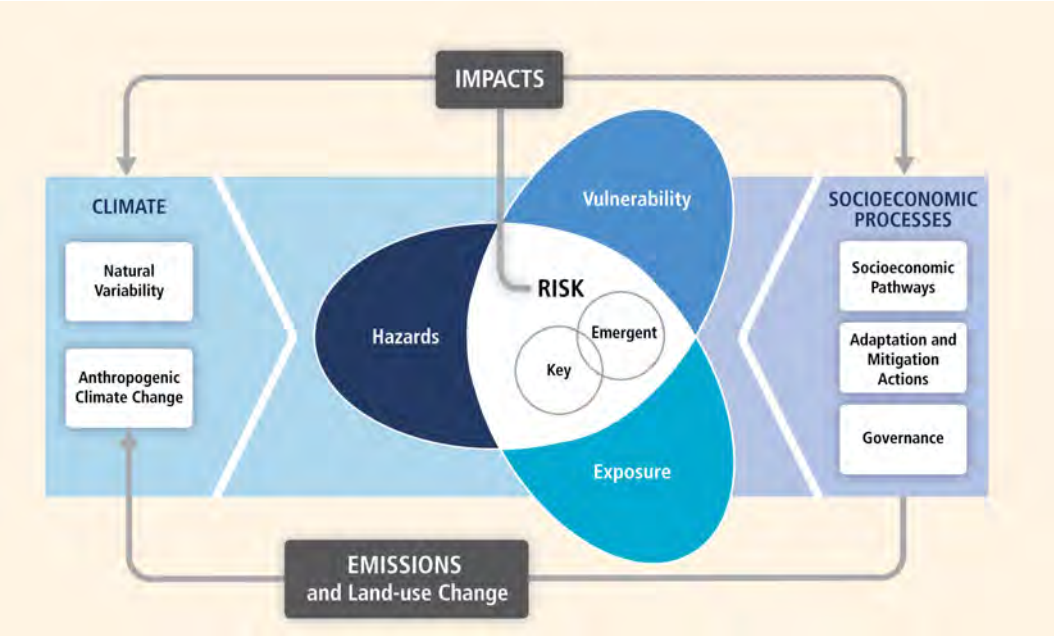

Figure 1.1: Factors affecting climate related risks (source: Oppenheimer et al., 2014).

Countries in southern Africa are particularly vulnerable to extreme events such as droughts, floods, tropical cyclones and heat waves because of low adaptive capacity due to limited access to information, finances, technology, and capital assets (Washington et al., 2004). Disasters caused by extreme events in southern Africa are estimated to have caused around US 10 billion of economic losses since 1970-2012 (WMO, 2014). For instance, Mozambique experienced extreme rainfall associated with Tropical Cyclone Eline in 2000, resulting in severe flooding and displacing over a million people (Reason and Keibel, 2004). During austral summer of 2014/2015, high amounts of precipitation were received throughout southern Africa. The core of the heaviest accumulations (>100mm) focused over much of southern Zambia, northern Zimbabwe and western Mozambique. These torrential precipitation triggered flooding in Malawi, Mozambique and Zimbabwe displacing 120000 people as of 16 January 2015 (OCHA, 2015). Further, trends in disaster losses have been increasing (WMO, 2014; Seneviratne et al., 2012) and whilst some of these increases are due to increased exposure of assets and populations, increases in weather and climate extremes, may play a role. The combination of an increase in exposure, vulnerability and frequency and magnitude of extreme events increases the associated

disaster risk (Seneviratne et al., 2012). Thus, understanding the changes in extreme events that may occur under future climate is important for adaptation planning, policy making and targeting investments to build resilience to the impacts of these extremes.

There is increasing evidence from observed climate trends that globally extreme precipitation events are becoming more frequent and more intense (e.g. Tebaldi et al., 2006; Alexander and Arblaster, 2009; Groisman et al., 2005; Donat et al., 2013). And results from climate models suggest that these trends will continue under enhanced greenhouse conditions (e.g. Kharin and Zwiers, 2000, 2005; Shongwe et al., 2009; Tebaldi et al., 2006; Sillmann et al., 2013b) in the future. However, it is less clear how these changes will evolve regionally together with circulation patterns and weather systems.

The primary tools used to provide such information are General Circulation Models(GCMs) (Tebaldi et al., 2006), however they cannot represent extreme precipitation adequately, primarily due to limitations in simulated dynamics and required parameterizations, a consequence of their coarse spatial resolutions (McGregor, 1997; Wilby and Wigley, 1997; Hudson and Jones, 2002). Thus, a regionalization process to resolve small scale weather events can improve the ability to model extreme precipitation. This is usually achieved through either statistical or dynamical downscaling (Hewitson et al., 2013).

Relatively few studies on future changes in extreme precipitation over southern Africa are available in the literature, and these are commonly based on the results from a single Regional Climate Model (RCM) (e.g Pinto, 2011; Engelbrecht et al., 2012) or lower resolution GCMs (e.g Mason and Joubert, 1997; Shongwe et al., 2009; Rocha et al., 2008). A common message emerging from the studies cited above is that the nature of climate extremes is changing and this could exacerbate existing problems

in Africa, where communities have a high dependence on the natural environment and therefore high risk to factors that have an impact on this.

However, in order to sample the uncertainty associated with future projections of climate, multi-model GCM/RCM/statistically downscaled ensembles are required. Furthermore, many RCMs downscaling provided better precipitation climatology than that of the global driving data; this supports the potential for added value of high-resolution RCMs by resolving small-scale processes (Di Luca et al., 2012; Feser et al., 2011; Dosio et al., 2015; Laprise et al., 2013).
In recent years, the World Climate Research Program (WCRP) CO-ordinated Regional Downscaling Experiment (CORDEX) (Giorgi et al., 2009) has been established in order to provide a global coordination of regional climate downscaling. As a result of this, there is a great opportunity for scientists to explore the envelope of future climate extremes, which can contribute to the information needs of climate change adaptation and impact assessment communities.

Given the need of higher resolution, downscaled climate information for climate change adaptation and impact assessment, the **aim of this thesis is to investigate the spatial and temporal characteristics of extreme climate events in CORDEX RCM simulations for present and future climate over southern Africa**. To support the aim, the thesis addresses the following hypothesis:

- The CORDEX RCMs can reasonably simulate extreme precipitation events in the present climate;
- The downscaling adds value to the global climate model output;
- The frequency and magnitude of extreme precipitation in the future, as projected by the CORDEX models, increases compared to base period simulation for the same locations;

- Large scale synoptic circulation environments can be associated with extreme rainfall and projected changes in extreme rainfall characteristics are attributable to changes in the frequency of occurrence of these synoptic drivers.

1.2 Background

1.2.1 Southern Africa climate and rainfall characteristics

The climate of southern Africa has been well documented (Nicholson, 2000; Tyson and Preston-White, 2000). However, to provide an informed analysis and discussion of the results presented in other chapters, the climate of the region is described briefly here. Southern Africa, defined here as a region bounded in the north by latitude 10°S, consists primarily of arid or semi-arid climatic regions. Most of the region is associated with summer (December-January-February) rainfall, with the exception of the relatively small areas along the eastern and southern coasts that receive rainfall throughout the year, and the south-western part of the Western Cape Province of South Africa which receives rainfall during winter (June-July-August) (Taljaard, 1986; D'Abreton and Lindesay, 1993; Tyson et al., 2002). The highest annual rainfall occurs in the northeast parts of the subcontinent and gradually decreases towards the southwest following roughly anti-cyclonic path (Taljaard, 1986). Rainfall in southern Africa is affected by a multiplicity of forcing including topography, contrasting oceanic surroundings and atmospheric dynamics (Taljaard, 1986; Tyson and Preston-White, 2000).

Influence of topography and the Ocean

The geographical distribution of rainfall over southern Africa is, to a large extent, controlled by the topography (Taljaard, 1986). Much of the subcontinent lies on an elevated plateau at altitudes well above a 1000 m, while the coastal margins are narrow, particularly in the south and southeast (Joubert et al., 1999; Taljaard, 1995).

Another factor controlling the rainfall is the unique oceanographic setting (Tyson and Preston-White, 2000; Nicholson, 2003). The Agulhas Current drives relatively warm water to the east coast while the water to the west coast is relatively cold as a result of the Benguela Ocean Current. Rainfall in southern Africa is also influenced by sea-surface temperature (SST) variability in the tropical Pacific Ocean. Large-scale warming of the equatorial eastern and central Pacific together with an associated oscillation of atmospheric pressure over the south Pacific Ocean - El Niño-Southern Oscillation (ENSO) - is frequently associated with below normal rainfall over much of southern Africa (Mason and Jury, 1997; Mason, 2001; Jury et al., 2004; Reason and Jagadheesha, 2005).

Influence of atmospheric circulation patterns

Rainfall events in southern Africa are also conditioned by the mean circulation of the atmosphere (Taljaard, 1995; Tyson and Preston-White, 2000; Taljaard, 1986). Due to the geographical location, the climate and weather are influenced by tropical, subtropical and mid-latitude circulation regimes. The two subtropical high-pressure cells are the dominant features of the general circulation of southern Africa. Except near the surface, circulation patterns are anticyclonic for much of the year (Tyson and Preston-White, 2000). These circulation patterns are most frequent during winter (June-August (JJA)). The basic pressure distribution and movement of air masses for winter are presented in figure 1.2. The two high pressure system features move northwards in winter due to the shift in the seasonal solar radiation bringing westerlies to the south western and southern coasts of the region. Therefore, along the southern and western coast, winter rainfall occurs, resulting from frontal systems associated with the passage of the waves in the westerlies of the middle and upper troposphere (Taljaard, 1995; Tyson and Preston-White, 2000). The east part of the subcontinent is influenced by the south-east trade winds (S. E. Trades), but because the north-eastern Monsoon (N. E. Monsoon) is absent, no convergence takes place, and therefore the likelihood of rainfall occurring diminishes.

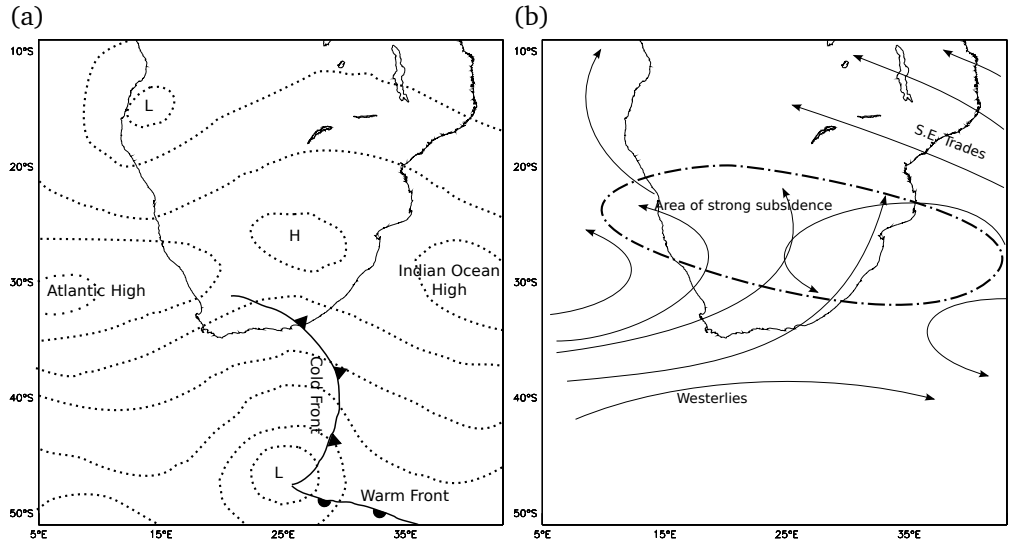

Figure 1.2: Features of the pressure distribution (a) and basic movement of air masses (b) over southern Africa during winter (after Hurry and Van Heerden (1982))

During summer, high pressure systems move southwards by almost five degrees of latitude on both sides of the subcontinent, and the influence of the westerlies becomes somewhat diminished. The basic pressure distribution and movement of air masses for summer (December-February (DJF)) is displayed in figure 1.3. All circulation features are found further south than they were in winter. During this season the air over southern Asia is cooler and denser than the west Indian Ocean leading to the establishment of a stronger pressure gradient which gives rise to the N. E. Monsoon. The N. E. Monsoon crosses the equator converging with the S. E. Trades from the Indian Ocean forming the Inter Tropical Convergence Zone (ITCZ) (Hurry and Van Heerden, 1982). The ITCZ is a region of pronounced convective activity and thus play a major role in southern Africa climate variability (Tyson and Preston-White, 2000). Strong summer heating causes a heat low (shallow-low pressure system) to develop over northwest of the subcontinent. The S. E. Trades from the Atlantic high pressure system move clockwise around this heat low, and change to south-western Monsoon (S. W. Monsoon) winds. Where these winds meet the S. E. Trades from the Indian Ocean, a secondary convergence zone, the Congo Air Boundary (CAB), is formed. This convergence zone influences rainfall patterns particularly over the

western half of the subcontinent (Tyson and Preston-White, 2000).

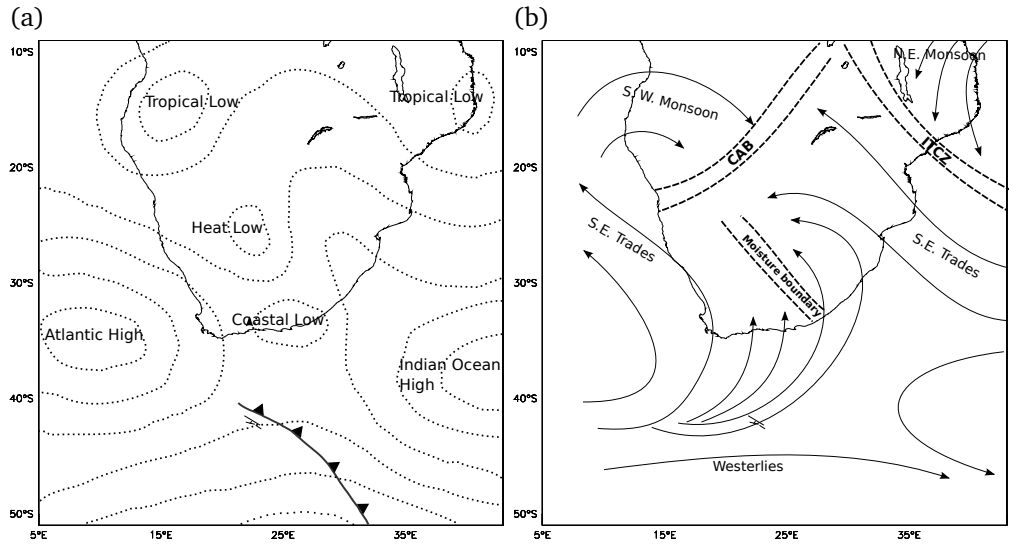

Figure 1.3: Features of the pressure distribution (a) and basic movement of air masses (b) over southern Africa during summer (after Hurry and Van Heerden (1982))

Extreme precipitation over southern Africa are typical associated with closed mid-tropospheric low-pressure systems: Tropical Cyclones in the southwest Indian Ocean, which occasionally make landfall over Mozambique (Dyson and van Heerden J., 2001) and intense cut-off lows (Singleton and Reason, 2006, 2007; Favre et al., 2013). Southern Africa is also regularly affected by extended periods of heavy rainfall when tropical and temperate disturbances interact, referred to as tropical-temperate troughs (TTT, Todd and Washington, 1999; Hart et al., 2012). They form when a tropical disturbance such as an easterly wave or a tropical low (e.g. Angola-low) combines with a subtropical low or temperate westerly wave (Harangozo and Harrison, 1983; Todd et al., 2004), thus establishing a interaction between the tropics and midlatitudes. Thus, when considering projected changes in extreme weather events over southern Africa, it is important to investigate the projected changes in the characteristics of synoptic circulation systems. Analysis of changes of circulation systems under future climate conditions are becoming available in literature as climate models runs becomes available Hope (2006); Cassano et al. (2006); Lynch et al. (2006). These studies only recently have been conducted for southern Africa Engelbrecht

et al. (2012). The authors used a RCM to downscale one GCM and showed that the frequency of closed low pressure systems detected at 500 hPa over southern Africa should decrease while in parallel extreme rainfall events should generally increase for the period 2070-2100 under the A2 SRES scenario relative to 1975-2005. Understand the changes in the synoptic drivers of precipitation enhance the robustness of projected local climate change.

1.2.2 Extreme events

Definitions of extreme events can vary widely due to heterogeneity of climate at different locations and the nature of the research undertaken (Stephenson, 2008) i.e. the intended application or sector of interest. In this thesis, extreme events are defined statistically in terms of their probability of occurrence, i.e. with respect to given percentiles (eg. 10th, 90th percentile) of the observed distribution function of variables (e.g. IPCC, 2007), and with respect to specific return frequencies(e.g. 1 in 20 year event) (e.g. Zwiers and Kharin, 1998). An extreme climate event can be classified as a pattern of extreme weather that persists for some time, especially if it yields an average or total that is itself extreme (e.g., drought or heavy rainfall over a season) (IPCC, 2007). The distinction between an extreme weather event and an extreme climate event is not well defined. An extreme weather event typically occurs within a time-scale of less than a day to one week, and an extreme climate event typically occurs within a time scale longer than a week and up to as long as a season. For simplicity, both extreme weather events and extreme climate events can be referred to as “climate extremes” (Seneviratne et al., 2012) .

In order to gauge how changes in climate extremes could influence society and ecosystems, it is useful to conceptually address how such extremes could change in a statistical sense. These statistical properties are captured by the probability distribution of a climate variable. For example, figure 1.4 presents a typical distribution

of a climate variable, here temperature, that is normally distributed and shows how the tails of the distribution might change in a warming world. Shaded areas indicate the extremes, which are high/low value events which are represented by the tails of the distribution. If there is a simple shift in the mean of the distribution (no change in shape or skewness) in a future climate toward higher values, there will be a disproportionate increase in extremes events on the upper end and a disproportionate decrease at the lower end (figure 1.4a); if this occurs in reality, an increase in the mean temperature will produce a large increase in the number of extreme hot days and a large decrease in the number of extreme cold days (Meehl et al., 2000). However, a change in the mean does not imply any change in variability (IPCC, 2001). An increase in variability, even without a change in the mean, would cause an increase in the probability of both hot and cold extremes (figure 1.4b). According to Katz and Brown (1992), a change in the variance of a distribution can have a greater effect on the frequency of extremes events than a change in the mean. Increases in both the mean and the variability are also possible (figure 1.4c) and this would dramatically affect the probability of hot and cold extremes, with many more frequent hot events and many fewer cold events (IPCC, 2001). According to the IPCC (2001), for variables that are not well approximated by normal distributions, such as precipitation, the situation is even more complicated, especially for dry climates. For example, changes in the mean total precipitation can be accompanied by other changes like the frequency of precipitation or the shape of the distribution including its variability. All these changes can affect the various aspects of precipitation extremes including the intensity of precipitation (amount per unit time).

Observed and projected changes in extreme events

The Special report on Managing the Risks of Extreme Events and Disasters to Advance Climate Change Adaptation (SREX) (IPCC, 2012), assesses changes in extreme events from observations gathered since 1950 for many regions of the world. The

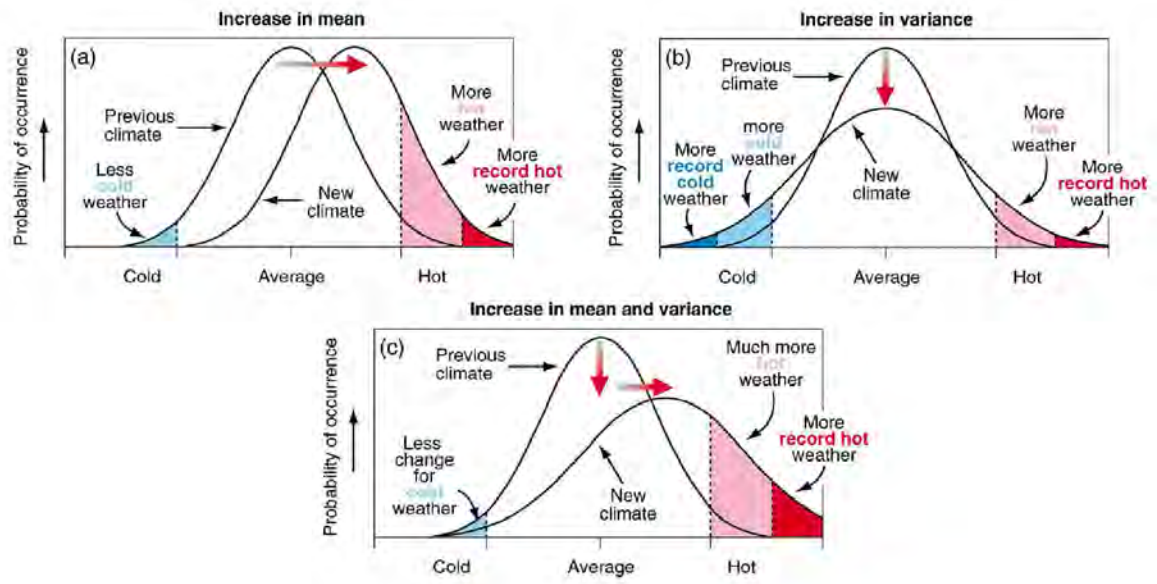

Figure 1.4: Theoretical changes in the normal distribution of climate variable (a) change in mean, (b) change in variance and (c) change in both mean and variance (source: IPCC, 2001).

report suggests that is very likely that there has been an overall decrease in cold extremes and an overall increase in warm extremes, at the global scale. Also, there are statistically significant trends in the number of heavy precipitation events in some regions of the world. Evidence from climate models shows that at least some types of extreme events will become more frequent and more severe in the future (e.g. Kharin and Zwiers, 2000, 2005; Frei et al., 2006; Meehl et al., 2005; Tebaldi et al., 2006; Alexander and Arblaster, 2009)

Because of the limited availability of observed daily data, which is desirable for studying certain types of extreme events, few examples of work related to observed changes in extremes across Africa are available in the literature. One notable study, by New et al. (2006), analysed climatic extremes in southern and west Africa over the period 1961-2000. The authors detected a decrease in regionally averaged annual precipitation, accompanied by increases in average daily precipitation intensity, along with the amount of precipitation falling on extreme precipitation days across southern Africa. They defined extreme precipitation days as days with annual total precipitation above the 95th and 99th percentile of daily precipitation. Mason et al. (1999)

found increases in the intensity of extreme precipitation events between 1931-1960 and 1961-1990 over approximately 70% of South Africa. Fauchereau et al. (2003) also identified regions of South Africa which experienced more extreme precipitation events in the later decades of the 20th Century. Groisman et al. (2005) empirically assessed the observed changes of very heavy precipitation (upper 0.3% of daily precipitation events) during 1906-1997 over eastern parts of South Africa. The authors found a statistically significant increases in the frequency of very heavy precipitation. Kruger (2006) found an increase trends in the number of extreme rainfall days in the Eastern Cape, southern Free State and parts of KwaZulu-Natal.

Despite the different definitions used for extreme precipitation in the literature cited above, there is evidence that the characteristics of extreme precipitation over southern Africa has changed over the last 50-100 years. It is also likely that the characteristics of extreme precipitation will continue to change in intensity, frequency and duration as a result of increases in green house gases.

Assessments of changes in precipitation and/or temperature extremes in southern Africa due to increases in greenhouse gas concentrations have been investigated in a number of studies using a variety of techniques which utilise GCM simulations (e.g., Mason and Joubert, 1997; Shongwe et al., 2009) as well as RCM simulations (e.g., Pinto, 2011; Engelbrecht et al., 2012). Mason and Joubert (1997) used the Commonwealth Scientific and Industrial Research Organization (CSIRO9) GCM to investigate possible changes in the frequency and intensity of extreme daily rainfall events over southern Africa resulting from a doubling of atmospheric carbon dioxide concentrations. They found an increase in the magnitude of extreme daily rainfall events with return periods of 10 and 30 years over the entire subcontinent. Results were similar for changes in the frequency and intensity of precipitation extreme events of five-day duration even in areas where decreases in mean annual rainfall were simulated. However, their findings are sensitive to the model representation of topographic features in Southern Africa. Shongwe et al. (2009) used an ensemble of global climate

models to investigate consistently simulated changes in mean and extreme precipitation for the period of 2046-2065 and 2081-2100 over southern Africa. The authors found increases in the intensity of dry extremes over the western parts of southern Africa during summer months (December-January-February). Pinto (2011) investigated projected changes in extreme temperature and precipitation events for the period of 2031-2049 based on high resolution (25 km) RCM simulations using PRECIS (HadRM3P) over Mozambique. Extreme precipitation was defined as the amount of precipitation above 95th and 99th percentile of daily precipitation. The study found a simulated overall increase in the intensity and a change in the distribution of daily precipitation extreme events over Mozambique. Engelbrecht et al. (2012) used a variable resolution GCM, the Conformal-Cubic Atmospheric Model (CCAM), over southern Africa at a resolution of about 60 km to simulate the frequency of occurrence of closed-lows and extreme rainfall events. The authors found that despite the projected general decrease in closed-lows and associated extreme rainfall (defined as events where more than 20 mm of rain falls within 24 hours over a grid box of dimensions 0.5° X 0.5° in longitude and latitude), extreme rainfall events in general are projected to increase over large parts of southern Africa by the end of century.

Climate modelling and extreme events

Some extreme events, by their very nature of being small in spatial scale and short in duration, cannot be adequately represented in a coarse resolution GCM grid box, which is sometimes of the order about 300 x 300 Km (Frei et al., 2006; Christensen et al., 2007; Buonomo et al., 2007). Despite the concerns raised about their resolution, studies of climate extremes have been carried out using GCMs (e.g. Kiktev et al., 2003; Wehner, 2004; Kharin and Zwiers, 2005; Emori et al., 2005). These GCM studies are often the starting point for most climate impacts analyses, however they lack the regional detail that such studies often need. In view of the need for regional detail, regionalization techniques have been developed to allow development of regional scale climate change projections through downscaling GCM output.

There are two main downscaling approaches, statistical and dynamic. The statistical approach, also referred to as empirical downscaling, relates large scale circulation features to a local variable of interest. Once the relationships are established, these are used to estimate the values of the local variable from GCM projections (Hewitson and Crane, 1996; Wilby et al., 2004).

The dynamical approach uses fine scale RCMs driven by GCMs (Giorgi, 1990). A number of studies have shown that RCMs are valuable tools for studying changes to extreme events (e.g. McGregor, 1997; Hudson and Jones, 2002; Jones et al., 2004). Their advantage over the GCM is that they provide highly resolved spatial and temporal information that enhances assessment of spatial and temporal changes to extreme events. Several studies have used RCMs to examine the effect of increased green house gases (GHG) on the characteristics of extreme events (e.g. Christensen et al., 2007; Pinto, 2011). Durman et al. (2001) and Jones et al. (2004) found that RCMs represent extremes events better than GCMs on the finer grid-scale and RCMs reproduce more precipitation extremes at scales not accessible to GCMs (e.g. Frei et al., 2003; Huntingford et al., 2003; Seneviratne et al., 2012) as well as cyclones (Hudson and Jones, 2002). However, the accurate representation of frequency and intensity of precipitation in RCMs remains a challenge. This is due to many complex processes that contribute to the duration, onset and intensification of precipitation events such as cloud microphysics, cumulus convection, planetary boundary layer processes and local-scale circulations.

1.2.3 Model ensembles

It is important to note that the studies by for example Pinto (2011) and Engelbrecht et al. (2012) were based on a single model and only used one emissions scenario (SRES A2, Nakicenovic et al. (2000)). Regional climate model projections of changes in temperature and precipitation differ considerably between models. This uncertainty is primarily due to two sources; uncertainty in forcing from the boundary

conditions(BCs),for example the driving GCM and uncertainty in the representation of physical processes in a given regional model (Noguer et al., 1998; Jones et al., 2004). Even if the BCs are the same, for example a reanalysis dataset like NCEP (Kalnay et al., 1996), different regional models can produce different climates for the same region (e.g. Nikulin 2011). Therefore, regionally specific future changes produced by a single model should not be viewed in isolation and should not be used in decision making structures. One way to overcome this is to consider several RCMs so that the results are considered within a multi-model framework, where areas of agreement/disagreement between models can be identified.

Various international projects have produced coordinated dynamical downscaling experiments using multiple RCMs for assessing climate variability, climate change, impacts and vulnerability for different regions across the globe. PRUDENCE and ENSEMBLES from Europe (Christensen et al., 2007; Hewitt, 2005); NARCCAP from North America (Mearns et al., 2009); CLARIS-LPB from South America (Menéndez et al., 2010); ARCMIP from the Arctic region (Curry and Lynch, 2002); RMIP from Asia (Fu et al., 2005).

Within the CORDEX, Africa has been the focus of a multi-model downscaling project for the first time. CORDEX is a World Climate Research Programme (WCRP) sponsored program to organise an international coordinated framework to provide an improved generation of regional climate change projections worldwide for input into impact and adaptation studies (Giorgi et al., 2009). CORDEX provides numerous RCM simulations of both present-day and future time periods covering most land areas in the world to a resolution of 50 km, with an initial focus on Africa (Giorgi et al., 2009). The CORDEX multi-model dataset provides the unique opportunity of using an ensemble of multiple dynamical and statistical downscaling models considering multiple GCMs forced with different greenhouse gas concentration scenarios from the Coupled Model Intercomparison Project Phase 5 (CMIP5) archive.

1.3 Thesis structure

This thesis is composed of six chapters. This introductory chapter outlines the need for this research and gives an overview of extremes events and southern Africa climate. **Chapter two** describes the model data and outlines the methodologies used. The section on methods also includes theoretical explanations on the techniques of extreme value modelling. **Chapter three** addresses the models ability to reproduce important features of southern African climate, and their role as drivers of precipitation and how these might change in the future. **Chapter four** expands on the assessment of the previous chapter by investigate how well the models capture extreme precipitation over the region followed by model projections of extreme precipitation events in future climate simulations in **Chapter five**. **Chapter six** summarises the findings, concludes the thesis and proposes future work in this area of study.

2

Data and Methodology

This chapter provides a description of the models, data and methods used in the study. It begins with a description of the two models followed by a brief description of the observation data used. Finally, a description of the techniques used in the core analyses is provided. The Self-Organizing maps (SOM) technique is used to identify the synoptic regimes. The non-parametric and parametric methods are used to assess downscaled moderate and rare extremes respectively against observed rainfall data.

2.1 Data

2.1.1 Model simulations

In this study, climate simulations for southern Africa region were made available throughout the CORDEX project. The Rossby Center (SMHI) regional climate model (RCA4) (Dieterich et al., 2013) and the Consortium for Small-scale Modelling (COSMO) Regional Climate Model (COSMO-CLM) (Panitz et al., 2014) were used to downscale four coupled atmosphere ocean general circulation models (AOGCMs) from the new CMIP5 global climate projections (table 2.1).
All simulations were performed at a grid resolution of 0.44°x 0.44°, giving grid spaces of approximately 50 km over the same Africa domain (Fig. 2.1).

The GCMs projections are forced by the Representative Concentration Pathways (RCPs)

Table 2.1: The downscaled CMIP5 models by RCA4 and CCLM for RCP4.5 and RCP8.5 (for detailed information, refer to http://cmip-pcmdi.llnl.gov/cmip5/availability.html).

GCM CMIP5	Expanded model name	Institution	Reference
CNRM-CM5	Centre National de Recherches, Meteo-rologiques Coupled, Global Climate Model, version 5	Centre National de Recherches Meteo-rologiques, Meteo-France, France	Voldoire et al. (2011)
EC-Earth		EC-EARTH consortium	Hazeleger et al. (2010)
HadGEM2-ES	Hadley Centre Global En-vironment Model, version 2-Earth System	Met Office Hadley Centre, UK	Collins et al. (2011)
MPI-ESM-LR	Max Planck Institute Earth System Model, low resolution	Max Planck Institute for Meteorology, Germany	Stevens et al. (2013)

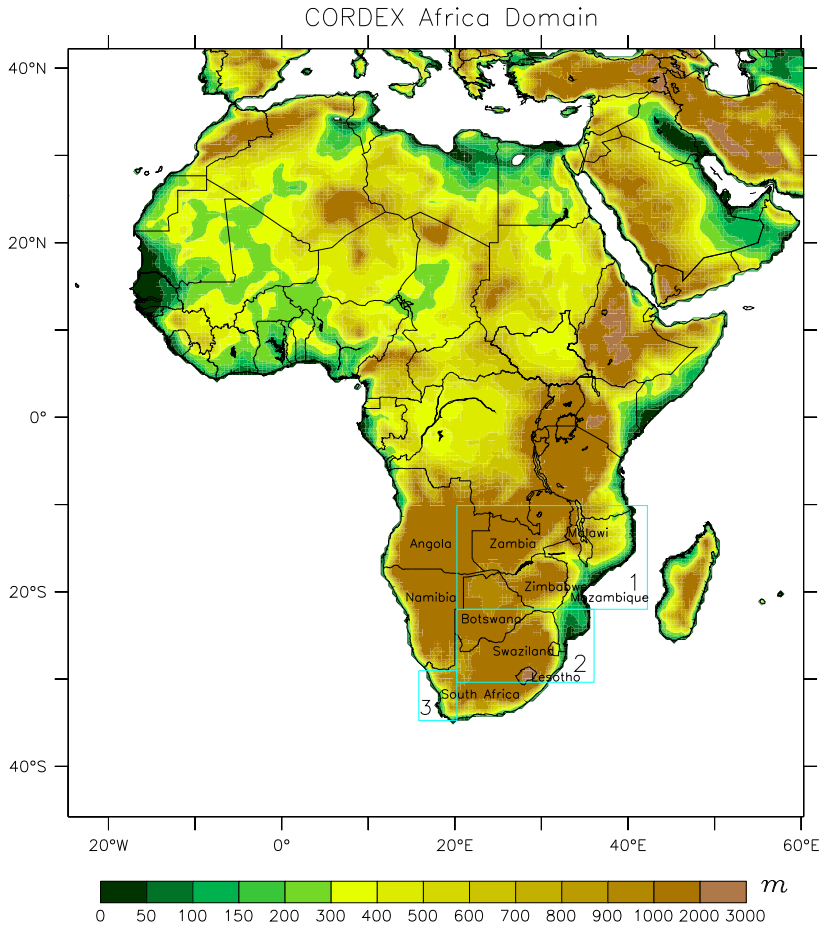

Figure 2.1: Topography of the CORDEX-Africa domain and location of the three sub-regions.

(Moss et al., 2010). The RCPs are prescribed greenhouse-gas concentration pathways throughout the 21st century, corresponding to different radiative forcing stabilisation levels by the year 2100. Two RCPs are available, RCP4.5 and RCP8.5, which represent a mid and a high-level emission scenario respectively. RCP4.5 corresponds to a radiative forcing after 2100 of approximately 4.5 W/m^2 , equivalent to ≈650 ppm CO_2, which is larger than that in the SRES (Special Report on Emissions Scenarios) B1 scenario (≈550 ppm) and lower than that in the SRES A1B scenario (≈720 ppm). RCP8.5 corresponds to a rising radiative forcing pathway leading to 8.5 W/m^2 in year 2100 equivalent to ≈1370 ppm CO_2 (Moss et al., 2010). Common to all simulations is the use of ERA-Interim (EI) reanalysis (Dee et al., 2011) as driving data for the period of 1989-2008 to assess the structural bias of the RCMs (e.g. Nikulin et al., 2012; Endris et al., 2013; Kalognomou et al., 2013). It should be noted that data from an earlier version of the RCA model, RCA3 (Samuelsson et al., 2011), was used in the CORDEX-related papers cited above. The RCA4 is in many respects the same model, but has been re-coded and updated, mostly with respect to surface processes and convective parameterizations.

Both models use mass flux convection schemes. CCLM uses the Tiedtke scheme (Tiedtke, 1989) while RCA4 the Kain-Fritsch/Bechtold (KF/B) scheme (Bechtold et al., 2001). The main difference in the schemes is that the Tiedtke scheme is based on moisture convergence closure assumption while the KF/B scheme is based on convective available potential energy (CAPE). In the Tiedtke scheme convection is triggered if the parcel's temperature exceeds the environment temperature by a fixed temperature threshold of 0.5 K. In the KF/B scheme the onset of convection depends on the large-scale vertical velocity. The Tiedtke and the KF/B scheme distinguish penetrative and shallow convection. The Tiedtke scheme additionally considers mid-level convection, convection starting above the planetary boundary layer (PBL). This is not separately considered in the KF/B scheme since the trigger criterion is also applied above the PBL.

2.1.2 Observations

Daily precipitation gauge datasets are scarce over Africa. As a result, few examples of work related to observed changes in extreme precipitation across Africa are available in the literature (e.g. New et al., 2006; Aguilar et al., 2009). And these observed dataset are insufficient for quantifying model biases as a consequence of limited spatial and temporal coverage of stations. Gridded rainfall data based on gauge-satellite products are an alternative for evaluating climate models (e.g Shongwe et al., 2009; Sylla et al., 2013; Nikulin et al., 2012). However, discrepancies exist across different datasets as a result of stations availability, extraction algorithms, merging and interpolation techniques (Sylla et al., 2013; Nikulin et al., 2012; Kalognomou et al., 2013). The ability of the downscaled simulations to reproduce extreme precipitation observations for the present (or validation) period 1997-2005 is assessed using Global Precipitation Climatology Project One-Degree Daily (GPCP 1DD Verion 1.2) (Huffman et al., 2001) dataset. The GPCP 1DD (hereafter GPCP) is a satellite-derived precipitation dataset that are bias corrected using of continental observational station records. While the GPCP dataset provides complete spatial coverage across southern Africa, some regions outside South Africa have sparse observational station records and hence extremes in these regions may be less reliable compared to regions with denser station network. This dataset is available from 1997 to 2005 at 1°latitude-longitude resolution. In addition the Tropical Rainfall Measuring Mission (TRMM 3B42 version 7, Huffman et al. (2007)) 0.25° latitude-longitude resolution from 1998 to 2005 was used. The ERA-Interim (EI) precipitation is not used because it is a model product that is not constrained by precipitation observations. In order to allow for a comparison between gridded observation and model simulations for the present period, the two dataset were remapped to the common grid (0.44°latitude-longitude) of the models.

2.2 Methods

2.2.1 Synoptic types

The basic aim of synoptic climatology is to relate local or regional climates to the large scale atmospheric circulation (Yarnal, 1993). This require classifying atmospheric circulation types and then relating a local variable (e.g. temperature, precipitation) to these circulation types. In order to gain confidence in the simulated historical climate and projected changes in extremes events, the atmospheric circulation at regional scale is analysed. This offers a valuable additional source of information to assess the robustness and value of downscaled climate (Hewitson, 2010). The non-linear classification method, the SOM, described in detail by Kohonen (2001) is used to classify the regional atmospheric circulation. The SOM reduces a high dimensional data set into a 2-dimensional matrix of reference vectors, or nodes (SOM map), which summarises key aspects of the larger data set. The nodes are arranged with similar types located adjacent to each other in the two-dimensional ordered array, facilitating interpretation of the synoptic types and their relationship. In comparison with more traditional approaches to investigating multi-dimensional data (e.g. cluster analysis and principal component analysis) the SOM approach is more robust and less subjective, i.e, no assumptions regarding the resulting patterns are made by the user. In addition, it offers a powerful means of visualising the continuum of data space with distinct advantages in interpreting underlying physical processes (Hewitson and Crane, 2002).

A review of SOMs and the application to synoptic climatology have been described in detail by Hewitson and Crane (2002). Other applications include extreme climate events, GCM evaluation, weather regime classification and season definition and classification (Cazavos, 2000; Tennant and Hewitson, 2002; Brown et al., 2010; Radic and Clarke, 2011; Lennard and Hegerl, 2014). Detailed description on the SOM training algorithm can be found in Sang et al. (2008).

The size of the SOM array has a strong influence on the range of synoptic situations represented. The fewer the number of nodes in the SOM array the more general each pattern must be, while with a greater number of nodes a wider range of situations can be represented. South African synoptic systems have been generalised into eight primary circulation types (Tyson and Preston-White, 2000). For example, Lennard and Hegerl (2014) and MacKellar et al. (2010) have used a 12-node SOM size over southern Africa. On testing various sizes a 20-node SOM patterns (5 x 4) was selected to span the range of synoptic conditions for all seasons. The size of the SOM node was based on an optimal number of nodes where there are not too few to result in generalisations, neither too many so as to make the analysis complex. Daily sea level pressure (PSL) ERA-Interim reanalysis data (Dee et al., 2011) with 0.44° horizontal resolution is used to train the SOMs as it was shown to be a good indicator of regional climate (Tyson et al., 1996b,a). The domain covers southern Africa from 9°S to 44°S. This latitude range includes synoptic weather system of both tropical and mid-latitude origins. The longitude range is from 6°E to 45°E and encompasses processes from the oceans around the sub-continent. The procedure to train the SOM begins with a random initialisation of the SOM array, followed by a two step training process with passes of 50000 iterations each. For the first training process the learning rate 1 was set to 0.05 and the initial radius of training area set to five which decreases linearly to one during training. On the contrary, the second training process the initial radius was set to three, with a training rate of 0.025. The second training process develops the finer aspects of the SOM array. Each day is therefore mapped to a particular SOM node and is associated with the same day of the downscaled GCMs for the present period (1976-2005) and future (2036-2065 and 2069-2098) simulations.

To better understand the the synoptic circulation over the region, moisture transport is calculated from the u-, v-wind components ($\overrightarrow{V}$) and specific humidity (q) at 850

hPa (equation 2.1).

$$Q = q * \overrightarrow{V} \tag{2.1}$$

Then all the days in the period that mapped to a particular SOM node are averaged to construct a composite of moisture transport.

Extreme precipitation days

Extreme precipitation days are defined as days with at least 10% of grid points with precipitation above the 95th percentile of daily rainfall distribution from 1997-2005. Extreme precipitation days are extracted from GPCP gridded data set and mapped to the SOMs to identify synoptic conditions associated with extreme precipitation. The same procedure is applied in the downscaled GCMs for the present and future. Three sub-regions are selected based on Global Precipitation Climatology Centre (GPCC)(Rudolf et al., 2010) standardised annual precipitation cycles over Africa, which are distinguished into nine classes using the k-means method (Kalognomou et al., 2013). The location of the sub-regions and their topography is shown in Fig. 2.1. The sub-regions are the centre and northern Mozambique, Zimbabwe, Zambia, northern Botswana and east parts of Angola (region 1), southern Mozambique, central and east coast of South Africa (region 2) and the south-western Cape of South Africa (region 3). Region 1 experience rainfall in summer that results from mesoscale convective systems, tropical storms and tropical cyclones from Mozambique Channel (MC) (Kalognomou et al., 2013). Region 2 is also a summer rainfall that results from mesoscale convective systems, warm fronts, subtropical lows, mid- to upper-tropospheric troughs, and cloud bands. Region 3 is a winter rainfall region that receives the bulk of its annual rainfall from frontal systems (Kalognomou et al., 2013).

2.2.2 Assessment of extreme events

Extreme weather and climate events are normally studied using two approaches, parametric and a non-parametric. In the non-parametric approach extreme precipitation indices are estimated from the empirical distribution of the daily data. These indices characterise moderate and statistically robust extreme events with reoccurrence times of a year or shorter (Klein Tank et al., 2009). The parametric approach based on the extreme value theory (EVT) (see Gnedenko, 1943; Fisher and Tippett, 1928; Gumbel, 1984) complements the descriptive indices in order to evaluate the intensity and frequency of rare events that lie far in the tails of the probability distribution of weather variables (e.g. events that occur once in 20 years).

Moderate extremes

The World Meteorological Organization (WMO) Commission for Climatology and the Expert Team on Climate Change Detection and Indices (ETCCDI) developed a set of 27 indices based on daily temperature and precipitation. Of these, the six indices that are based on daily precipitation are used to asses the performance of the RCMs at simulating precipitation extremes across southern Africa for the 1997-2005 validation period and to demonstrate future projected changes in extreme events for mid Century (2036-2065) and end of the Century (2069-2098). These indices have been widely used in detection, attribution, and projection of changes in climate extremes (e.g., Alexander and Arblaster, 2009; Min et al., 2011; Orlowsky and Seneviratne, 2011; Donat et al., 2013; Sillmann et al., 2013b). Detail of these indices are shown in Table 2.2, and a full descriptive list of the indices can be found on the ETCCDI website http://etccdi.pacificclimate.org/list_27_indices.shtml.

Table 2.2: Definitions of the indices of precipitation extremes used in this study.

Label	Index Name	Index definition	Units
R10mm	Heavy precipitation days	Number of days (per year/season) with precipitation amount $\geq$ 10 mm. Let PR_{ij} be the daily precipitation amount on day *i* in period *j*. Count the number of days where $PR_{ij} \geq 10$ mm	days
R20mm	Very heavy precipitation days	Number of days (per year/season) with precipitation amount $\geq$ 20 mm. Let PR_{ij} be the daily precipitation amount on day *i* in period *j*. Count the number of days where $PR_{ij} \geq 20$ mm	days
CDD	Consecutive dry days	Maximum (annual/seasonal) number of consecutive dry days. Let PR_{ij} be the daily precipitation amount on day *i* in period *j*. Count the largest number of consecutive days where $PR_{ij} < 1$ mm	days
Rx5day	Highest 5-day precipitation amount	Maximum (annual/seasonal) precipitation sums for 5-day interval. Let PR_{kj} be the precipitation amount for the 5 day interval ending *k*, period *j*. Then maximum 5 day values for period*j* are: $RX5day_j = \max(PR_{kj})$	mm
SDII	Simple daily intensity index	Average precipitation from wet days. Let PR_{wj} be the daily precipitation amount on wet days, PR $\geq$ 1 mm in period *j*. If *W* represents number of wet days in *j*, then: SDII*j* = $(\sum_{W=1}^{W} PR_{wj})/W$	mm/day
R95pTOT	Very wet days	Annual/seasonal total precipitation from days with PR $\geq$ 95th percentile of the distribution of daily precipitation amounts at days with 1 mm or more precipitation in the 1976-2005 baseline period. Let PR_{wj} be the daily precipitation amount on a wet day *w* (PR $\geq$ 1 mm) in period *i* and let $PR_{wn}95$ be the 95th percentile of precipitation on wet days in the baseline period (1976-2005). If *W* represents the number of wet days in the period, then: $R95p_j = \sum_{W=1}^{W} PR_{wj}$, where $PR_{wj} > PR_{wn}95$	mm
PRCPTOT	Total wet-day precipitation	Annual/seasonal total precipitation from wet days. Let PR_{ij} be the daily precipitation amount on day*i* in period *j*. If *I* represents the number of days in *j*, then: PRCPTOT*j* = $\sum_{i=1}^{I} PR_{ij}$	mm

The simple daily intensity (SDII) and the total wet-day precipitation (PRCPTOT) represent average precipitation conditions. These two indices are also useful to understand variations in extreme precipitation. The PRCPTOT index can be compared with the number of wet days to investigate rainfall intensity changes - a fewer number of wet days with no change in PRCPTOT would infer more intense rainfall, which should also be reflected on SDII. All indices are calculated for each of the downscaled RCM simulations independently and the results averaged across the eight downscaled members to provide a multimodel mean. While for a single given diagnostic, the mul-

timodel performance might be significantly better than a single model (Nikulin et al., 2012), there remains a range of uncertainty with it. Therefore, model spread are presented for each index for three specific subregions with homogeneous rainfall annual cycle patterns.

Rare extremes

The EVT approach have been used in hydrology (e.g., Katz et al., 2002), atmospheric science (e.g., Palutikof et al., 1999; Buishand, 1989), finance and insurance (e.g., Embrechts et al., 1997) and many other fields of applications. In this study the EVT approach follows that used in Zwiers and Kharin (1998) and Kharin and Zwiers (2000). The diagnostics of primary focus is to estimate extreme events in terms of T-year return values. The T-year return value is defined as the threshold that is expected to be exceeded on average, once every T year, where T is the return period or waiting time. These thresholds are estimated by the block maximum technique (Coles, 2001), where a generalised extreme value (GEV) distribution is fitted to a sample of annual/seasonal maxima at every grid point. The GEV distribution is the asymptotic distribution that describes the behaviour of block maxima and as the form:

$$F(x) = \begin{cases} \exp\left[-\left(1+\kappa\left(\frac{x-\xi}{\alpha}\right)\right)^{-\frac{1}{\kappa}}\right], & \kappa < 0, x > \xi + \alpha/\kappa, \\ \exp\left[-\exp\left(-\frac{x-\xi}{\alpha}\right)\right], & \kappa = 0, \\ \exp\left[-\left(1+\kappa\left(\frac{x-\xi}{\alpha}\right)\right)^{-\frac{1}{\kappa}}\right], & \kappa > 0, x > \xi + \alpha/\kappa. \end{cases} \tag{2.2}$$

where, ξ, α and κ are *location, scale* and *shape*. The GEV distribution (Eq. 2.2) encompasses the classical "three types" of extreme value distributions defined by κ, which determines the nature of tail behaviour of the maximum distribution. The flexibility of the GEV to describe all "three types" of tail behaviour makes it a universal tool for modelling block maxima (Naveau et al., 2005). The justification for the GEV distribution arises from an asymptotic argument. As the sample size in-

creases, the distribution of the sample maximum, say X, will asymptotically follow the classical "three types", either Fréchet distribution (κ>0), Weibull distribution (κ<0), or Gumbell distribution (κ=0) (Naveau et al., 2005). Each of the "three types"of distributions has distinct forms of behaviour in the tails (see Fig. 2.2). The Weibull distribution is bounded above, meaning that there is a finite value which the maximum cannot exceed. The Gumbel distribution yields a light tail, meaning that although the maximum can take on infinitely high values, the probability of obtaining such levels becomes small exponentially. The Fréchet distribution with a heavy tail, decays polynomially, so that higher values of the maximum are obtained with greater probability, that would be the case with a lighter tail (Gilleland and Katz, 2006).

L-moment method

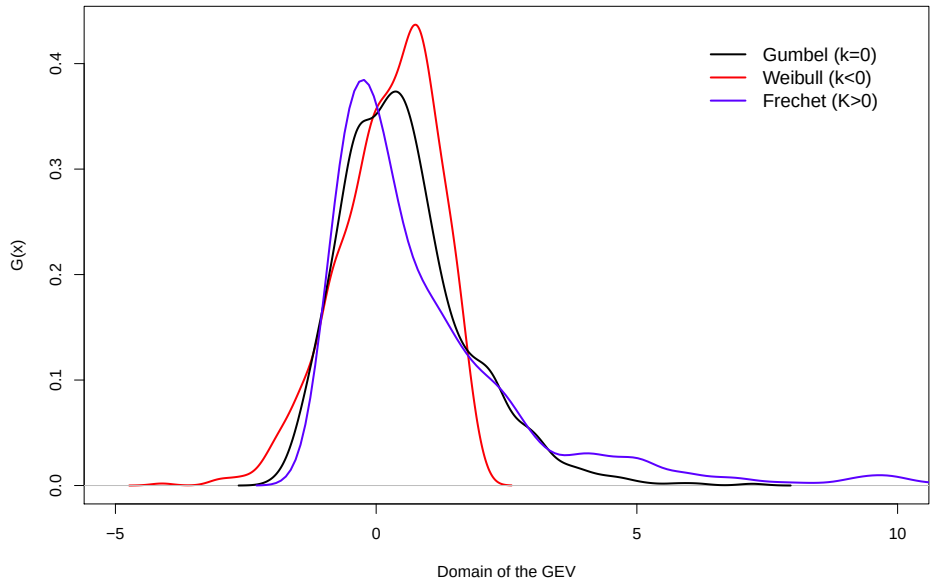

Figure 2.2: Density of the GEV distribution function for three choices of the shape parameter k

Various methods are used to estimate the parameters of the GEV distribution. The maximum likelihood estimators (Coles, 2001) are asymptotically optimal but they are not necessarily the best for finite sample sizes (Zwiers and Kharin, 1998; Kharin et al., 2005; Hosking et al., 1985), and thus less advisable choice in this study because the available samples are very short (16 annual extremes). The GEV distribution

parameters are estimated by the method of L-moments (LMOM) (Hosking, 1990). L-moments are linear functions of the expectations of order statistics and they can be viewed as an alternative system of describing the shapes of probability distributions. The main advantages of using the method of LMOM are that the parameter estimates are more reliable (i.e. smaller mean-squared error of estimation) and are more robust for short samples, and are usually computationally more tractable than the conventional moments and maximum likelihood (Hosking, 1990).

The first three L moments of a random variable *X* are defined in terms of its distribution function *F(x)* (Hosking, 1990) as follows:

$$\begin{aligned}
\lambda_1 &= EX = \int_0^1 x(F)dF, \\
\lambda_2 &= \frac{1}{2}E(X_{2:2} - X_{1:2}) = \int_0^1 x(F)(2F-1)dF, \\
\lambda_3 &= \frac{1}{3}E(X_{3:3} - 2X_{2:3} + X_{1:2}) = \int_0^1 x(F)(6F^2 + 6F + 1)dF.
\end{aligned} \tag{2.3}$$

where E denotes expectation and $X_{1:r}, X_{2:r}, ..., X_{r:r}$ are the order statistics obtained by sorting the sample of size r in ascending order. The L moments λ_1, λ_2, and λ_3 are in some ways analogous to the conventional central moments and may be regarded as measures of location, scale and skewness of the distribution.

For the GEV distribution, the first three L-moments in terms of its location (ξ), scale (α) and shape (κ) parameters are given by:

$$\begin{aligned}
\lambda_1 &= \xi + \frac{\alpha}{\kappa}[1 - \Gamma(1+\kappa)] \\
\lambda_2 &= (1 - 2^{-\kappa})\frac{\alpha}{\kappa}\Gamma(1+\kappa) \\
\lambda_3 &= \lambda_2[2\frac{(1-3^{-\kappa})}{(1-2^{-\kappa})} - 3]
\end{aligned} \tag{2.4}$$

where $\Gamma()$ represents the gamma function:

$$\Gamma(x) = \int_0^\infty t^{x-1} e^{-t} dt, x \geq 0 \tag{2.5}$$

The unbiased estimators of λ_1, λ_2 and λ_3 are:

$$\begin{aligned}
\hat{\lambda_1} &= \sum_i X_i/n \\
\hat{\lambda_2} &= \frac{1}{2} \sum_{i>j} (X_{i:n} - X_{j:n})/C_2^n \\
\hat{\lambda_3} &= \frac{1}{3} \sum_{i>j>k} (X_{i:n} - 2X_{j:n} + X_{k:n})/C_3^n
\end{aligned} \tag{2.6}$$

where $C_k^n = n!/[k!(n-k!]$.

To estimate the GEV distribution parameters, one needs to substitute the L-moments in Eq. 2.4 with the unbiased estimators of L-moments using Eq. 2.6. The resulting method of L-moments estimators are given by:

$$\begin{aligned}
\hat{\kappa} &= 7.8590z + 2.9595z^2 \\
\hat{\alpha} &= \frac{\hat{\lambda_2}\hat{\kappa}}{(1-2^{-\hat{\kappa}})\Gamma(1+\hat{\kappa})} \\
\hat{\xi} &= \hat{\lambda_1} + \frac{\hat{\alpha}}{\hat{\kappa}}[\Gamma(1+\hat{\kappa}) - 1]
\end{aligned} \tag{2.7}$$

where $z = (2/(3 + \hat{\lambda_3}/\hat{\lambda_2})) - (\ln 2/\ln 3)$.

Feasibility of the L-moment estimators

Dupuis and Tsao (1998) pointed out that the method of L-moments may yield non-feasible estimates in the sense of the estimated distribution may not contain all of the data from which distribution parameters are estimated. The percentage of nonfeasibiliy is small when $\kappa \leq 0.1$, but is considerably larger when κ is larger. The LMOM

estimates are not feasible when the following auxiliary constraints are violated

$$X_{n:n} \leq \hat{\xi} + \frac{\hat{\alpha}}{\hat{\kappa}} \quad \text{if} \quad \hat{\kappa} > 0 \tag{2.8}$$
$$X_{1:n} \geq \hat{\xi} + \frac{\hat{\alpha}}{\hat{\kappa}} \quad \text{if} \quad \hat{\kappa} < 0$$

where $X_{1:n}$ and $X_{n:n}$ are the smallest and the largest values in a sample of size n, respectively. Dupuis and Tsao (1998) proposed a hybrid estimator which always satisfies Eq. 2.8 by replacing nonzero $\hat{\kappa}$ by $\tilde{\kappa}$ when the estimate is nonfeasible

$$\tilde{\kappa} = \begin{cases} \hat{\alpha}/(X_{n:n} - \hat{\xi} & \text{if} \quad \hat{\kappa} > 0 \\ \hat{\alpha}/(X_{1:n} - \hat{\xi} & \text{if} \quad \hat{\kappa} < 0 \end{cases} \tag{2.9}$$

The method of LMOM and hybrid estimators are comparable in terms of bias and root mean square error (rmse) but the hybrid has the extra advantage that it is always feasible (Dupuis and Tsao, 1998).

The 20-year return values are estimated by fitting the GEV distribution to a sample of annual maxima and then invert the GEV cumulative distribution function 2.2:

$$X_T = \begin{cases} \hat{\xi} - \hat{\alpha}\{1 - [-\ln(1 - 1/T)]^{-\hat{\kappa}}\}/\hat{\kappa}, & \hat{\kappa} \neq 0, \\ \hat{\xi} - \hat{\alpha}\ln[-\ln(1 - 1/T)], & \hat{\kappa} = 0. \end{cases} \tag{2.10}$$

Goodness-of-fit test

It is important to test the goodness-of-fit (GOF) of the fitted distribution to examine whether the sampled annual maxima are realisations of a random process with the GEV distribution. The standard Kolmogorov-Smirnov (KS) GOF is applied, and is defined as the maximum absolute difference between two cumulative distribution

functions

$$D = \max_{x \in \mathbb{R}} |F(x) - G(x)| \tag{2.11}$$

where $F(x)$ is the fitted distribution function and $G(x)$ the empirical distribution function estimated from the sample.

Since the GEV distribution parameters are estimated from the data, the critical values taken from statistical tables should not be employed (von Storch and Zwiers, 1999). In this case, more appropriate estimates of the critical values are determined by parametric bootstrap procedure (e.g., Kharin and Zwiers, 2000). In this procedure 1000 samples of the same size as observed or modelled series of seasonal/annual maxima are generated from the fitted GEV, and the values of D are derived for each generated sample. The 90% quantile of the distribution of D is then used as the critical value of the test at the significance level α=0.10. The null hypothesis that the seasonal/annual extremes are drawn from the distribution $F(x)$ is rejected when D exceeds the critical value.

2.2.3 Value added by RCMs

The added value (AV) concept (Di Luca et al., 2012, 2013) is used to test whether the RCMs show improvements over the coarse-resolution models used as large-scale forcing. It is defined as a measure of the difference between the large scale forcing or boundary condition (BC) and the downscaled RCM squared errors and was computed as:

$$AV = \frac{(X_{BC} - X_{OBS})^2 - (X_{RCM} - X_{OBS})^2}{Max((X_{BC} - X_{OBS})^2, (X_{RCM} - X_{OBS})^2)} \tag{2.12}$$

where, X_{BC}, X_{OBS} and X_{RCM} represents the index calculated from the BC (ERA-Interim or GCM), observation (GPCP), and RCMs, respectively. The normalization is introduced so that -1 $\leq$ AV $\leq$ 1 (e.g. Dosio et al., 2015). It is worth mentioning that for this analysis, only GPCP is used in the spatial distribution of the added value. A

positive value of AV provides a measure of the added value afforded by dynamical downscaling with an RCM. Various studies have assessed the added value issue using a scale decomposition method (Bresson and Laprise, 2011; Di Luca et al., 2012; Feser, 2006). Di Luca et al. (2012) separated the AV in two types. The first type is related with climate variability in scales that are not explicitly resolved by GCMs. The second type is related with spatial scales common to both the RCMs and GCMs that results from the upscaling of fine scales into large scales. The added value considered in this thesis is of the type one and for this the GCMs were regridded to common spatial resolution of RCMs using a billinear interpolation method.

The centered pattern correlation coefficient (PCC) is also calculated, and it indicates how well the spatial pattern is captured. Both GPCP and TRMM are used to account for uncertainties in the observed daily precipitation products.

3 Dominant synoptic systems

In the following section, the simulated historical and projected atmospheric circulation are investigated. It is essential to have a good understanding of how RCMs perform over southern Africa before considering how they simulate atmospheric circulation changes in the future. Of particular importance is the extent to which atmospheric circulation responds to changes in radiative forcing. In order to assess this response, mean sea-level pressure (MSLP) and wind fields at the 850 hPa level are used. The downscaled data is compared with ERA-Interim reanalysis to asses the ability of the models to simulate synoptic circulation over the region. Future changes on these synoptic circulations is also presented.

3.1 Synoptic systems in 20th century simulations

In order to explore the circulation patterns responsible for rainfall in Southern Africa a SOM was applied to the ERA-Interim (EI) data from the period 1989-2005, as described in the Section 2.2. The 20 SOM patterns of MSLP for the full 1989-2005 period of the EI reanalysis is shown in Fig. 3.1. The shaded region is MSLP and the arrows indicate the moisture transport over the region.

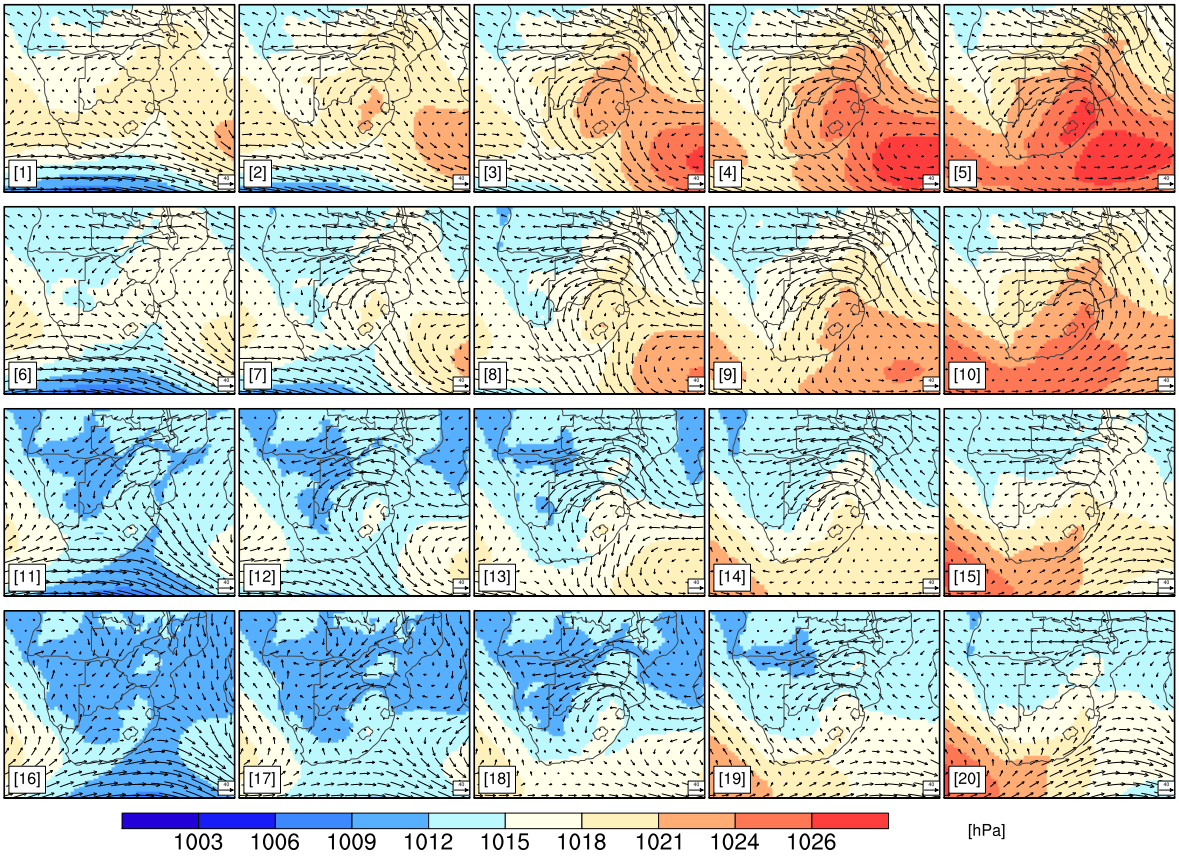

Figure 3.1: The 5x4 SOM built using 1989-2005 period of the ERA-Interim reanalysis SLP. The *reds* indicate high pressure and the *blues* lower pressure. Vectors represent moisture transport [units: g kg-1 m s-1] composite associated with each node.

The archetypal modes of MSLP and moisture transport are used to describe the characteristics circulations over southern Africa. Similar synoptic circulation patterns are clustered together across the node space while more distinct types are further apart as a consequence of the SOM mapping algorithm (Hewitson and Crane, 2002). Features of the low level circulation can be seen through the MSLP patterns - these include the South Atlantic and Indian anticyclone, mid latitude westerlies and the northeast monsoon. The circulation types displaying tropical troughs are in the lower portion of the SOM and types with broad regions of high pressure are near the top.

In the two bottom rows of the SOM array, nodes represent strong anticyclones ridging in over the east or west coast with a dominant South Atlantic High Pressure (SAHP),

and tropical troughs extending down from the equator.These nodes represent circulation patterns typical of austral summer (DJF) over the region. The mid-latitude cyclones in theses nodes are displaced southwards compared with nodes 1,2,6, and 7. The moisture is transported into southern Africa from the southwest Indian Ocean (IO) and from the southeast tropical Atlantic Ocean (AO) (Reason et al., 2006) through the Angola low (Cook et al., 2004; Tyson and Preston-White, 2000). The westerly moisture from the AO converges with a warm moist air from the IO in the heat low located over the interior of southern Africa which result in ideal conditions for strong vertical uplift and the formation of cloud bands. These features are commonly referred to as tropical-temperate troughs(TTTs) and contribute significantly to summer rainfall over southern Africa (Harangozo and Harrison, 1983) including heavy rainfall events (Hart et al., 2010). Over southern Africa, a TTT is formed when a easterly low or wave at surface combines with a westerly wave leading to the formation of northwest-southeast oriented cloud bands which extend over both continental southern Africa and adjacent southwest IO (Todd and Washington, 1999). Circulations represented by node 12 and 17 suggest a linkage between the mid-latitudes and subtropical low-pressure systems and represent conditions favourable for the formation of TTT. The high-pressure system located in the south-west of the domain, results in a poleward displacement of frontal systems and dry summers over south-western part of the Western Cape Province of South Africa.

Typical austral winter (JJA) circulation patterns for the region are located at the top rows of the SOM map. These nodes are associated with ridging highs from the AO, strong high pressure over the IO and the strong westerly wave with associated cold frontal systems. These cold fronts are the primary rain-bearing system along the southern coast and the south-western part of the Western Cape Province of South Africa (Tyson and Preston-White, 2000). The moisture flux in this region is westerly, in contrast to the easterly flux experienced across the bulk of the subcontinent.

During austral autumn (MAM) and austral spring (SON) transitions periods, synoptic situations typical of either winter or summer can occur.

Having derived characteristic circulation patterns, the average climatological frequency of daily events on each SOM node for the whole period (shown as a percent of the total days) is determined for all ensemble members (Fig. 3.2). Each bar represents the node frequency of occurrence of each individual ensemble member. For the trained data EI reanalysis, the frequency of occurrence of each synoptic node is in the expected frequency of 5% or 1/20 (i.e. the node frequency that would occur if each node occurred equally), indicating that the synoptic patterns attained by SOM are an even distribution across the whole training data.

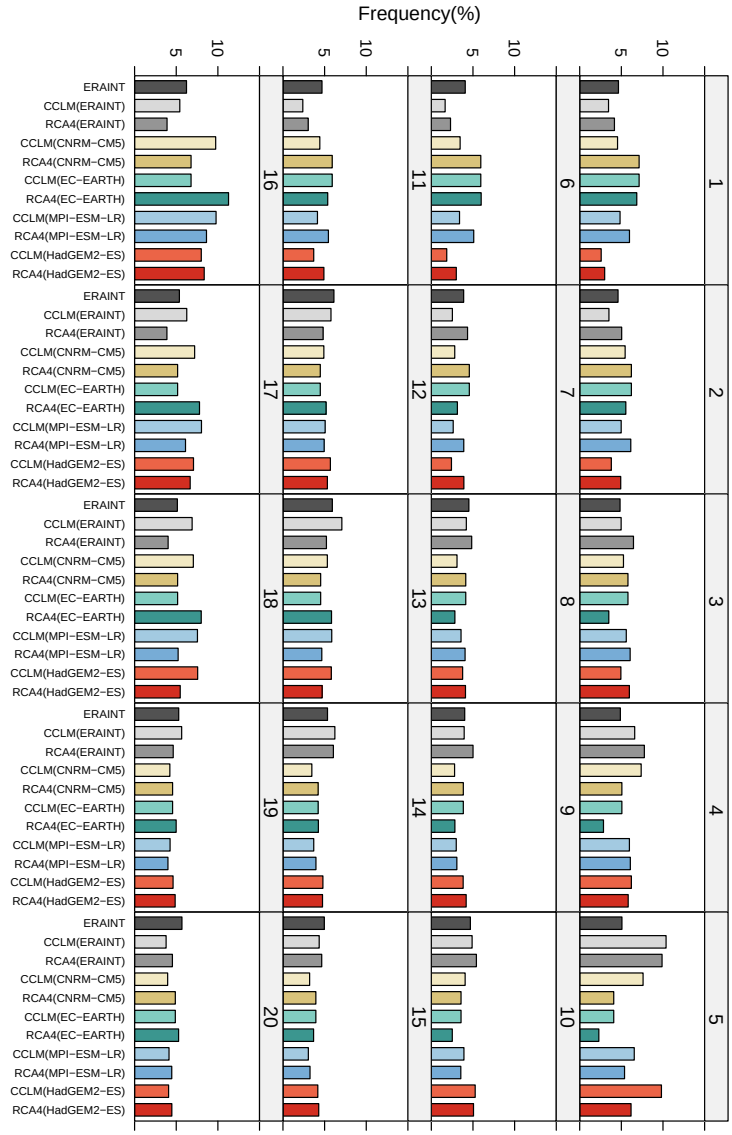

Figure 3.2: Frequency (%) of occurrence that map to each SOM node shown in fig. 3.1 for the period 1989-2005 (ERA-Interim and RCM(ERA-Interim)) and 1976-2005 (RCM(GCM)).

In evaluating the two RCMs (downscaled EI for the period 1989-2005, grey bars), most node mapping frequencies are similar to that of the EI reanalysis with the exception of node 5, which is over simulated by both models, and nodes 6,11 and 16 which are under-simulated.

When considering the downscaled GCM results for example in node 16, which show higher mapping frequencies than EI data and RCMs forced by EI, this would imply that the downscaled GCMs simulate this type of circulation too frequently.

The nodal loadings for austral summer (DJF), winter (JJA), autumn (MAM) and spring (SON) are presented in fig. 3.3. These show the frequency (as a percentage) that each node was mapped to in each respective season over the 17-year period.

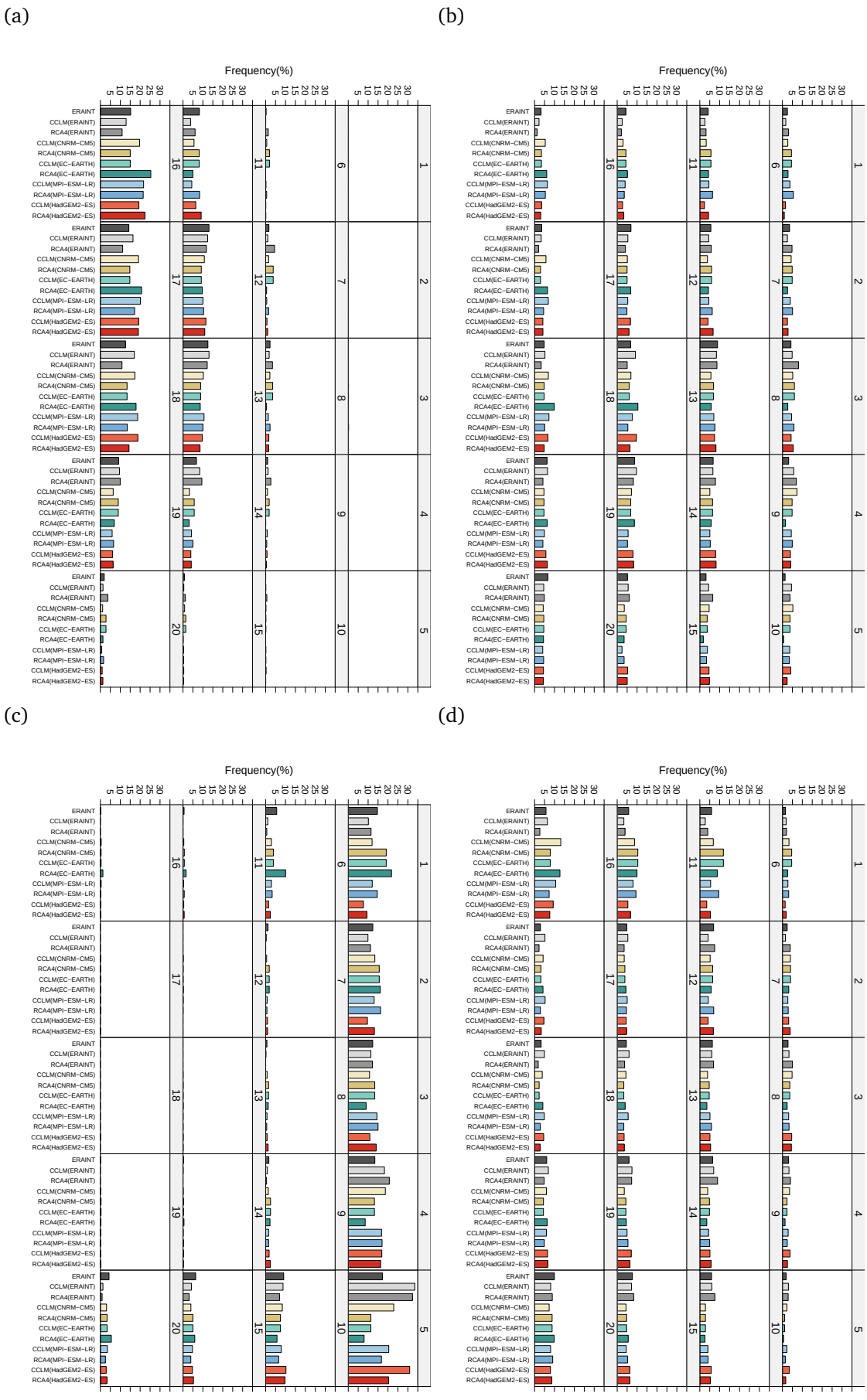

Figure 3.3: Frequency (%) of occurrence that map to each SOM node shown in fig. 3.1 on a seasonal basis (a) DJF, (b) MAM, (c) JJA and (d) SON.

Nodes in the bottom row of the SOM (node 11 to 14 and node 16 to 19) are mapped more frequently by models during DJF (Fig. 3.3(a)) and the nodes at the top row and right hand side (node 1 to 6 and node 10 and 15) appear more frequently during JJA (Fig. 3.3(c)). During transitions periods synoptic circulation of both winter or summer are evident, however with lower frequency (Fig. 3.3(b) and 3.3(d)). The bias in the EI downscaled results in node 5 is attributable to an over simulation of winter-time circulations dominated by high-pressure synoptics which may be a function of the southern most extent of the CORDEX-Africa domain. Here the minimum latitude of the domain is 45° S and likely retard the ability of the regional models to develop mid-latitude troughs that move northward through this latitude (e.g. Kalognomou et al., 2013). The lower frequency bias in nodes 11 and 16 seem to be present throughout DJF, MAM and SON. The majority of the downscaled GCMs overestimate the frequency of nodes 16, 17, 18 and 19 and underestimate nodes 12,13 and 14. During SON and MAM the inter-model variability of the downscaled GCMs is smaller compared with JJA and DJF.

3.1.1 Link between precipitation and circulation patterns

In order to identify the precipitation patterns associated with different circulation nodes, each day of the observed period was mapped to the closest SOM node to construct a composite of rainfall for each SOM node (e.g., Hope et al., 2006). The daily mapping was performed for the period 1997-2005 and the corresponding rainfall composited from GPCP dataset. The precipitation anomalies from this composite mapping are shown in Fig. 3.4. Brown shading indicates regions of less rainfall compared to the 1997-2005 mean while green shading indicates more. Nodes 11-14 and 16-18 in the SOM map are clearly responsible for most of the wet conditions for the bulk of the sub-continent, and most of this rainfall occurs during summer. Highest rainfall occurs over northern Mozambique and is attributable to the tropical low

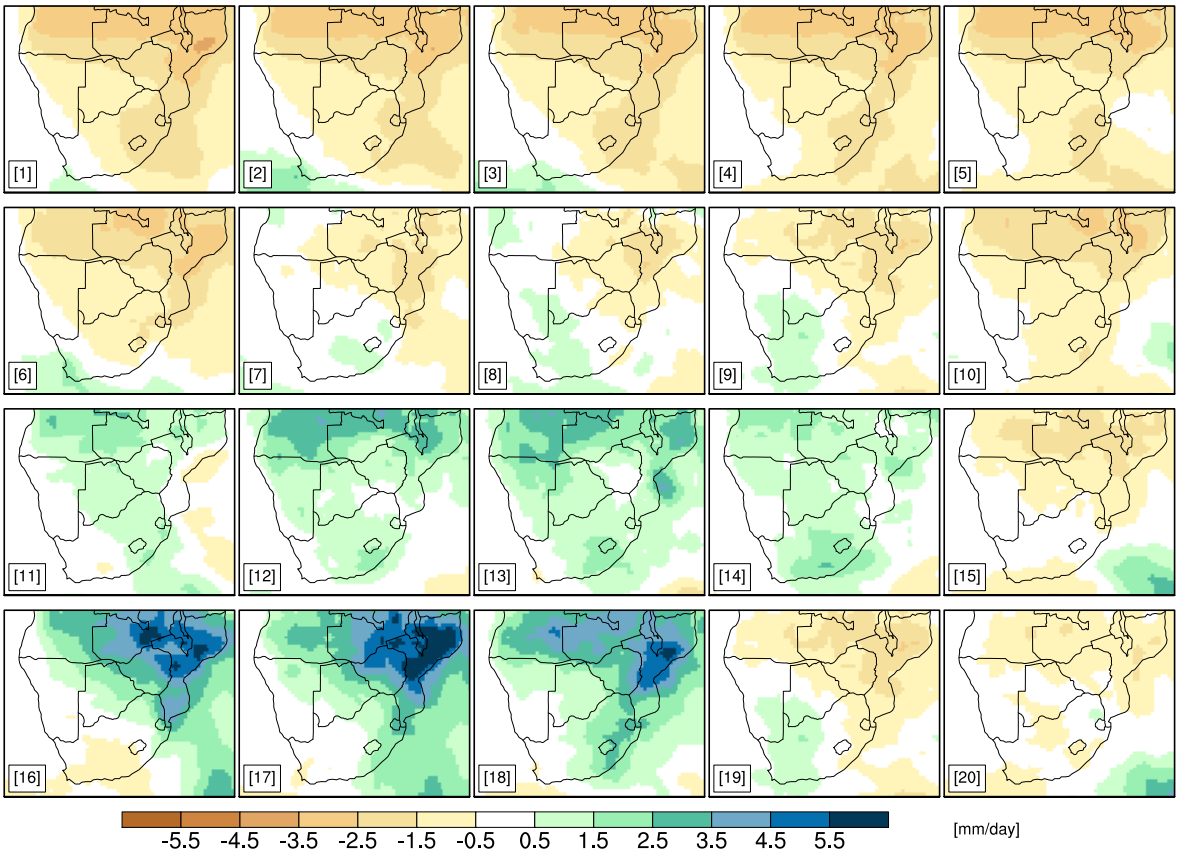

Figure 3.4: GPCP precipitation anomalies associated with each circulation type in the 5x4 SOM. Negative values indicates conditions drier than the 1979-2005 mean and positive values wetter than the mean.

formed at the MC that advects moisture into the region as demonstrated in nodes 17 and 18. The winter rainfall is largely associated with nodes 1-3 and would represent frontal rainfall.

3.1.2 Synoptic condition associated with extreme precipitation days

It is also possible to describe the driving synoptics of extreme precipitation days by mapping only these days to the trained SOM. The days with extreme precipitation are extracted from the observed data set (GPCP) and from the downscaled GCMs (Section 2.2). The seasonal frequency of extreme precipitation days from GPCP data

set is shown in Fig. 3.5.

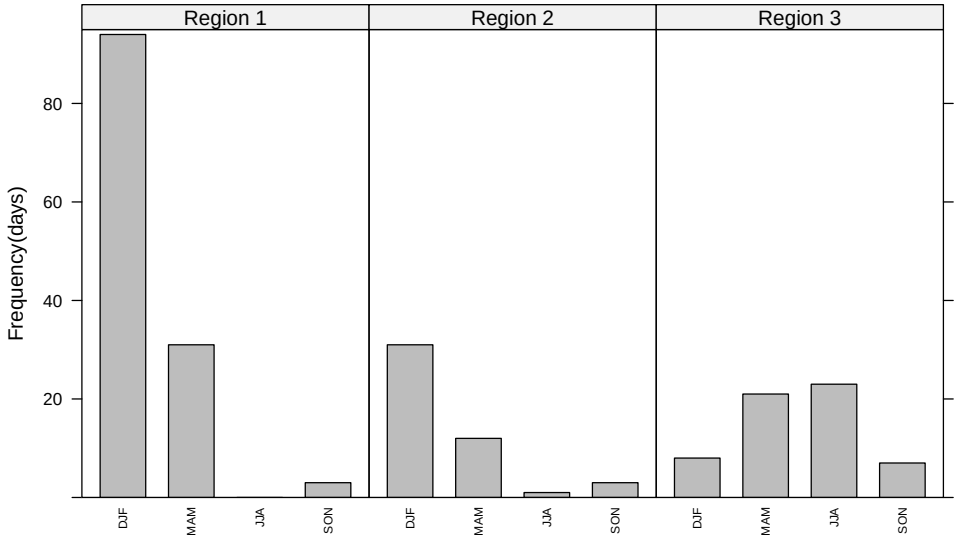

Figure 3.5: Seasonal frequency of extreme precipitation days as observed (GPCP) from 1997-2005.

The highest number of extreme precipitation occurs in summer over region 1 and 2 (see fig. 2.1 for the location of the regions), a season when most precipitation and extreme events typically occur (e.g Tyson and Preston-White, 2000). In region 3 the highest number of extreme precipitation days occurred in JJA and MAM. The composite of extreme precipitation days during this period associated with each synoptic circulation pattern is shown in Fig. 3.6.

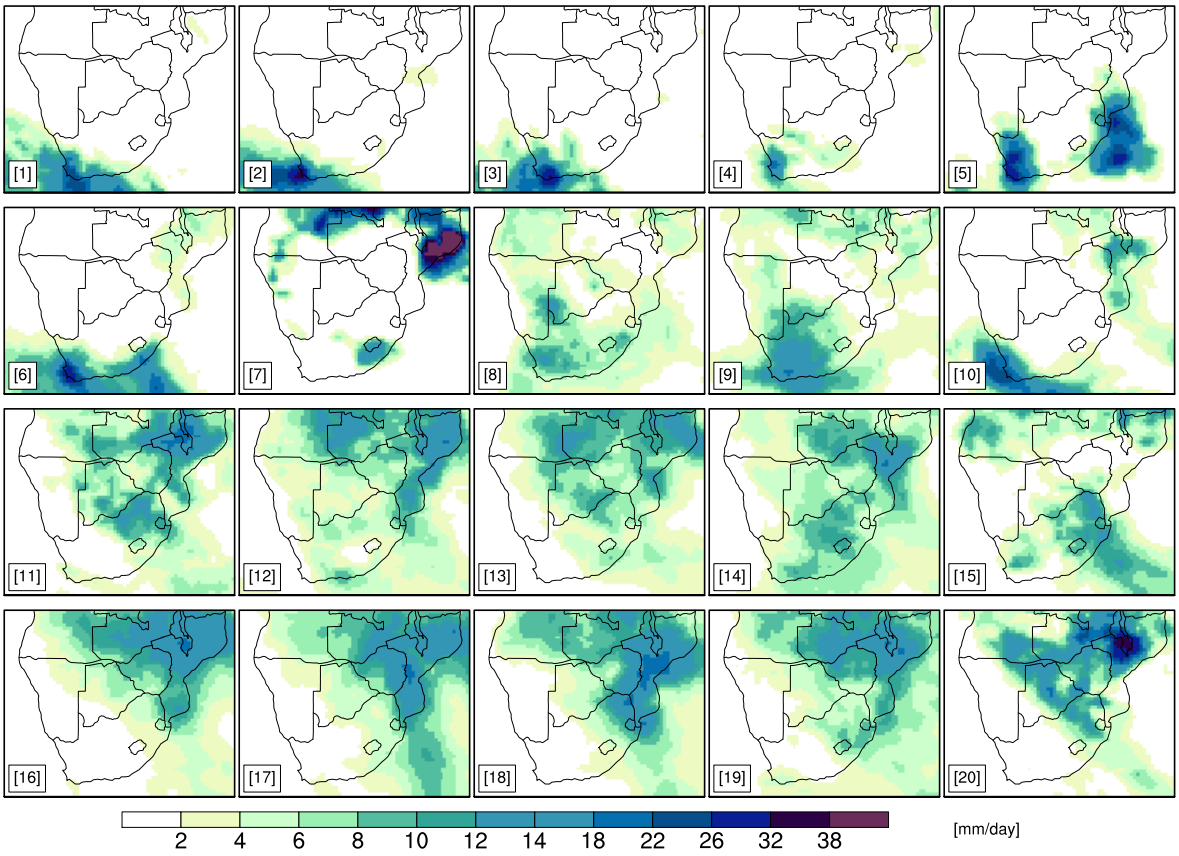

Figure 3.6: GPCP precipitation composites of days with extreme precipitation associated with each type in the 5x4 SOM.

Over region 1, the dominant summer month nodes (16-19) are associated with extreme precipitation and of these most of these extreme precipitation days map to nodes 16 and 17 (Fig. 3.7(a) - GPCP). Spatially, extreme precipitation mapping to these nodes is in the north east of the domain over Mozambique, Zimbabwe and Zambia where the extreme precipitation is associated primarily with westward moisture transport into the region from the MC.

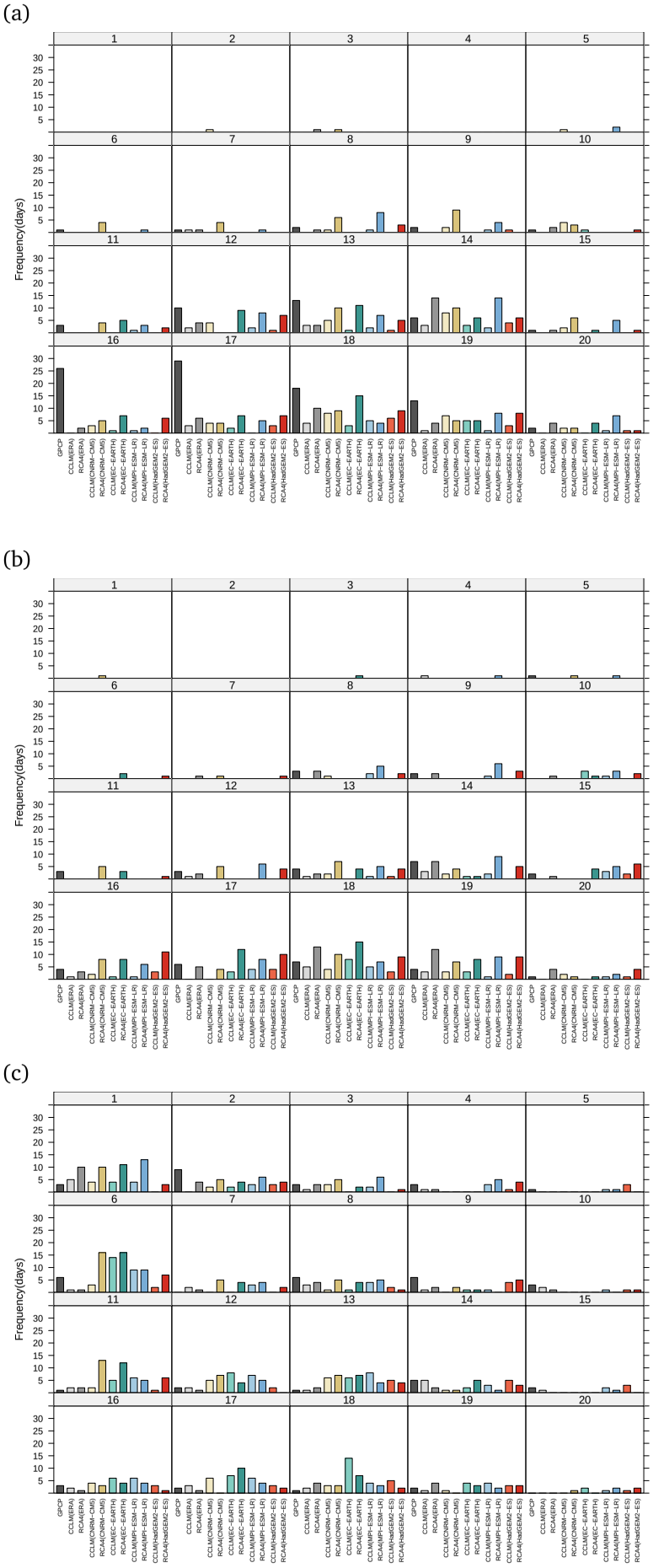

Figure 3.7: Frequency of occurrence of days with extreme precipitation during 1997-2005 that map to each SOM node shown in fig. 3.1 for each region (a) Region 1, (b) Region 2 and (c) Region 3.

Table 3.1 shows the number of extreme precipitation days for each ensemble member and observations for the three regions.

Table 3.1: Total number of extreme precipitation days for each region for the period of 1997-2005

	Region 1	Region 2	Region 3
GPCP	128	47	59
CCLM(ERA-INT)	17	15	35
RCA4(ERA-INT)	53	56	44
CCLM(CNRM-CM5)	52	16	41
RCA4(CNRM-CM5)	82	54	83
CCLM(EC-EARTH)	16	19	76
RCA4(EC-EARTH)	70	60	94
CCLM(MPI-ESM-LR)	17	22	78
RCA4(MPI-ESM-LR)	79	73	80
CCLM(HadGEM2-ES)	20	16	47
RCA4(HadGEM2-ES)	56	72	51

The RCMs do not capture the frequent mapping of extreme precipitation to nodes 16 and 17 in both the EI and GCM downscaling. This suggests that the regional climate models may have deficiencies in developing and advecting in the moisture necessary for such events, problems with the boundary layer and convective parameterization schemes are perhaps not able to simulate tropical cyclones, which are a primary cause of extreme precipitation in the region. It is likely a combination of these factors. However, it should be remembered that GCM simulations are not synchronous with the observed climate. Each GCM is initialised with atmospheric, sea and ice states in 1950 and left to develop its own climate - it is this non-real world climate that the RCM downscales. Despite this it would be expected that over the 9-year period the salient circulations responsible for extreme precipitation in the region would be captured. The poor EI result suggest even if the GCMs captured these drivers the downscaling would not be able to produce the expected extreme precipitation.

Spatially, extreme precipitation over region 2 lies largely in the bottom and bottom

second row of the SOM array and also node 8 and 9. This is apparent in the frequency mapping of extreme precipitation in this region, however nodes 16-19 also recorded equivalent mappings (Fig. 3.7(b)). Being a summer rainfall region these results are expected. Although the downscaled mappings in this region appear better than in region 1 when compared to GPCP, as was noted earlier the RCA4 model produced too many extreme precipitation events and the CCLM too few giving overall lower number of extreme precipitations days when averaged. The RCA4 overestimates the frequency of extreme precipitation days when compared with CCLM. This is due to the model cores as well as differences in physical parameterizations.

Region 3 includes the winter rainfall region of South Africa and spatially extreme precipitation is associated with mid-latitudes cyclones. Extreme precipitation days in this region map most frequently to nodes 1 and 6 (Fig. 3.7(c)) and these synoptic systems would take the form of deep mid-latitude cyclones and cut-off lows. However, extreme precipitation days are not only influenced from synoptic circulation typical from JJA but also from other seasons (e.g. Lennard et al., 2013) as evident especially nodes 13,14 and 19. This is because the northern part of this region lies in a region that is also influenced by summer rainfall regimes.

3.2 Future changes in synoptic systems

The change in synoptic circulation is defined as the difference between the simulated climate under future and current forcings. The difference in the number of days matching each synoptic type in the SOM map are shown in Fig. 3.8 at seasonal timescale for the middle (2035-2065) and late (2069-2098) 21st Century relative to 1976-2005 for the two reference concentration pathways (RCP4.5 and RCP8.5). The stationary hypothesis over climate dynamics is assumed, that is, the historical synoptic types remains valid throughout the 21st Century and rainfall results from the same synoptics. Boxes indicate the interquartile model spread (25th and 75th quantiles)

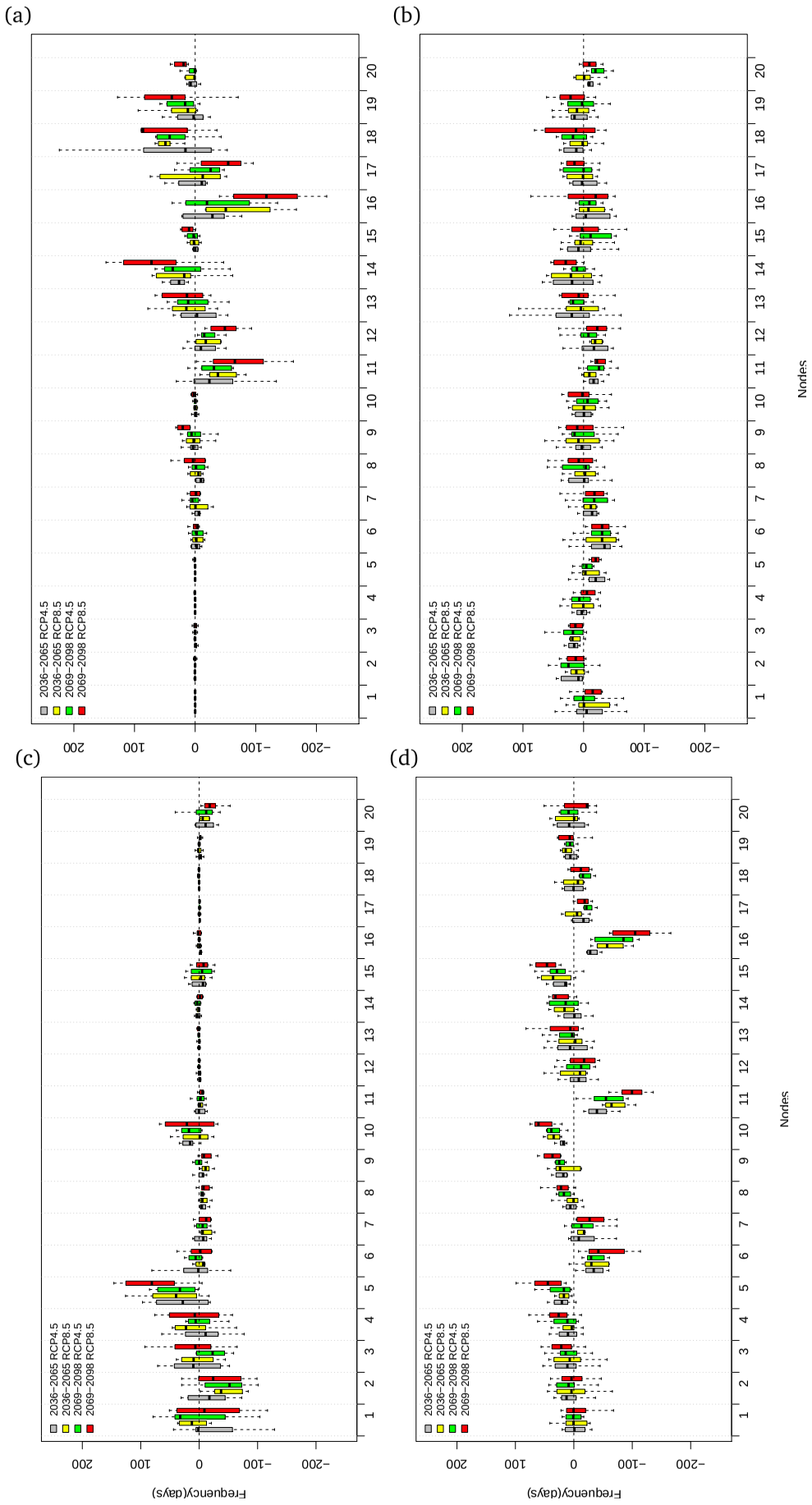

Figure 3.8: Projected changes in the frequency of occurrence that map to each SOM node shown in fig. 3.1 on seasonal basis, (a) DJF, (b) MAM, (c) JJA and (d) SON, over the periods 2036-2065 and 2069-2098 relative to 1976-2005 under RCP4.5 and RCP8.5.

with the horizontal line indicating the ensemble median and the whiskers showing the extreme range of the ensemble members. The extreme range of the ensemble members indicate the spread of the indicated change from the different models. The magnitude of change of the frequency of the synoptic types of the ensemble median is higher for RCP8.5 for most of the nodes compared with RCP4.5 for the same period. Decreases are projected for the frequency of occurrence of nodes in the bottom portions of the map (wet nodes) across the seasons. This suggests a decrease in circulation patterns that favour the occurrence of precipitation over most of southern Africa.The increasing frequency of occurrence of nodes in the top of the map (dry nodes) implies an increase in circulation patterns that are associated with reduced precipitation events. In general, these changes represent a projected increased occurrence of the oceanic high-pressure systems, a more dominant high-pressure circulation poleward of the continent and a decreased occurrence of patterns of continental lows and mid-latitude lows. Seasonally, the spread of the change is larger for DJF and JJA than the shoulder seasons (SON and MAM).

Comparisons of circulation patterns associated with extreme precipitation days from the downscaled GCMs for the mid and late 21st Century with the past where done and the results are shown in Fig. 3.9. Nodes 16 and 17, associated with higher occurrence of extreme precipitation days during DJF in region 1 are projected to decrease. However, projected increases in the occurrence of nodes 13,14,18 and 19 suggest an increase in the frequency of occurrence of extreme precipitation days over region 1 and 2. The circulation patterns associated with extreme precipitation days over region 1 are in general projected to increase. Days with extreme precipitation that map node 11,12,16 and 17 are projected to increase. However, these nodes are projected to decrease (Fig. 3.8(a)). This means that when this type of circulation occurs in the future, they are more likely to favour extreme precipitation days. For region 2, extreme precipitation days are projected to increase in association with nodes 18 and 19. For region 3, most of the nodes associated with extreme precipitation are

(a)

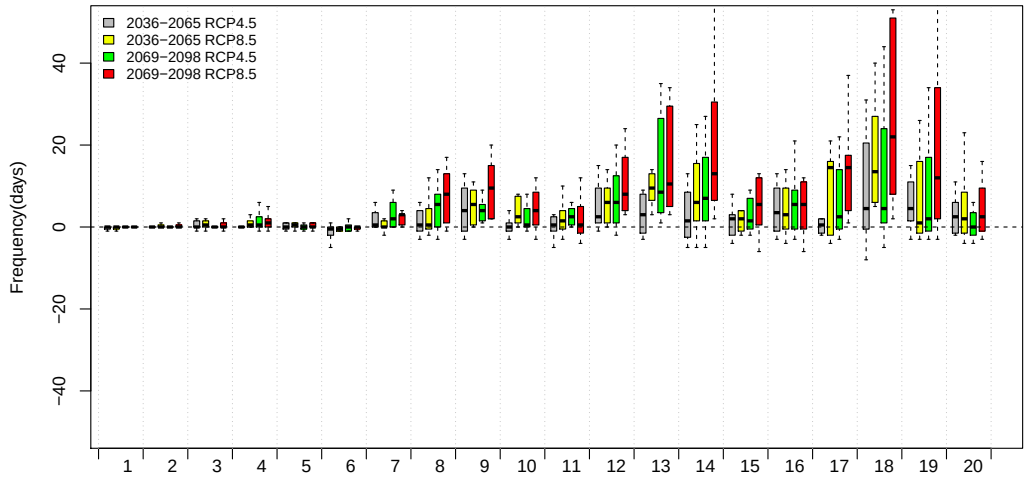

(b)

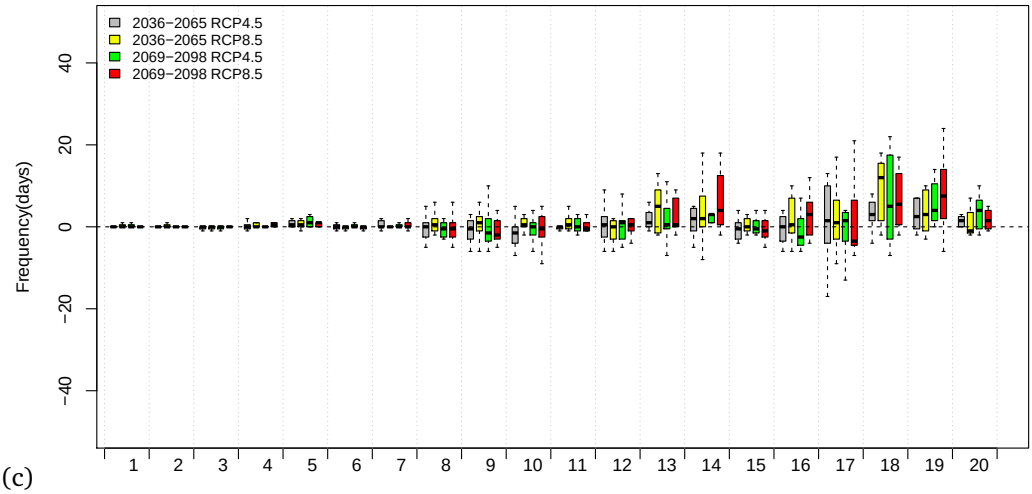

(c)

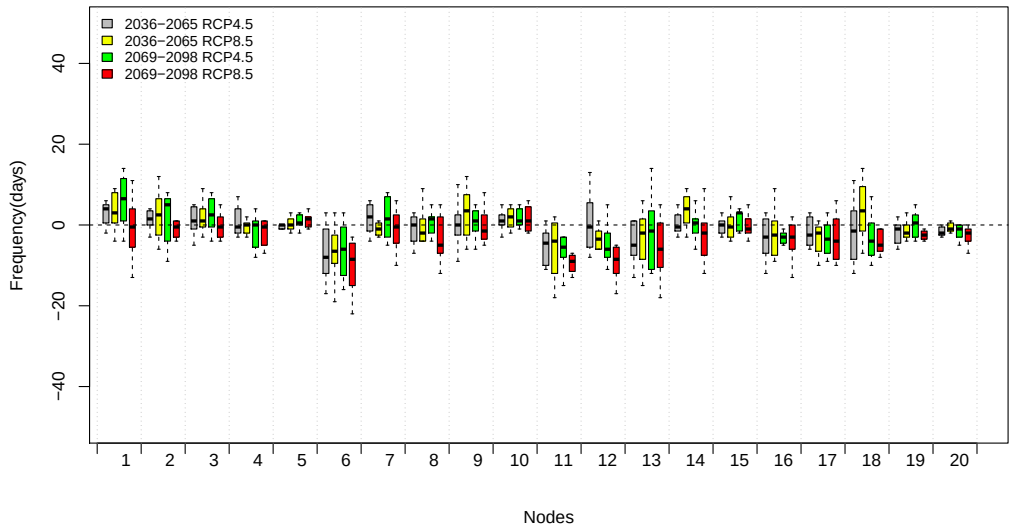

Figure 3.9: Projected changes in the frequency of occurrence of extreme precipitation days that map to each SOM node shown in fig. 3.1 for (a) region 1, (b) region 2 and (d) region 3, over the periods 2036-2065 and 2069-2098 relative to 1976-2005 under RCP4.5 and RCP8.5.

projected to decrease with the exception of node 1. This suggests less extreme precipitation days for this region.

3.3 Summary

The models capture the features of low level circulation reasonable well over southern Africa in the historical period as well as a general rainfall states. Extreme precipitation days are more frequent during DJF and MAM over region 1 and 2 while in region 3 extreme precipitation days are more frequent during MAM and JJA. Region 3 does include the all year rainfall region of South Africa so is not purely a winter rainfall region and extreme rainfall in summer for this region is not unexpected. The downscaling does not capture the frequency mapping characteristics of extreme rainfall in region 1 and generally the CCLM model produces fewer extreme rainfall synoptic states than the RCA model for all regions. The regional climate model' s poor representation of extreme rainfall might be a combination of factors such as grid resolution (at 0.44 degrees convective activity is not adequately resolved), parameterizations of microphysics, boundary layer processes and convection and the model core. The synoptic states that reduce precipitation are projected to increase, while synoptic states that enhance precipitation are projected to decrease over time. These results will be used as a basis to identify connections between rainfall and atmospheric circulation over southern Africa in the following chapters.

4

Model-simulated historical climate extremes

The assessment of the ability of RCMs to simulate extreme precipitation events in the present climate is presented in this chapter. The simulations are evaluated against two gridded observation datasets. Spatial analysis of both simulated and observed extremes events are plotted and correlations calculated between the simulations and observation. The added value generated by the RCM with respect to the stand-alone GCM simulation is also assessed. The synoptic circulation features assessed in the previous chapter are used here as means to give a dynamical reason for model bias.

4.1 Moderate extremes

Within CORDEX, an ensemble of RCM downscaling over Africa, forced by EI reanalysis has been completed at grid resolutions of 0.44 degrees (about 50 km). The individual models representations of the historical spatio-temporal patterns of African rainfall have been evaluated by Nikulin et al. (2012); Endris et al. (2013); Kalognomou et al. (2013); Kim et al. (2013) and, Panitz et al. (2014). These authors confirm the ability of the RCMs to capture the broad precipitation characteristics, however biases remain and are found to be specific to individual models, regions and seasons. Furthermore, these authors did not explicitly evaluated model representation of extreme precipitation nor projections thereof. The spatial distribution of total annual wet-day precipitation (PRCPTOT) from the GPCP and TRMM "observed" data and the CCLM and RCA4 driven by (1) EI reanalysis data and (2) boundary condi-

tions from the four GCMs as well the multi-model ensemble mean is shown in Fig. 4.1.

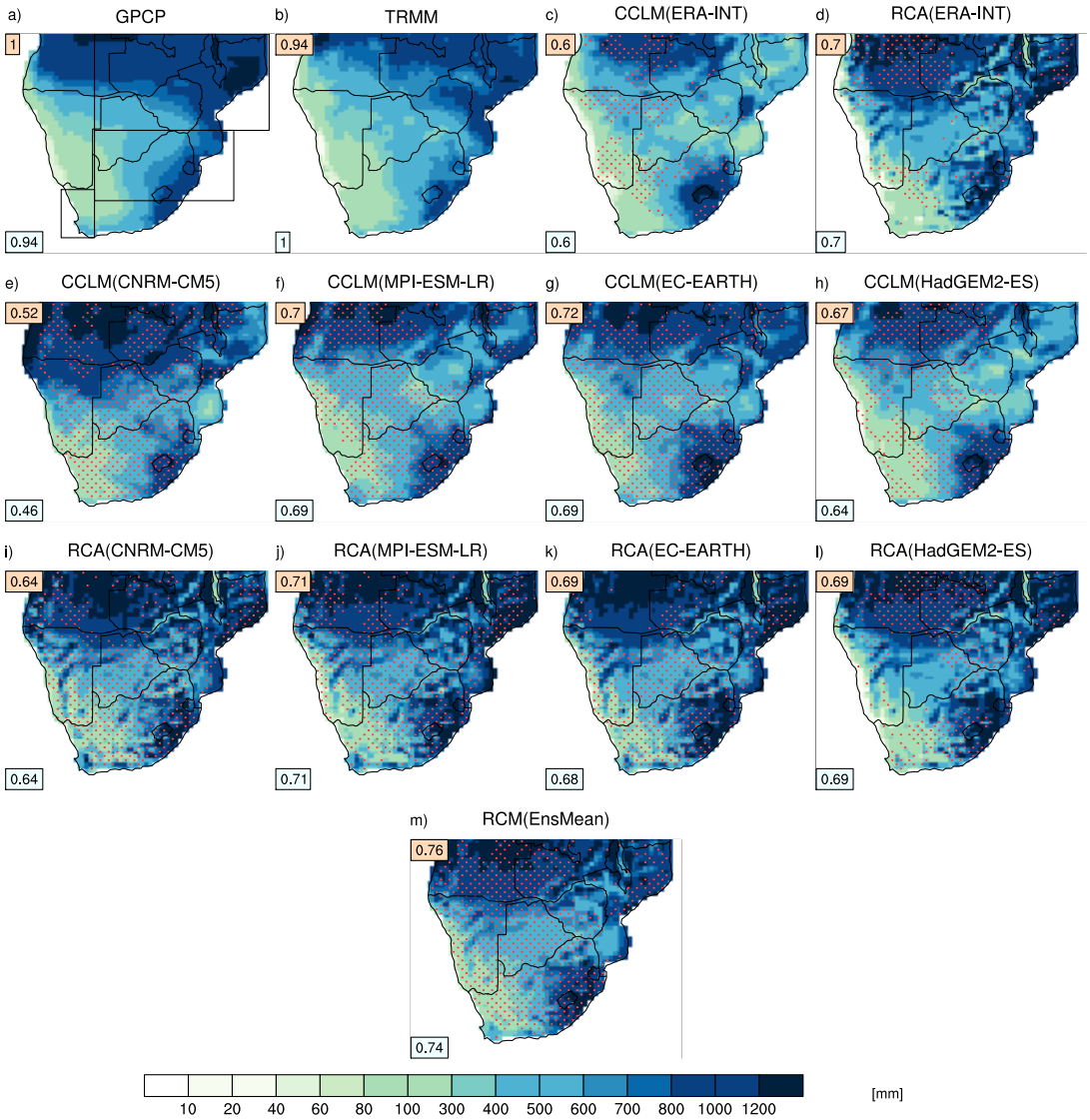

Figure 4.1: Total annual wet day precipitation (PRCPTOT) for the period 1997-2006 for (a) GPCP, (b) TRMM (1998-2005) , CCLM forced by (c) ERA-Int. and different GCMs (e-h), RCA forced by (d) ERA-Int. and different GCMs (i-l) and (m) multi-model ensemble mean of CCLM and RCA4 forced by GCMs. Stippling indicates grid points where there is added value by the dynamical downscaling. *Squares* in (a) indicate the locations of the evaluation regions as defined in Kalognomou et al (2013). The top left number is the PCC with GPCP and the bottom left with TRMM

The multi-model ensemble mean is the average of the CCLM and RCA4 driven by the GCMs. The stippling in Fig. 4.1-4.4 represents areas where there is added value (AV) in the indices from the RCMs compared to the indices from EI and GCMs for the reference period. The top left number represent the centred pattern correlation co-

efficient (PCC) between model simulations and GPCP data and the bottom left with TRMM.

In both observed data sets GPCP and TRMM, PRCPTOT maxima are located over the complex terrain of eastern part of South Africa, Mozambique and the northern parts domain along the ITCZ. Differences can be found across the observation datasets with regard to the magnitude and spatial extent of PRCPTOT. GPCP shows higher PRCPTOT over northern Angola and northern Mozambique. The PCC exceeding 0.9 is found between GPCP and TRMM indicating a good level agreement in PRCPTOT patterns. Comparing both observed datasets with RCMs, it is found that the main features of the climatological pattern of PRCPTOT is reasonably captured. In particular the west-east gradient in precipitation totals over South Africa and the band of relatively low precipitation that stretches from Namibia in the west over Botswana to Zimbabwe. Differences exist, however, between the observations and the model simulations and among the individual model simulations. The CCLM underestimates the actual magnitude of PRCPTOT both in EI and individual GCM downscaled runs, especially over the east part of the domain. This underestimation of PRCPTOT might be caused by the misplacement of the monsoon rainbelt by the driving GCMs and an underestimation of associated rainfall intensity (Panitz et al., 2014; Dosio et al., 2015). A common tendency to overestimate PRCPTOT over the Lesotho highlands and Drakensberg areas is found in all simulations. The overestimation in precipitation over mountains are largely due to the finer resolution of the RCMs causing enhanced topographical forcing and dynamical uplift, and this is known to be problematic for RCMs (e.g. Engelbrecht et al., 2009; Kalognomou et al., 2013). The RCA4 forced by individual GCMs generally overestimate PRCPTOT over most of southern Africa, and the effect of topography is more evident in this model. Over the northwest region rainfall is overestimated in all ensemble members and is likely influenced by the overestimation of the frequency of occurrence of the circulation patterns represented by nodes 16, 17 and 18 as seen in Fig. 3.2. These nodes show the presence of the Angola low, a semi- permanent feature of tropical southern Africa circulation

during summer (Reason et al., 2006). The Angola low facilitates moisture transport that bring most of the summer rainfall across subtropical southern Africa (Hart et al., 2010; Reason et al., 2006). For the pattern correlation of PRCPTOT, averaging across all GCM downscaled ensemble members gives better correlation with observations than any individual model as a result of the cancellation of spatial errors from the individual model simulations. This limited sample suggests that the use of multi-model ensembles using different RCMs driven by different GCMs might provide an optimal approach to the provision of climate change scenarios over Southern Africa. However, in order to sample the uncertainty associated with future projections of climate, a large number of multi-model GCM/RCM downscaled ensembles are required. Giorgi and Coppola (2010) noted that at least four to five models is needed to obtain a robust regional precipitation change estimates.

The large scale pattern of the maximum number of consecutive dry days (CDD), which in many areas represents the length of the dry season is shown in Fig.4.2. The magnitude of CDD is higher in TRMM dataset over South Africa and Mozambique when compared with GPCP. However, the PCC (0.9) shows a good level of agreement between both datasets. The pattern of CDD is reasonably well represented in the simulations when compared to both observed datasets. However, the number of CDD is overestimated over the central areas of the domain in both RCMs forced by EI. This is likely because the EI captures synoptic states associated with dry days (e.g. high pressure systems) and consequently the precipitation field reflects observed CDD, whereas the RCMs are overly responsive to high pressure forcing during the autumn and spring season. During these two seasons the RCMs forced by EI overestimate the frequency of occurrence of circulation patterns typical of high pressure (nodes 3,4,5,10 and 15) (Fig. 3.3(b) and 3.3(d)). A comparison of model ensembles with observation data shows that both CCLM and RCA are closer to the TRMM data. The spatial distribution of heavy precipitation days (R10mm) (Fig. 4.3) is similar to the spatial pattern of PRCPTOT, and R10mm events are generally underestimated/overestimated as described for PRCPTOT. Both GPCP and TRMM indicate a

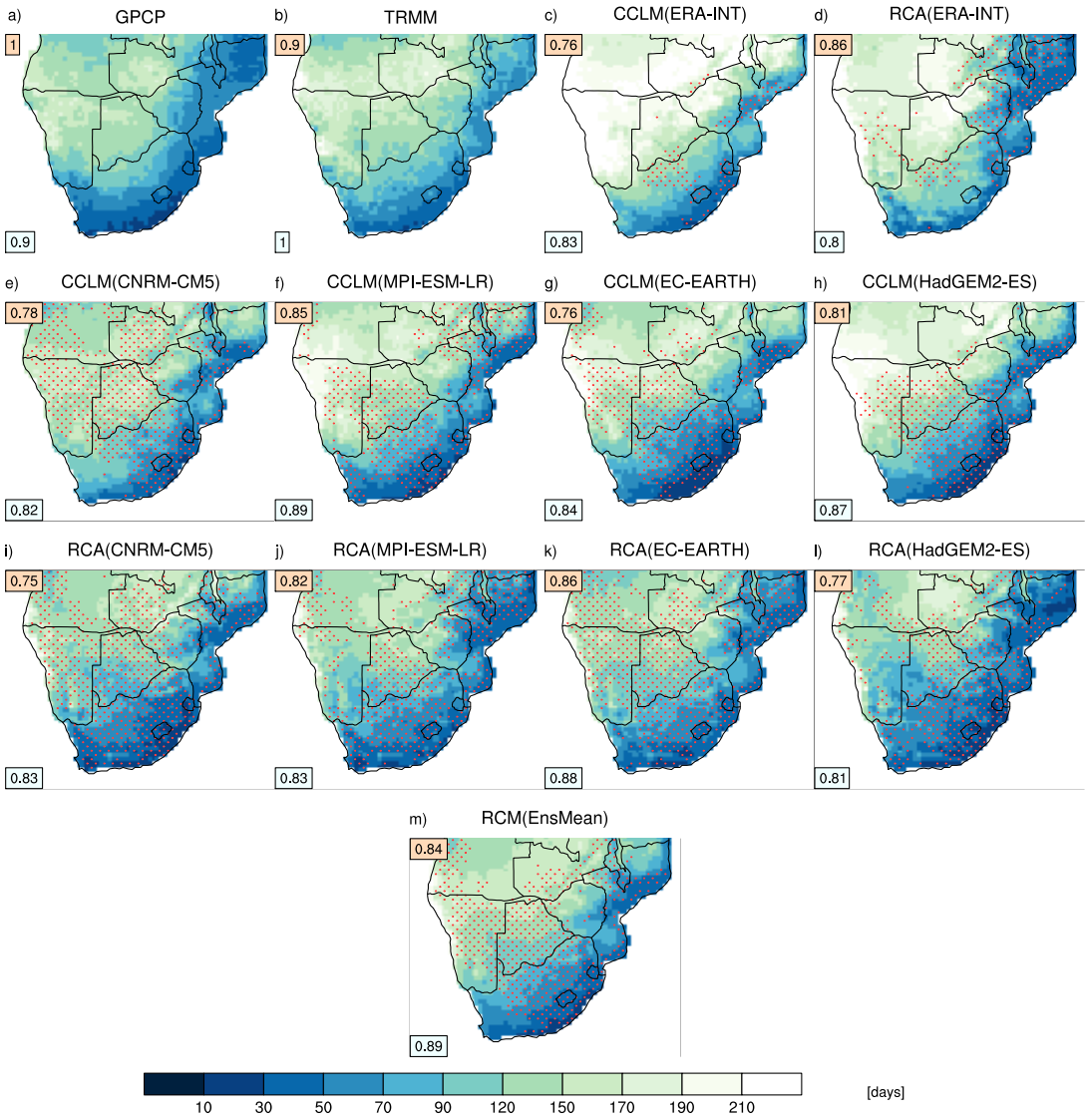

Figure 4.2: Same as Figure 4.1 but for maximum number of consecutive dry days (CDD).

good level of agreement with PCC exceeding 0.9. The ensemble mean again shows a better correlation pattern compared with individual models.

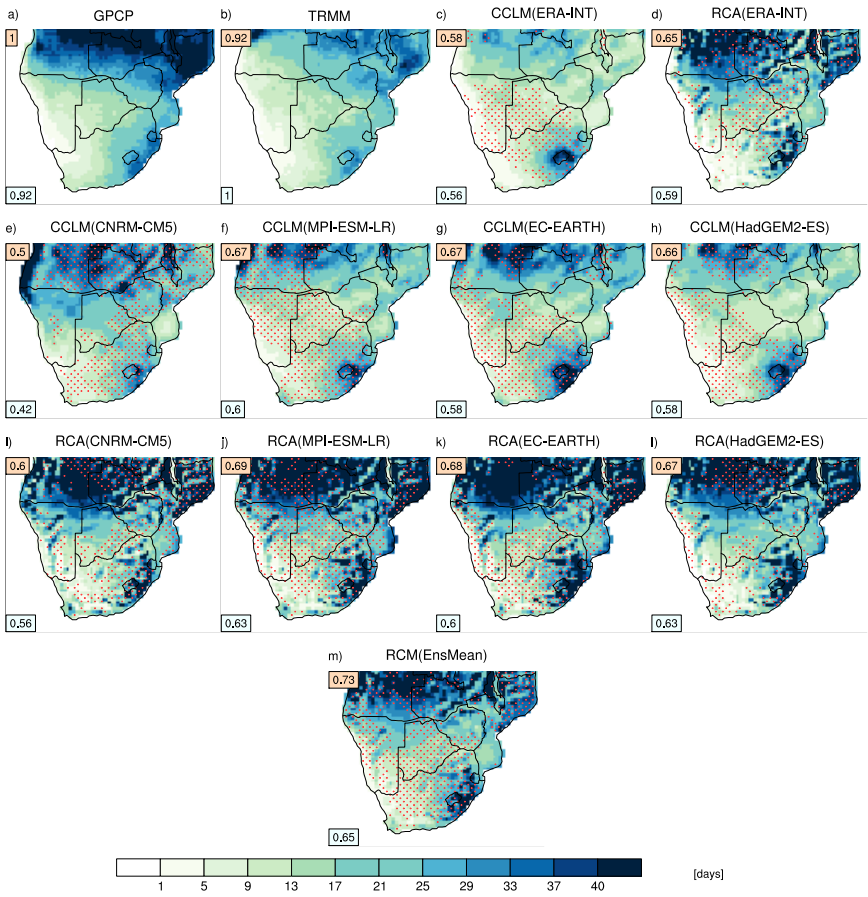

Figure 4.3: Same as Figure 4.1 but for heavy precipitation days (R10mm).

The pattern of precipitation on very wet days (R95pTOT) is also similar to that of PRCPTOT, showing a decrease from east to the very dry region in the west (Fig. 4.4). Both observed datasets have a good level of agreement (PCC=0.92) however, the ensemble mean is closer to the TRMM data (PCC=0.82) than GPCP (PCC=0.78). The spatial distribution of the maximum 5-day precipitation (Rx5day) (Fig. 4.5) and precipitation intensity (SDII) (Fig 4.6) are generally better represented in RCA4 than in CCLM. Both indices are overestimated over the northern parts of the domain. This is likely due to overestimation of the frequency of circulation patterns that brings moisture to the region (nodes 16, 17 and 18).

For a more detailed regional analysis of the difference between observations and model simulations are investigated over the three sub-regions shown in Fig. 4.1a. Again the subtropical region 1 experience rainfall in summer that results from mesoscale

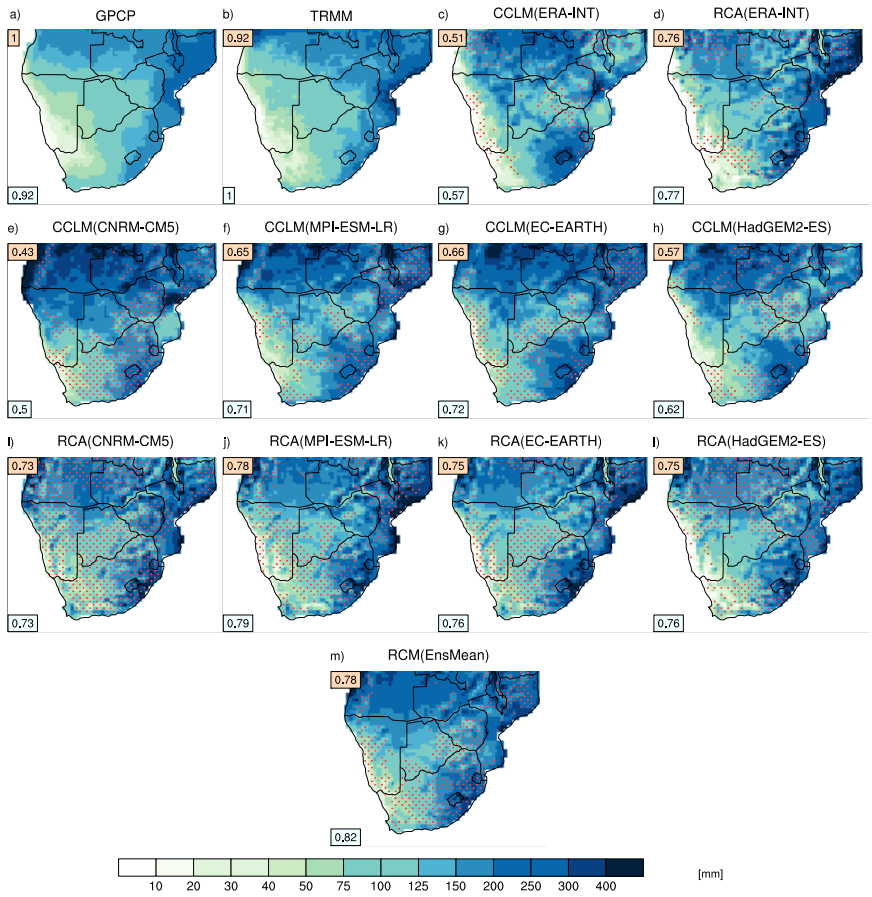

Figure 4.4: Same as Figure 4.1 but for annual total precipitation greater than or equal to the daily 95th percentile (R95pTOT).

convective systems, tropical storms and tropical cyclones from MC. Region 2, is also a summer rainfall due to mesoscale convective systems, warm fronts, subtropical lows, mid- to upper-tropospheric troughs, and cloud bands. Region 3 is a winter rainfall region that receives the bulk of its annual rainfall from the passage of cold fronts.

The interquartile model spread of extreme precipitation indices in each region is shown in Fig. 4.7. The ensemble mean (RCM(EnsMean)) is also shown in this figure. The magnitude of extreme precipitation indices decrease from region 1 to region 3 miming the west-east gradient of the total annual precipitation over the region. In many aspects the RCM(EnsMean) is comparable with the ensemble median. Both observed gridded products, GPCP and TRMM represent each indices with varying magnitudes.For most indices, the difference between TRMM and GPCP is not as large as the intermodel spread. For R95pTOT and Rx5day both GPCP and TRMM

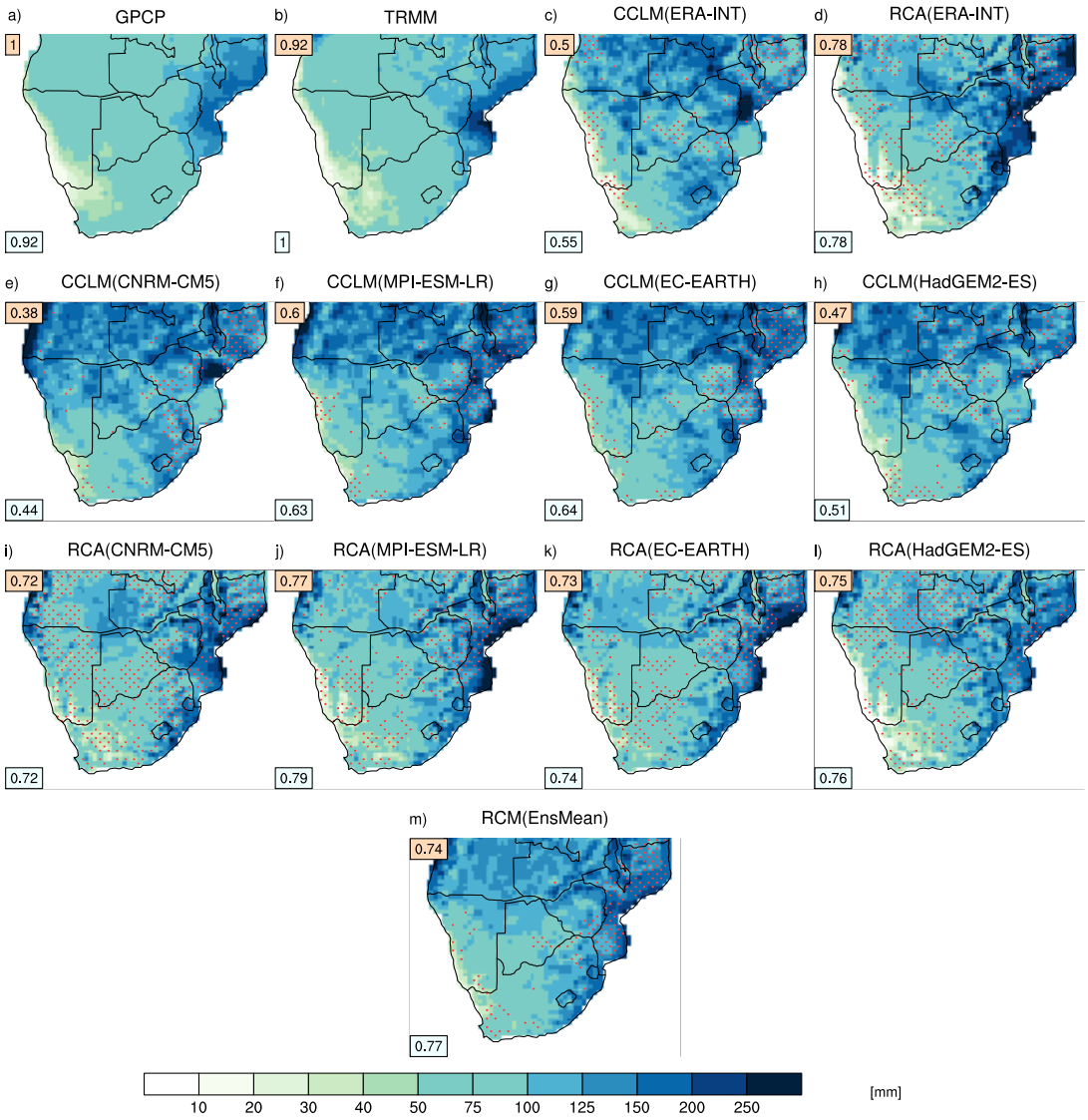

Figure 4.5: Same as Figure 4.1 but for maximum 5 day precipitation (Rx5day).

are similar and are generally overestimated by the models except for RCA4(ERAINT) and CCLM(ERAINT) over region 3. For PRCPTOT both GPCP and TRMM are in close agreement. The difference between GPCP and TRMM found in CDD might be due to the dry precipitation bias on the TRMM dataset in the entire north part of southern Africa during the wet season compared to GPCP (e.g. Nikulin et al., 2012). And the difference in other wet extremes will in part due to differences in spatial resolution (GPCP 0.5 degrees and TRMM 0.25 degrees), since precipitation rates tend to increase when observed or modelled at higher resolution.

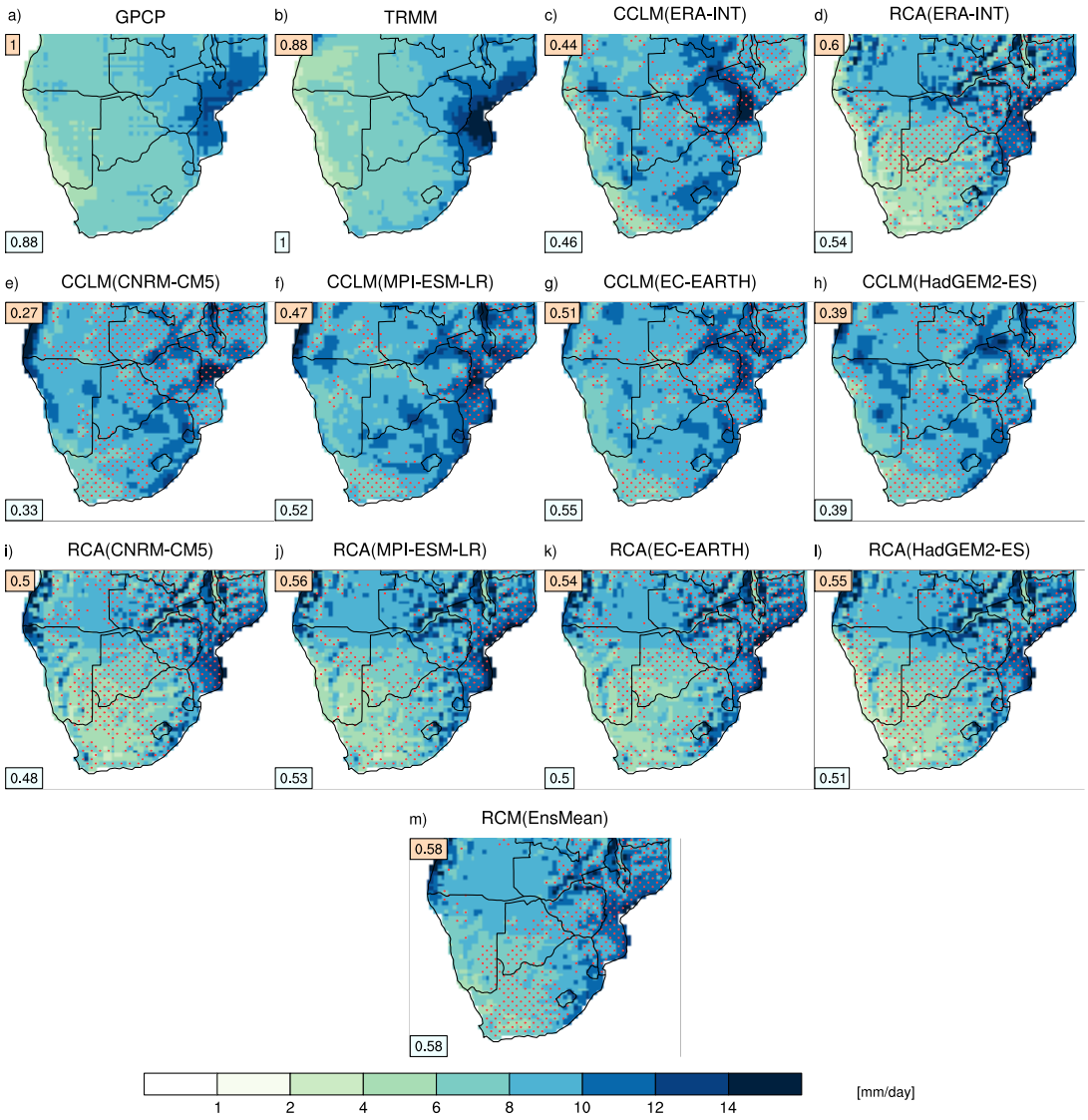

Figure 4.6: Same as Figure 4.1 but for single daily precipitation intensity (SDII).

4.2 Added value of RCMs compared to driving global data

This section aims to show the added value generated by the RCM with respect to the stand-alone GCM simulation. The climatology of moderate extremes events from the RCMs are compared to the driving GCMs and ERA-Interim for the period of 1997-2007. The added value is shown as stippling in Fig. 4.1-4.4. Feser et al. (2011) have shown that AV depends upon a variety of factors such as the season and time scale, the variable and the climate statistics of interest, the region of analysis and the kind

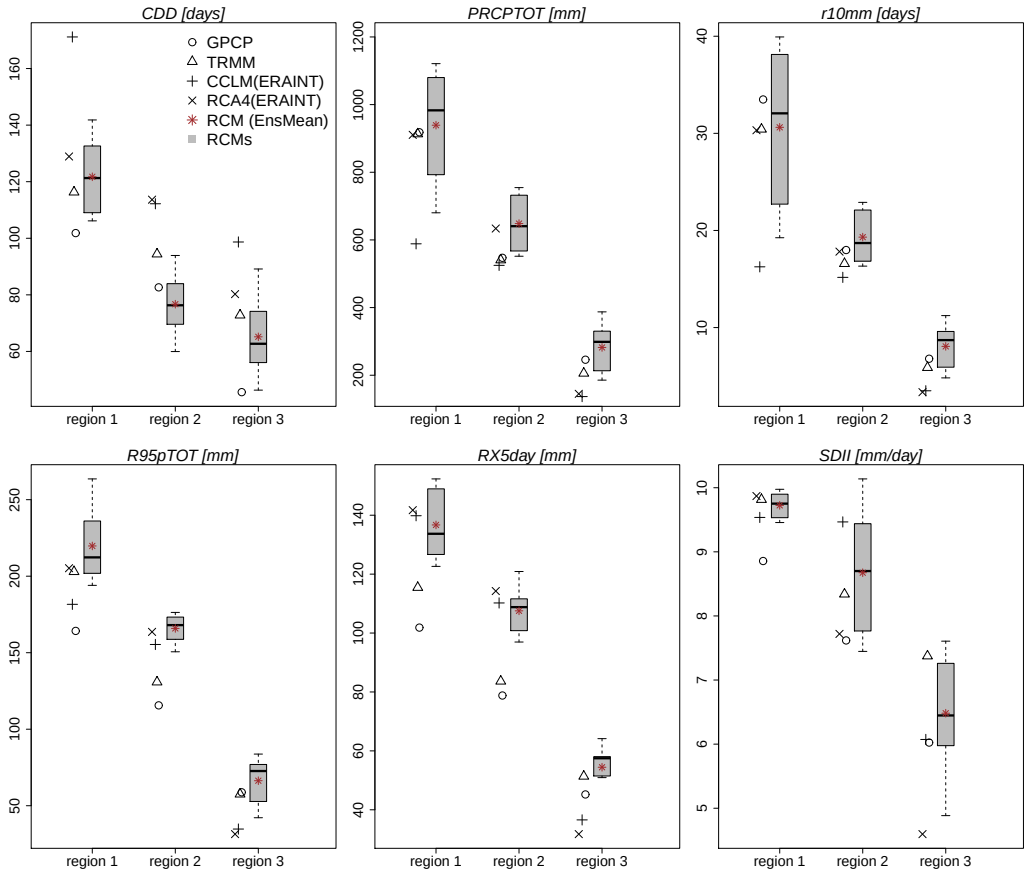

Figure 4.7: Box-and-whisker plots for precipitation indices calculated from CCLM and RCA4 forced by GCMs for the period 1998-2006. GPCP, TRMM, CCLM(ERAINT), RCA4(ERAINT) and RCMs(EnsMean) are indicated in different shapes. The boxes indicate the interquartile model spread (range between the 25th and 75th quantiles), the black solid marks within the boxes show the multimodel median and the whiskers indicate the full intermodel range

of application. For variables that are spatially quite homogenous such as air pressure the overall added value is small. The added value of RCMs is mainly expected in the simulation of topography-influenced phenomena with relatively small spatial or short temporal character such as precipitation (Feser et al., 2011). Although RCMs are capable of adding value to the forcing global climate models, there is a limit to what can be corrected by the downscaling of imperfect driving conditions. For instance, Dosio et al. (2015) showed that CCLM not always improves on the GCM seasonal average precipitation climatology, but found that the number of consecutive wet days (i.e., daily precipitation $>$ 1 mm) and dry days, and the number of intense precipitation events (i.e., number of rainy days when precipitation exceeds the 95^{th} percentile) are better reproduced by CCLM. Gao et al. (2012) found that RCM down-

scaling leads to better large-scale monsoon precipitation patterns for East Asia than in the global models used for boundary conditions.

For PRCPTOT (fig. 4.1) the downscaling by RCA4 and CCLM adds value to the GCMs for most parts of southern Africa with the exception of the eastern region of the domain. For this particular region, GCMs produce reasonable precipitation pattern amounts as a result of overestimation of frequency of wet days (e.g. Sun et al., 2006). As can be seen in Fig. 4.8, the RCM downscaled simulations improves the GCMs frequency of wet days.

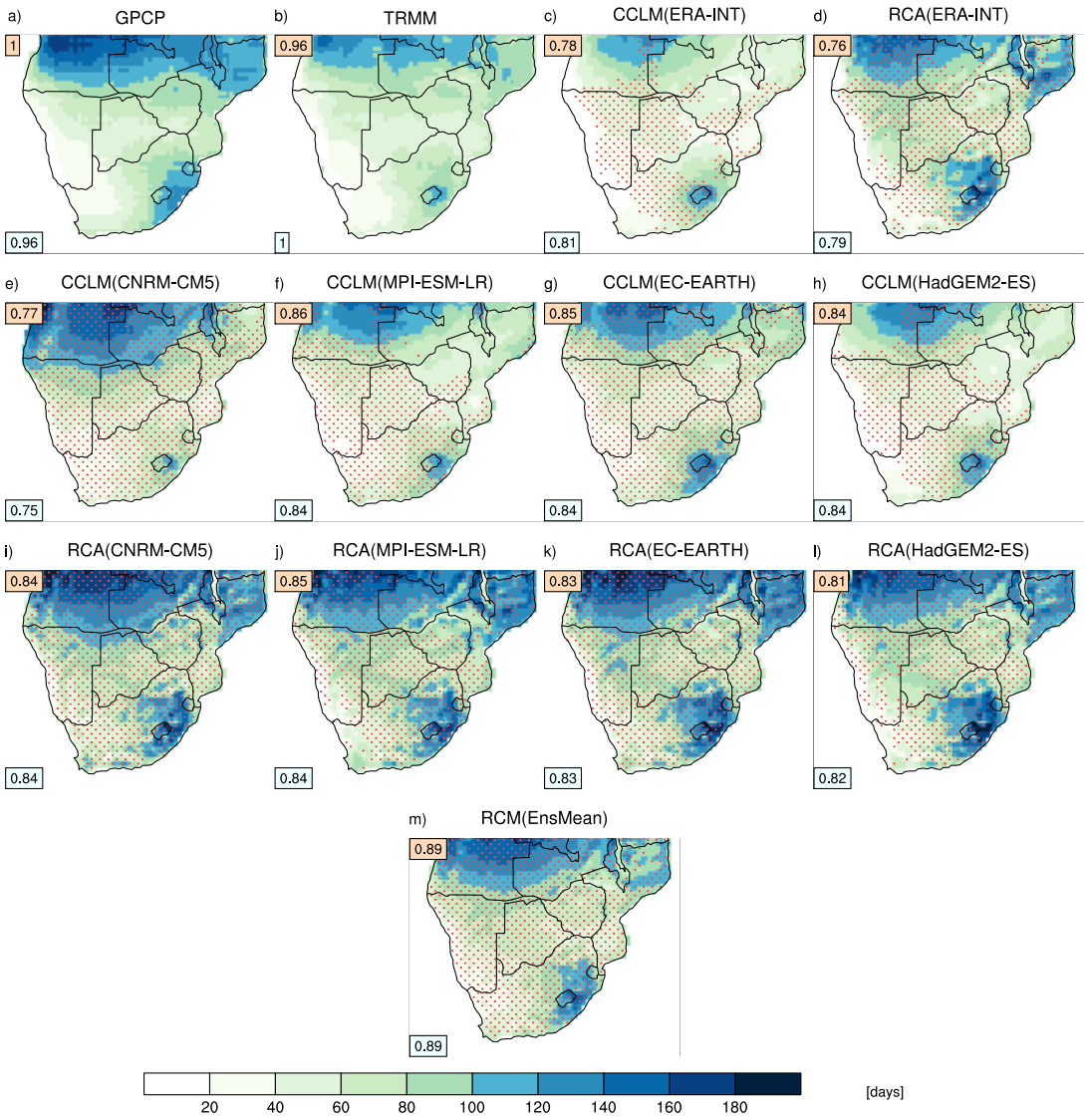

Figure 4.8: Same as Figure 4.1 but for annual precipitation frequency.

This supports the idea that RCM are able to resolve processes and feedbacks that

operate at a sub-grid scale GCM resolution (e.g. Giorgi, 1990; Di Luca et al., 2012). Although the individual RCMs offer some improvements in PRCPTOT compared to the driving GCMs, the best performances are captured in the RCM ensemble mean. The added value in CDD is mostly seen in the downscaled GCMs over large parts of South Africa, Namibia, Botswana, southern Zambia and central parts of Mozambique (Fig. 4.2). The added value in R10mm (fig. 4.3) is similar to that found in CDD. Added value in R95pTOT is found over South Africa, Namibia, Zimbabwe and north Mozambique in the multi model ensemble mean (fig. 4.4). In contrary to previous indices, Rx5day shows added value only over Mozambique in the multi model ensemble mean. The added value in the downscaled GCMs multi model ensemble mean for SDII is found over Mozambique, South Africa and Zimbabwe. The downscaling of GCMs over these areas will be much more useful for users aiming at performing impact studies. However, as pointed out by Barsugli et al. (2013) there are other elements (e.g. credibility, salience, and legitimacy) in addition to explicitly documented added value that come into the choosing between global or regional models.

4.3 Rare extremes

Spatial patterns of the estimated 20-year return value for GPCP, TRMM, both RCMs driven by the ERA interim and ensemble mean of both RCMs driven by GCMs is shown in Fig. 4.9.

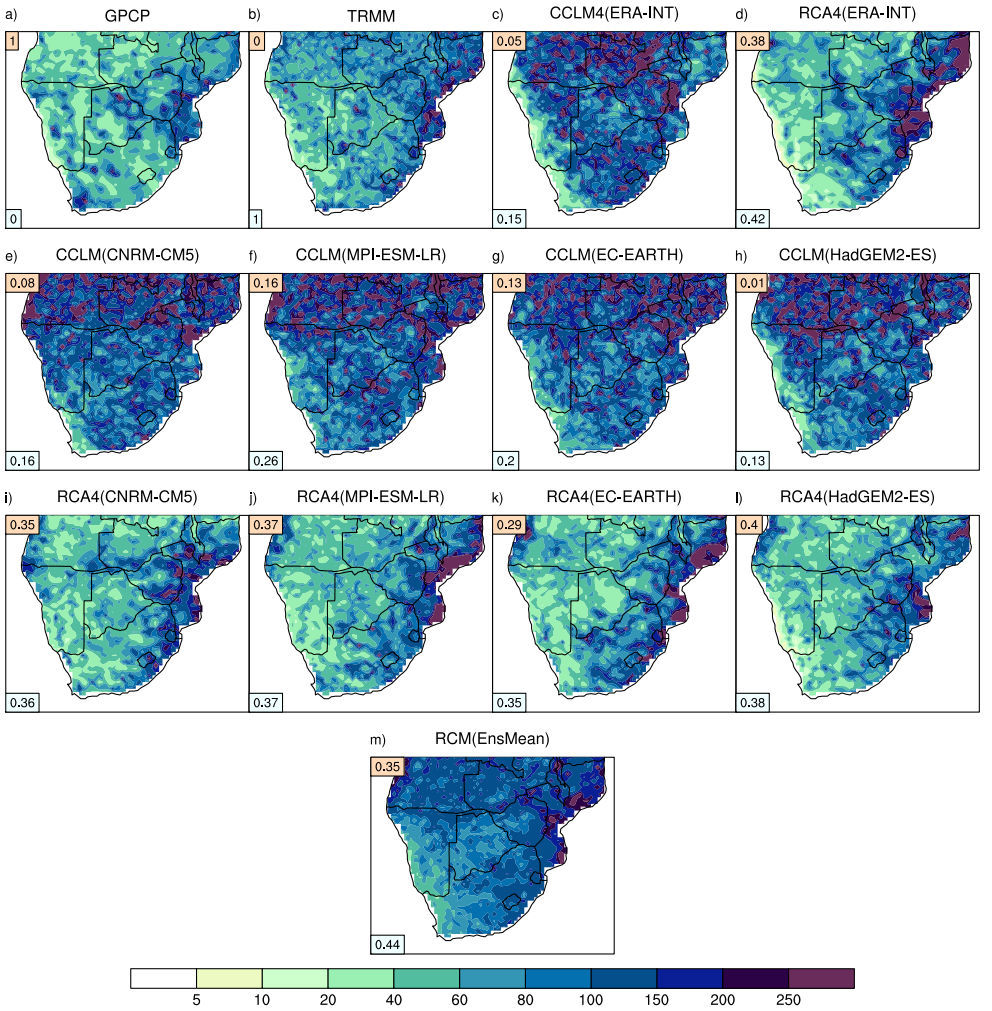

Figure 4.9: 20-year return values of annual maximum daily precipitation (P_{20}) for the period 1997-2006 for (a) GPCP, (b) TRMM (1998-2005), CCLM forced by (c) ERA-Int. and different GCMs (e-h), RCA forced by (d) ERA-Int. and different GCMs (i-l) and (m) multi-model ensemble mean of CCLM and RCA4 forced by GCMs.

The PCC of 0 indicate a poor level of agreement between GPCP and TRMM datasets. The magnitude of 20-year return value is generally higher in the TRMM than in GPCP. The spatial pattern from the downscaled models show a complex structure defined by local topographical conditions. The Kolmogorov-Smirnov goodness-of-fit test has been applied to verify the accuracy of the GEV fits. At the 5% significance level, no grid box GEV distributions are rejected. This indicates that the GEV distribution is a reasonable approximation for the distribution of annual precipitation maxima at

each grid box. The individual RCMs driven by GCMs reproduce the 20 year return values with varying magnitude. However, they show a coherent spatial distribution of precipitation extreme and there is minimal spread between the members of the ensemble driven by the same RCM indicating that rare extremes are mostly controlled by model physics. The RCMs consistently simulate maximum 20-year return values to the east of southern Africa, whereas minima occur to the very dry region to the west. CCLM simulates maximum 20-year return values over the north of the continent which is not seen in neither the GPCP and TRMM data nor RCA4. The RCA4 forced runs are in better agreement with the observed 20-year return value estimated from the GPCP and TRMM data compared to the CCLM runs. The pattern correlation is lower compared with the pattern correlation of moderate extremes suggesting that the spatial distribution of rare extremes is not well captured by these models.

4.4 Summary

The ability of the RCMs to simulate the past extreme rainfall climate and to add value to the GCM output has been assessed. It was found that both RCMs are able to improve several aspects of the present climate simulated by the GCMs used as boundary conditions. This shows the added value of dynamical downscaling. This added value of RCMs is sourced in the topographical detail that cannot be resolved by GCMs, such as coasts or complex terrain (Arritt and Rummukainen, 2011) and better representation of mesoscale circulations. This supports the idea that downscaling of GCMs may improve the quality of the model at regional scales. Validation of the downscaled GCM and reanalysis ERA-Interim realisations under present conditions shows that the RCMs simulate the climatology of extreme precipitation over southern Africa reasonably well. However there are some differences in the simulations with respect to the observations that might be attributed to RCM internal variability and observation

uncertainty. For the pattern correlation, averaging across models gives better correlation with observations than any individual model for most of the indices, which is consistent with the argument that spatial errors are being reduced by averaging multiple models (e.g. Nikulin et al., 2012; Kalognomou et al., 2013; Panitz et al., 2014). Both models (RCA4 and CCLM) are not able to capture rare extremes when compared to GPCP and TRMM gridded data possibly due to models internal noise.

5

Projected changes in climate extremes

In this chapter, the downscaled projected changes of precipitation climate extremes for 21st Century are presented for the multi-model ensemble mean. Time interval of 30 years, 1976-2005, 2036-2065 and end of 21st Century (2069-2098) were chosen and the time means for these periods were compared. Spatial maps of the ensemble time average at annual and seasonal timescales and box-and-whisker plots that summarise regional and features of the projected changes of moderate extremes are presented.

5.1 Changes in moderate extremes

The multi-model ensemble mean of projected changes in PRCPTOT under RCP4.5 and RCP8.5 at annual and seasonal timescales for middle and end of 21st Century are shown in Fig. 5.1.

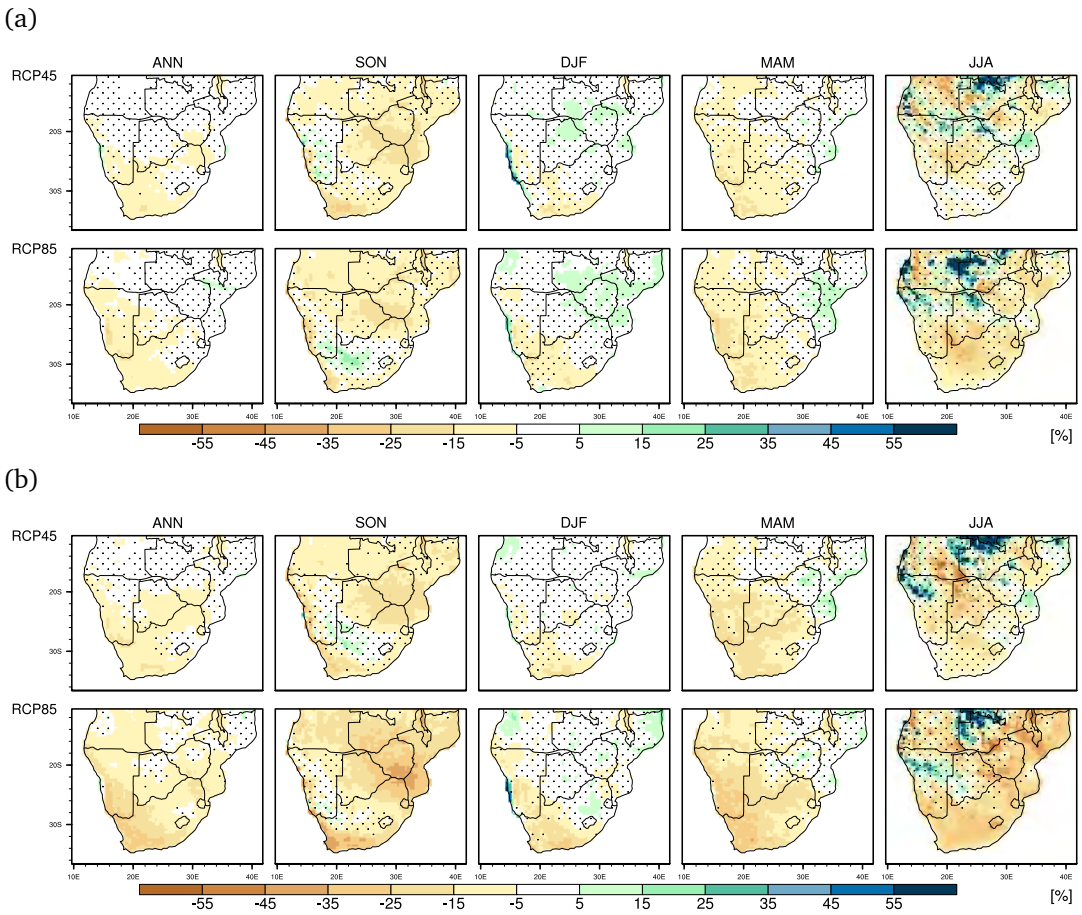

Figure 5.1: The multi-model mean of temporally averaged changes in total wet-day precipitation (PRCPTOT) by 2036-2065 (a) and 2069-2098 (b) under RCP4.5 and RCP8.5, relative to the reference period 1976-2005 for the entire year (ANN) and four seasons (SON, DJF, MAM,JJA). Stippling indicates grid points where changes are not significant at the 5% significance level.

Changes that are not significant at the 5 % significance level are indicated by stippling. The significance of the changes was tested with a Student-t test. There are significant decreases in projected annual PRCPTOT over most of South Africa, southern Botswana and Zimbabwe under the RCP4.5 scenario. Under RCP8.5 the projected magnitude of the decrease is greater, especially by the end of 21st Century, and it covers a wider spatial area that also includes Namibia, Angola and Mozambique. There is projected statistically significant decreases (15-25 %) in PRCPTOT during SON over Zambia, Zimbabwe, Botswana, southern Mozambique and southwest province of South Africa. Using a statistical downscaling of seven GCMs forced using the SRES A2 emissions scenario, Tadross et al. (2009) also found a projected

reduction in SON and increases in MAM precipitation in mid 21st Century (2046-2065) over southern Africa north of 20° S, suggesting a shift of the rainy season to later dates. During MAM, PRCPTOT is projected to decrease over most of South Africa with higher changes occurring over the western province. By the end of 21st Century, PRCPTOT is projected to decrease over the winter rainfall region during JJA. During DJF the projected changes in PRCPTOT are not statistically significant over most of the subcontinent. The increases in PRCPTOT during DJF over north-east of the domain may be linked to an increase in frequency of southeasterly trade winds that increase moisture supply into the region and enhancing precipitation. This is shown by the increases in frequency of nodes 14,18,19 (Fig. 3.8). At annual time scale, the maximum number of consecutive dry days (CDD) are projected to increase over the entire subcontinent with longer dry spells projected over Namibia, Botswana, northern Zimbabwe and southern Zambia (Fig. 5.2).

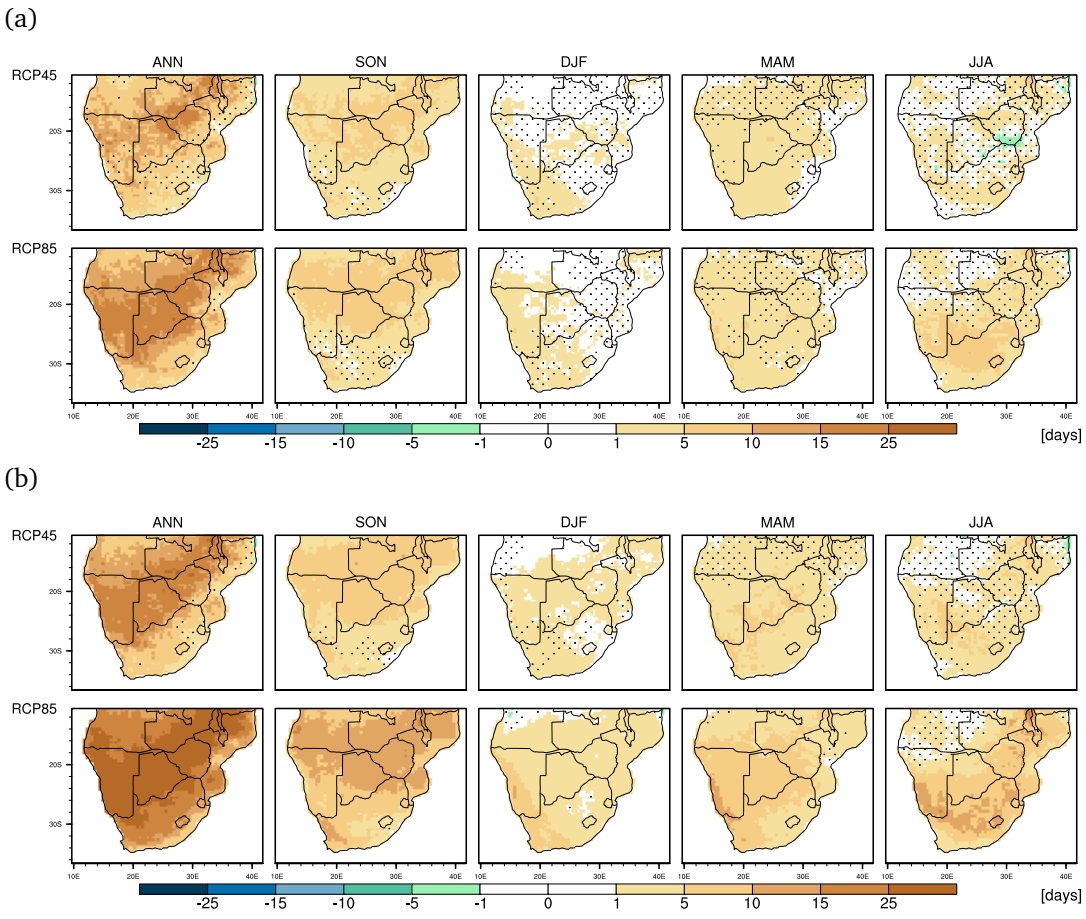

Figure 5.2: Same as figure 5.1 but for consecutive dry days (CDD)

Comparing seasonal changes, SON is the season with higher changes in CDD following MAM and JJA. Drier conditions during SON are associated with increases in frequency of occurrence of high pressure circulation pattern (Fig. 3.8d). Increases in CDD over southern Africa were also found by Giorgi et al. (2014) for the period of 2071-2100 under RCP4.5 compared to 1976-2005. Reductions in PRCPTOT together with increases in CDD have implications for seasonal precipitation onset in southern Africa (e.g. Tadross et al., 2005) and is likely to have negative impacts in agriculture, particularly in the areas of traditional rain-fed agriculture and water resources. The pattern of change of SDII for both mid and late 21st Century are similar (Fig. 5.3). The model projections shows increases in SDII with significant changes over Mozambique, Zimbabwe, Botswana, Zambia at annual timescales and during DJF for RCP8.5.

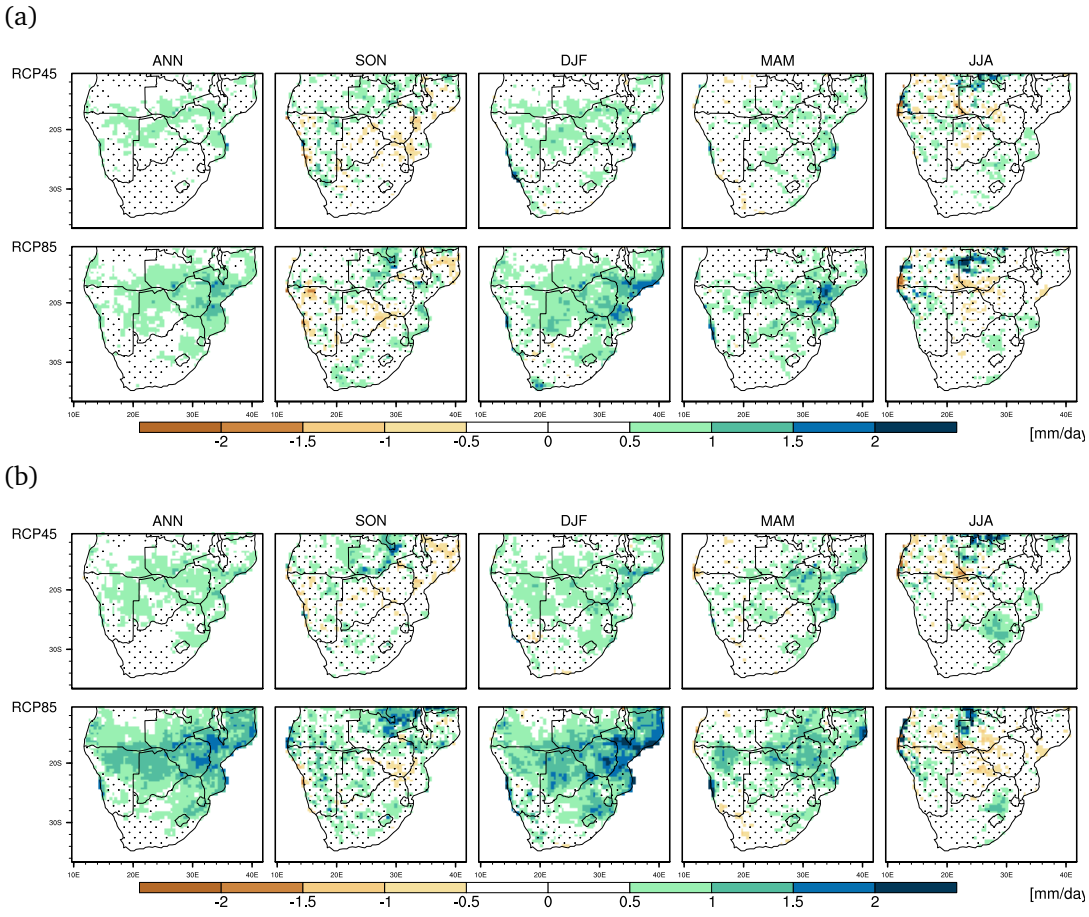

Figure 5.3: Same as figure 5.1 but for single daily precipitation intensity (SDII).

In order to understand the relationship between dry days and precipitation, the con-

tribution of dry days to annual total precipitation changes is investigated and shown in Fig. 5.4.

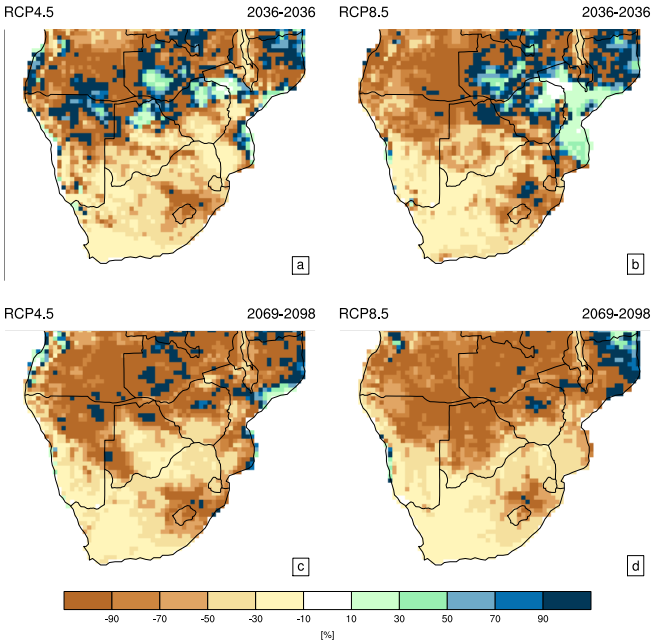

Figure 5.4: Multi-model ensemble mean percentage contribution of changes in dry days to changes in total annual precipitation.

This is done by assuming that an addition dry day in a given month in the future decreases the total annual precipitation by an amount equal to the average precipitating day in the same month in the historical period (Pierce et al., 2013). As in Pierce et al. (2013), the day's month is used because changes precipitating days during winter months have less effect on the annual average than loss of a January precipitating day. The effects of changes in precipitation intensity are then calculated as the actual change in precipitation minus the change that is due to dry day frequency. For example in RCP8.5 for the time slice 2069-2098 over the northern parts of Zimbabwe, 90% of the rainfall change (decrease) is primarily due to an increase in the number of dry days. Over the broader southern African region increases in dry-day frequency account for more than half of the change in total-annual precipitation by the end of 21st Century. By the mid 21st Century the projected increases in PRCPTOT under

RCP8.5 over most of Mozambique is caused by decreases in dry days. Since SDII is projected to increase, decreases in PRCPTOT are caused primarily by increases in dry day frequency.

The changes in PRCPTOT and increases in CDD are consistent with increasing frequency of high pressure systems and decreases in the frequency of cold fronts (cf., section 3.2).

The pattern of change of maximum consecutive 5-day precipitation total (Rx5day), which represent extreme aspect of precipitation distribution, is similar for both periods (Fig. 5.5). However the magnitude of change is higher for the RCP8.5.

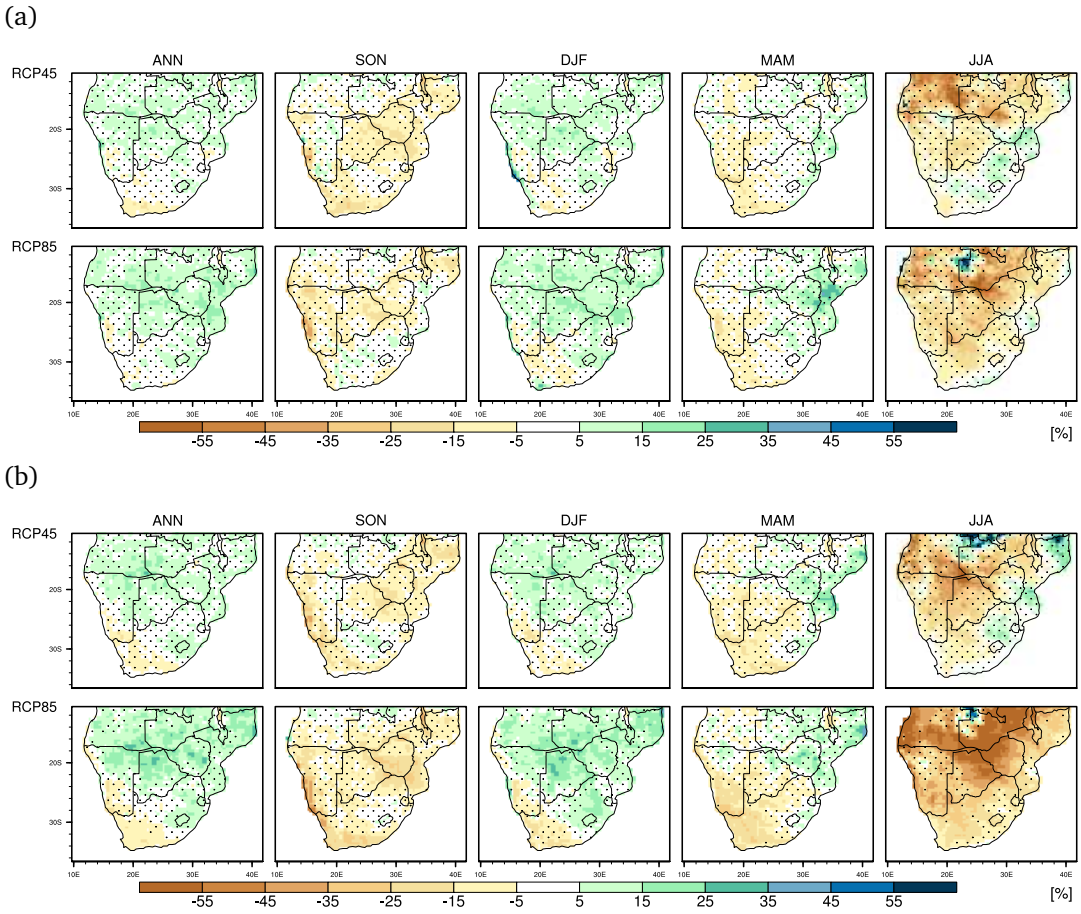

Figure 5.5: Same as figure 5.1 but for maximum 5-day precipitation (Rx5day).

The highest project increases is found in the centre of the domain and north of Mozambique at annual timescales and during DJF. In general during SON, MAM and JJA Rx5day is projected to decrease. These changes are associated with increases in frequency of circulation types characterised by node 18 (cf. Section 3.2).

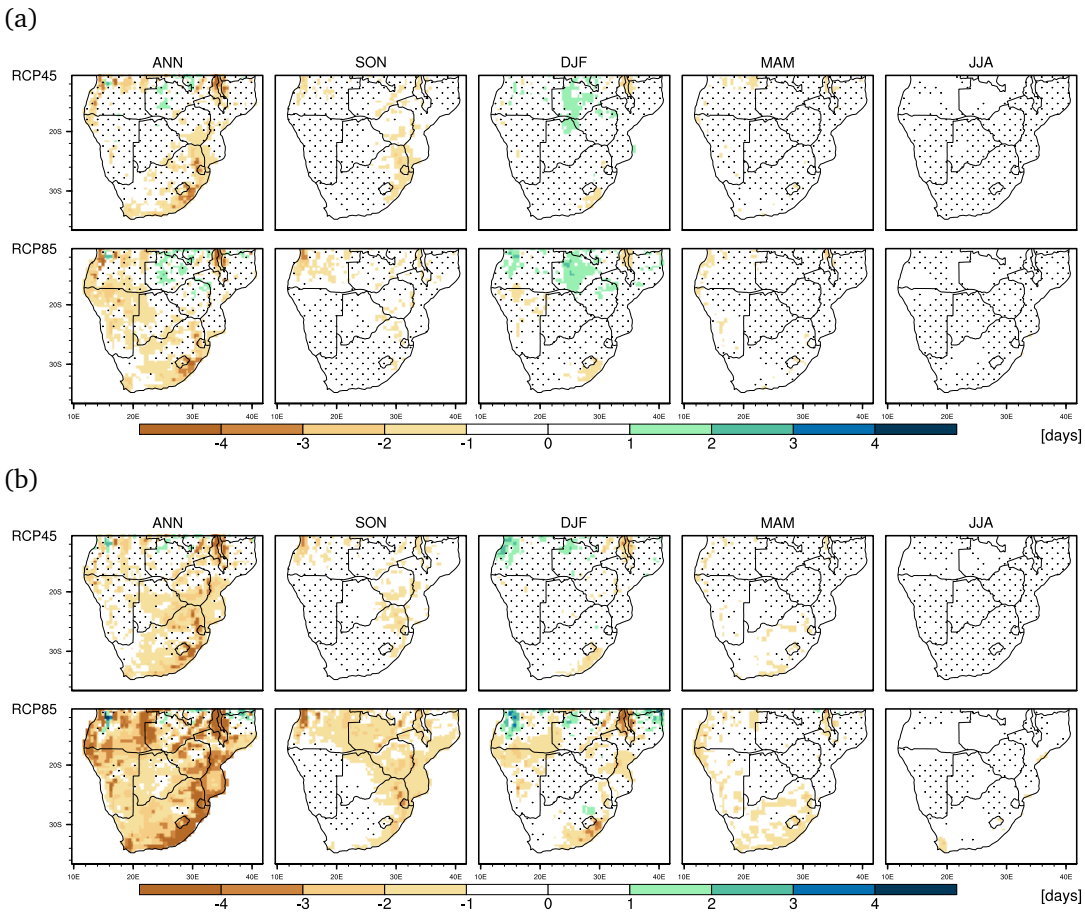

Figure 5.6: Same as figure 5.1 but for heavy precipitation days (R10mm)

In general, heavy precipitation days (R10mm) is projected to decrease in most of southern Africa (Fig. 5.6). At seasonal timescales, the projections shows no change for most of the region. Similar pattern of change in Rx5day are found in very wet days (R95pTOT), indicating increase over the northern region of the domain but decrease in the south western parts of South Africa (Fig. 5.7).

5.2 Changes in rare events

Figure 5.8 shows the ensemble mean of the projected changes in rare extreme precipitation (here defined as 20-year return values) for the late 21st Century for both RCP4.5 and RCP8.5.

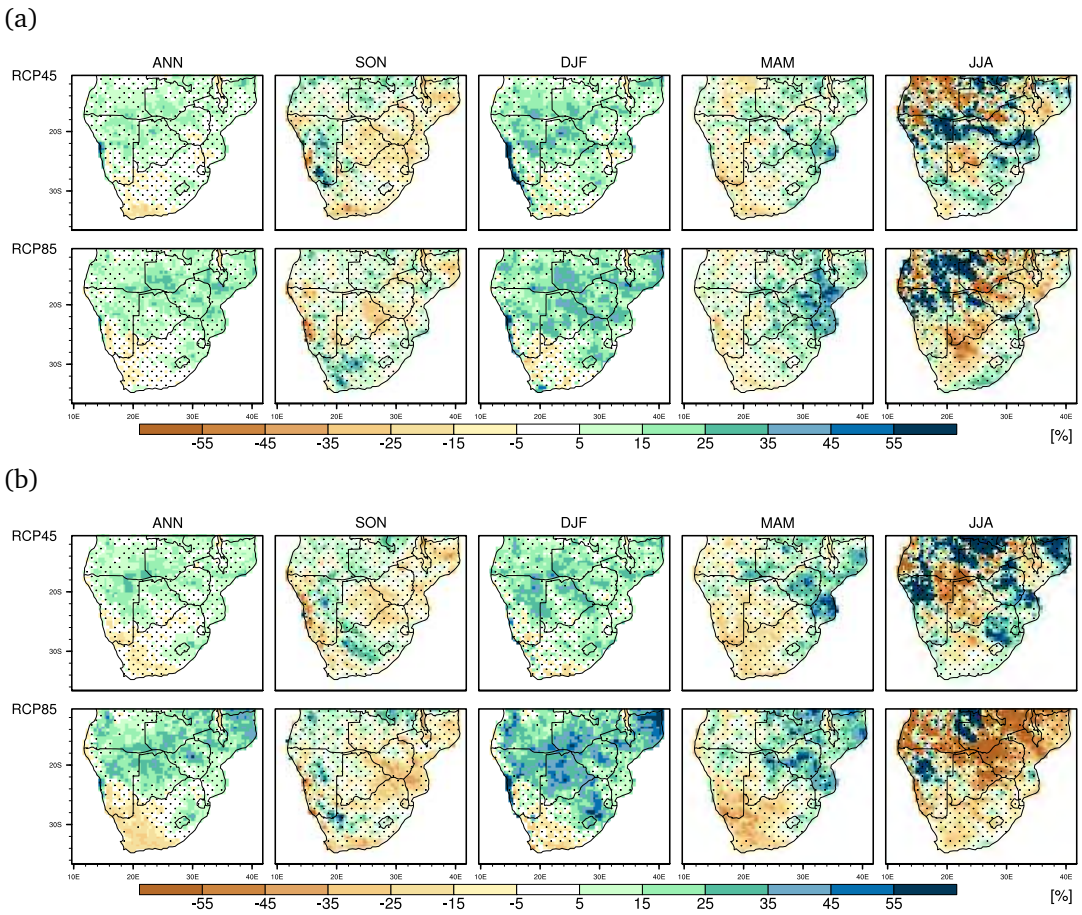

Figure 5.7: Same as figure 5.1 but for contribution of very wet days to the total wet-day precipitation (R95pTOT).

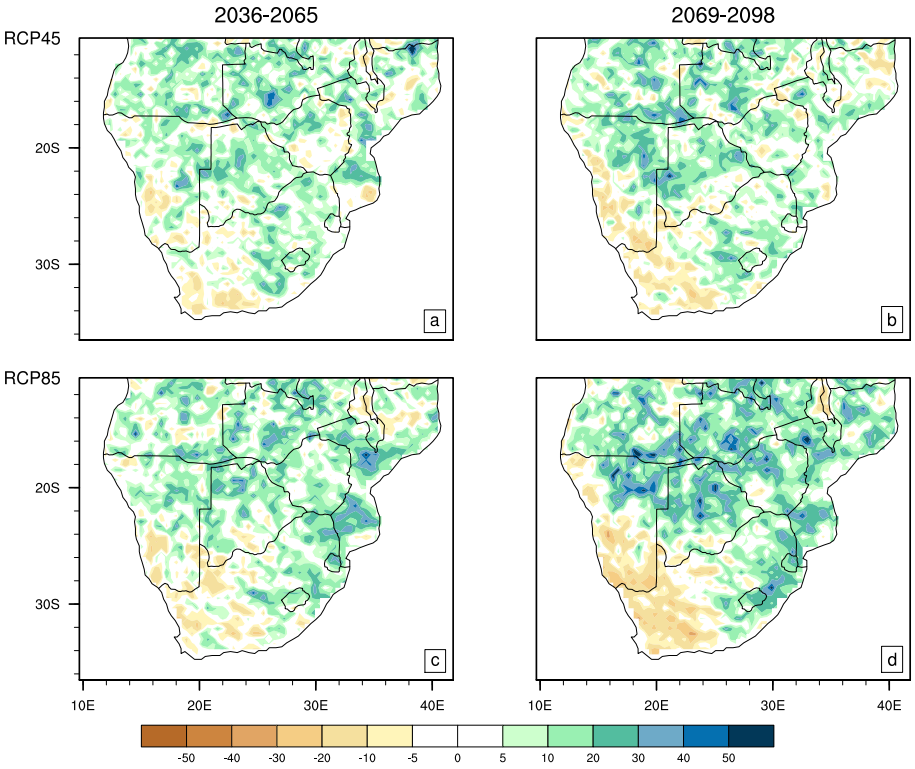

Figure 5.8: Projected multimodel mean changes 20-yr return values over the time period 2036-2065 (a and b) and 2069-2098 (c and d) as differences relative to the reference period (1976-2005) for RCP4.5 (a and c) and RCP8.5 (b and d).

A general increase in the magnitude of the 1-in-20 year extreme precipitation event is projected over the central and eastern parts of southern Africa and a decrease over western parts of South Africa and central and southern Namibia. This pattern of change in extreme precipitation is projected consistently across both scenarios although the magnitude of increases are generally higher under RCP8.5 in areas where the change is positive. The projected increases in return values imply more frequent recurrence and less time between currently defined extreme events.

Model agreement

Regional summaries of the projected changes by mid and end of 21st Century for the three sub-regions (cf. fig. 4.1) on annual basis are shown in Fig. 5.9 for moderate extremes and in Fig.5.10 for rare extremes. These figures show the model agreement on the sign of the change, and is assessed on the basis of the interquartile model spread (boxes) which correspond to an agreement on sign amongst at least 75% of models (Sillmann et al., 2013b).

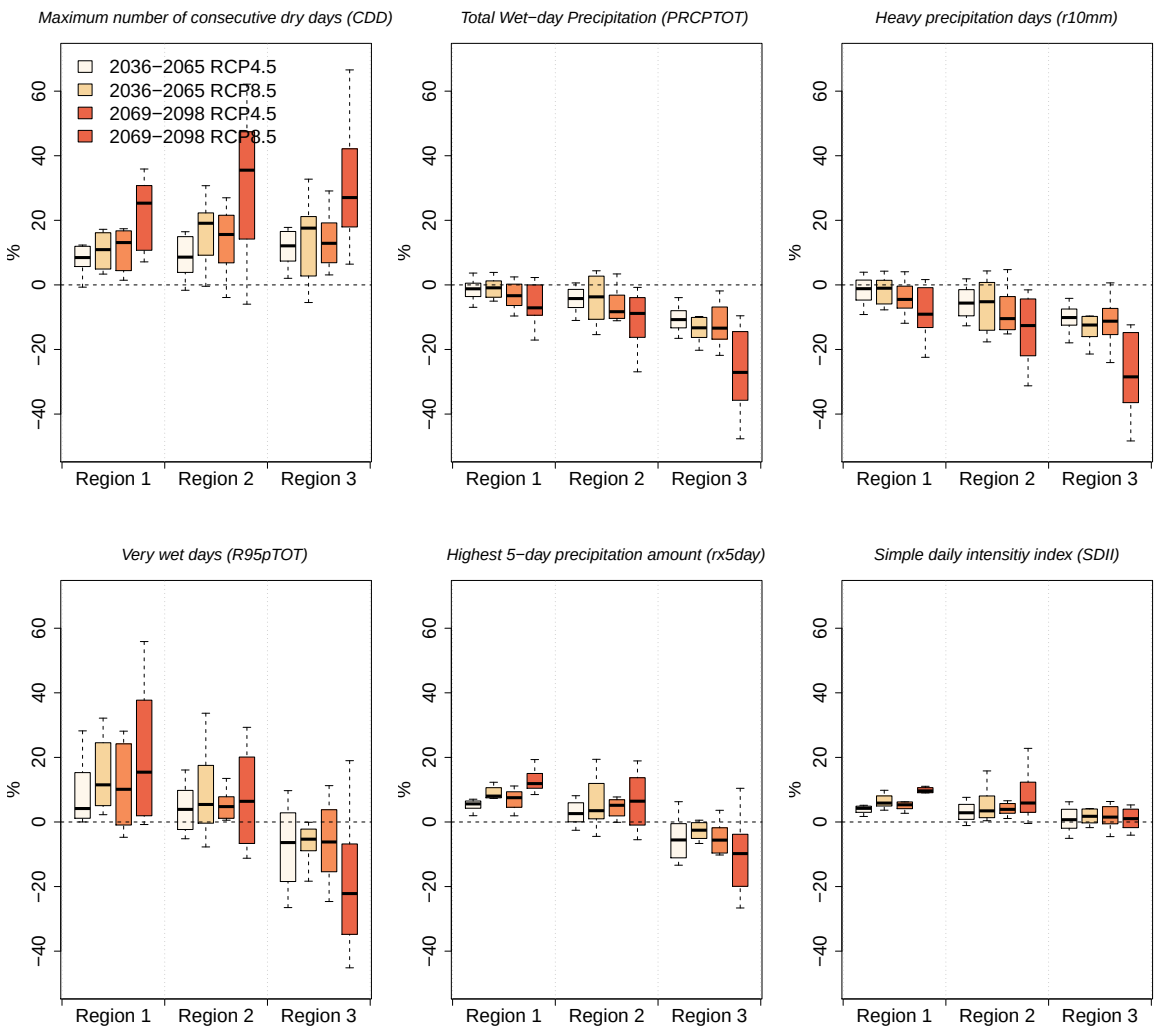

Figure 5.9: Projected changes in annual precipitation indices over the time period 2036-2065 and 2069-2098 as differences relative to the reference period (1976-2005) for RCP4.5 and RCP8.5

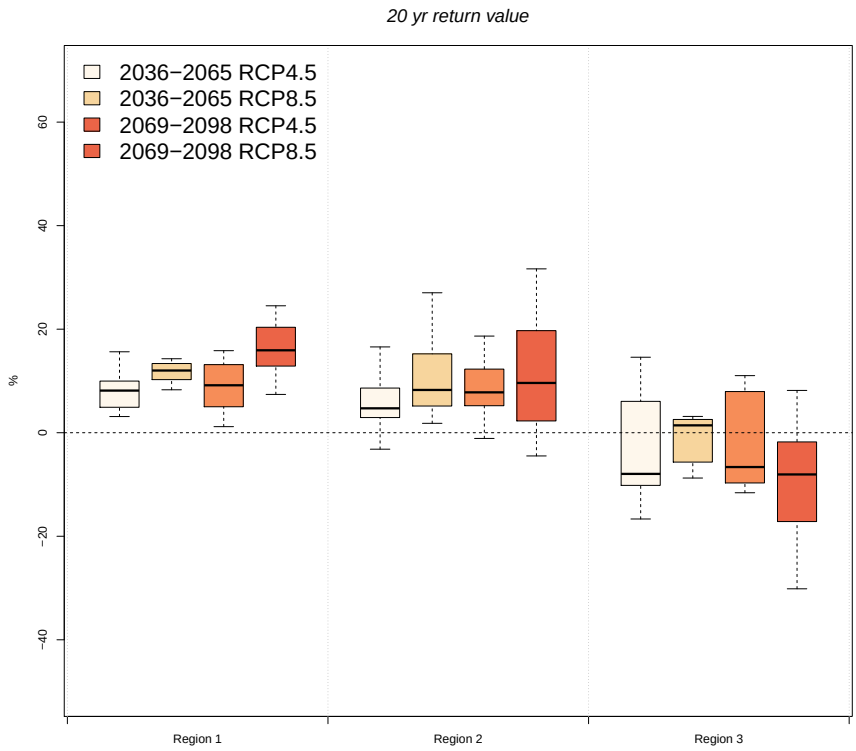

Figure 5.10: Projected changes in annual 20-yr return values over the time period 2036-2065 and 2069-2098 as differences relative to the reference period (1976-2005) for RCP4.5 and RCP8.5

The percentage of median changes of all indices are almost the same for regions 1 and 2. These two regions have similar climate conditions. There is a general agreement on the sign of change of all indices independent of the region considered for mid and end of 21st Century. Increases in CDD are projected in all regions followed by decreases in PRCPTOT and R10mm. Increases in R95pTOT, Rx5day and SDII are projected over region 1 and 2. Higher amount of change in PRCPTOT is found in region 3 together with decreases in R95pTOT, Rx5day and no change in median SDII. These changes are consistent with changes in physical mechanisms responsible for precipitation over south western South Africa. These include decrease in frequency of cold fronts (cf., section 3.2). The interquartile model spread is generally smaller in RCP4.5 compared to RCP8.5 probably due to different climate sensitivity in the models and feedback mechanisms. For rare extremes, the majority of the ensemble members models are in agreement on the sign of the change over region 1 and 2

implying more intense precipitation associated with 20 year return values. For region 3, all the models agree on the decrease of 20 year return values only by the end of the 21st Century under higher radiative forcing.

5.3 Summary

Projections of an ensemble of CORDEX RCMs, four downscaled GCMs by two RCMs (RCA4 and CCLM), has been presented for the mid and end of the 21st Century. In general the results suggests increases in wet extremes, such as R95pTOT and Rx5day in tropical and sub-tropical regions of southern Africa and decreases in these indices in the extra-tropical region. These changes are coherent with the changes in projected frequency of synoptic circulation associated to extreme precipitation. Dry extremes are also projected to increase in all three regions. In addition the magnitude 20-year return period precipitation events are projected to increase over most regions of southern Africa. The magnitude of the projected change are higher for the period 2069-2098 compared with 2036-2065 relative to 1976-2005. Comparing changes for both radiative forcing (RCP4.5 and RCP8.5), it was found that the magnitude of changes are higher for RCP8.5 compared with RCP4.5. The models agree on the sign of the change, increases in wet extremes and decreases in dry extremes.

6 Conclusions

A sharp rise in natural disasters such as catastrophic floods and droughts in southern Africa highlight the urgent need to look at the patterns of change in climate extremes at the regional level. The aim of this dissertation was to investigate the spatial and temporal characteristics of extreme climate events in CORDEX RCMs simulations of the present and future climate over southern Africa.

The following hypotheses were addressed to fulfil the aim of the thesis:

- The CORDEX RCMs can reasonably simulate extreme precipitation events in the present climate;
- The downscaling adds value to the global climate model output;
- The frequency and magnitude of extreme precipitation in the future, as projected by the CORDEX models, increases compared to base period simulation for the same locations;
- Large scale synoptic circulation environments can be associated with extreme rainfall and projected changes in extreme rainfall characteristics are attributable to changes in the frequency of occurrence of these synoptic drivers.

This chapter presents an overview and discussion of the key findings in view of the thesis hypotheses, followed by a discussion of problems and caveats, as well as rec-

ommendations for future work.

The analysis has been performed using data from two RCMs (COSMO-CLM and RCA4) that downscaled four GCMs, namely the MPI-ESM-LR, HadGEM2-ES, CNRM-CM5, and EC-EARTH. Thus, an eight-member ensemble of downscaled climate projections over the study region of southern Africa has been used. These were the ensemble members available at the time of the analysis. The study provides an initial step towards the delivery of downscaled climate information, however, the results need to be considered within the context of and uncertainty and caveats associated with dynamical downscaling.

The first set of present-day CORDEX simulations using ERA-Interim reanalysis and GCMs at the boundaries has been analysed in detail by Nikulin et al. (2012); Endris et al. (2013); Kalognomou et al. (2013); Kim et al. (2013); Hernández-Díaz et al. (2013); Panitz et al. (2014); Gbobaniyi et al. (2013). These authors focused mostly on precipitation climatology and confirm the ability of the RCMs to capture the broad precipitation characteristics. However, biases remain and are found to be specific to individual models, regions and seasons. It was also found that the multi-model ensemble (MME) mean generally outperforms any individual simulation and that the RCMs significantly improve the precipitation climate, often improving the performance of GCMs (e.g. Dosio et al., 2015; Laprise et al., 2013)). In fact, most of the previous studies have focused on mean precipitation climatology, examining in particular the ability of RCMs to improve the representation of the African climatology and variability. And none of the studies analysed the changes in the characteristics of extreme precipitation events using multiple RCMs.

The performance of individual models and their ensemble mean is analysed here for moderate and rare extremes. Validation of the downscaled GCM and reanalysis ERA-Interim realisations under present conditions shows that the downscaled climatology of extreme precipitation over southern Africa is generally consistent with observa-

tions. Maxima are well represented over complex terrains, although the models tend to overestimate extreme precipitation over high elevation areas. However, the relative performance of an individual model depends on the choice of the observed data set and the metric used for evaluation. For example, for the downscaled MME mean, the CDD is in higher agreement with the TRMM data while the annual PRCPTOT with GPCP data. And the downscaled MME single daily intensity index (SDII) and precipitation frequency is closer to both datasets. The MME outperforms most of the individual RCM ensemble members as a result of error cancellation between the different models, a phenomena found in many other studies (e.g Nikulin et al., 2011; Sillmann et al., 2013a).

As precipitation is controlled by synoptic circulation features, it is important that models adequately represent these controlling features over southern Africa. In chapter 3 of this study, a self-organising map (SOM) was used to construct a set of SLP patterns, or synoptic circulation types, and the corresponding observed and model rainfall patterns were examined. The rainfall for each synoptic regime was also decomposed into frequency to determine whether the models captured the distribution of rainfall associated with each regime. The SOM was able to identify characteristic circulation states that influence South African weather such as tropical lows, Atlantic and Indian Ocean High pressure systems and frontal systems as well as the seasonal characteristics of these. The individual models simulated the characteristics of circulation states over southern Africa reasonably well, although with varying magnitudes. Individual synoptic circulations facilitate a variety of precipitation responses due to the shift in intensities and locations of the dominant synoptic patterns throughout the seasons. Patterns representing a deeper continental low or mid-latitude cyclone are associated with more precipitation and extreme precipitation than other patterns. In general, SOMs offer a means to identify changes in driving synoptic environment of the surface rainfall response through an assessment of changes in the frequency of occurrence of synoptic circulation patterns. Since the atmospheric circulation is

relatively well simulated compared to, for example rainfall, the bias in precipitation are likely due to the representation of local subgrid-scale parameterized processes, such as convection and/or the representation of coastlines.

In terms of assessing the value added by the downscaling, the ability of RCMs to improve on the agreement of GCM data with observations was investigated. It was found that the downscaling of GCMs with the RCMs reduces biases in certain regions (Di Luca et al., 2012), in areas of strong topographical forcing (Arritt and Rummukainen, 2011; Elguindi and Grundstein, 2013) and with respect to convective precipitation (Rauscher et al., 2010). Kawazoe and Gutowski Jr (2013) compared six different RCMs and one GCM to two observational data sets and concluded that precipitation extremes were more representative in RCMs than in the GCMs. Seneviratne et al. (2012) also found that regional models run at higher resolution enables better simulation of extremes. The results of this thesis are in agreement with these authors, however, it was found that RCMs also deviate from the imposed driving boundary conditions. As suggested by Alexandru et al. (2007) and Liang et al. (2008) this seems to be mainly due to the regional climate model physical formulation and biases in the simulation. The added value in downscaling also depends on the index being considered. PRCPTOT and precipitation frequency, for example, both show improvements for most southern African regions, however, the Rx5day index shows no clear improvement on the GCM results. The fact that RCMs simulate precipitation frequency better than GCMs have been found in others studies (e.g. Sun et al., 2006). In general, this highlights the need to dynamically downscale global climate model output in order to provide future regional and/or local climate change information required for suitable impact studies that are related to extreme rainfall over southern Africa.

In chapter 5, future projections under two different climate change scenarios were examined. These suggest that changes in the characteristics of precipitation over

the southern Africa region can be expected by the middle (2036-2068) of and end (2069-2098) end of the 21st Century. At seasonal scales, the projected changes in the PRCPTOT index decrease during SON, followed by MAM, DJF and JJA. Statistically significant decreases in PRCPTOT over regions of southern Africa are projected for the future with greater changes at the end of the century. The models agree on the sign of the change at annual scales, although the magnitudes differ somewhat. Higher changes are expected over the mid-latitudes (region 3) followed by sub-tropical (regions 2) and tropical regions (region 1). The frequency of occurrence of cold fronts are projected to decrease in winter with the southern displacement of frontal rain bands by a strengthened descending limb of the Hadley circulation (Engelbrecht et al., 2009), resulting in decreases in precipitation over the winter rainfall region of South Africa. Eastern southern Africa is projected to become wetter in summer by mid century as the circulation changes favour the occurrence of precipitation, followed by a decrease in PRCPTOT by the end of 21st Century. Decreases in PRCPTOT during SON suggest a shift of the rainy season to later dates. This is in agreement with the trend toward a later onset that has been found over South Africa and Zimbabwe during the period 1979-2001 (Tadross et al., 2005) which is projected to continue into the future (e.g. Shongwe et al., 2009).

At seasonal scales, the projected change in the magnitude of CDD index shows the largest signal increase during SON, followed by MAM, JJA and DJF. This increasing dryness is expected to occur by the middle then intensify in the latter half of the century. The models show agreement on the sign of the change for all three regions with higher changes under the RCP8.5 radiative forcing. The dryness during SON is associated with increases in frequency of occurrence of synoptic circulation typical of winter, a result supported by the findings of Lennard and Hegerl (2014).

Both Rx5day and R95pTOT are project to increase during summer over Mozambique, south-east Angola, Zambia, northeast Namibia and Botswana. These regions, with the exception of Mozambique, coincides with the region of convergence of the Indian Ocean' s southeast trade winds and the recurved South Atlantic air, or the

Congo Air Boundary (CAB). This system brings widespread precipitation to the region, which becomes heavy when it is associated with the ITCZ. These increases are accompanied by increases in SDII. Increases in CDD are accompanied by increases in R95pTOT, suggesting an increase in dry spell duration, but that precipitation may be more extreme when it occurs. In addition the magnitude of 20-year return period precipitation events are projected to increase over most regions of southern Africa. These changes are strengthened by a consistent inter-model agreement on the sign of the change.

The projected changes in the synoptic drivers of the above results suggests that an increase in the frequency of occurrence of the continental surface low pressure trough during summer months, which is likely associated with increased surface warming, leads to an increase in atmospheric moisture content and convection potential over the summer rainfall region of the sub-continent. This explain the projected increase in extreme precipitation indices over these regions. Furthermore, an increase in the frequency of the occurrence of the Indian Ocean High during summer was also found, which facilitates an increase in air flow onto the continent from the east. As the Indian Ocean is the primary moisture source for the subcontinent Todd et al. (2004); Reason (2001); Washington and Preston (2006), this is of key relevance for the moisture transport into the region, especially as air can hold more moisture as the world warms, according to the Clausius-Clapeyron relationship. The increase in moisture content may result in an increase in rain per rainday rather than in the number of rain days Fowler and Hennessy (1995).

The spatial distribution of changes in extreme precipitation events are largely in line with previous studies based on coarser-resolved models (e.g Shongwe et al., 2009; Sillmann et al., 2013b; Fischer et al., 2013). These results imply that there would be a trend towards drier conditions over regions that is already dry and wetter conditions over wet regions over southern Africa and is consistent with past trends found by Donat et al. (2013).

The changes in extreme precipitation events is higher under the RCP8.5 radiative

forcing than under RCP4.5, implying that a reduction in emissions could mitigate some of the costs of climate change in the future. The increases in SDII, Rx5day, R95pTOT in the centre of the sub continent, in the boundary between Angola, Zambia, Namibia and Botswana are ascribed to increases in atmospheric moisture into the region. These increases will most likely result in higher surface runoff and potential floods in the Zambezi River Basin, especially in Mozambique. From a dynamic circulation perspective, the changes in extreme precipitation presented here are physically consistent with changes in circulation patterns. It should be noted that the projected changes that are not classified as statistically significant may still be sensitive to changes in radiative forcing given that (1) determining statistical significance is dependent on choice of analysis methods (e.g. McSweeney and Jones, 2012) and (2) it is not clear that changes in precipitation that are not significant will have no detectable impact, because of different levels of sensitivity of each sector or system (e.g. McSweeney and Jones, 2012).

In summary, the regional climate models are able to simulate moderate extreme events that are in agreement with observations. The RCMs add value to the GCM data, which justifies the additional computational expense of RCM downscaling to generate relevant climate information for regional application. However, rare events are not well captured by RCMs when compared with observed data possibly due to models internal noise. Downscaled projections suggest an increase in the frequency and intensity of extreme rainfall events in the future with greater magnitudes of change under RCP8.5. Future changes in precipitation characteristics are physically consistent with changes in the frequency of occurrence of circulation patterns associated with extreme rainfall that were presented in chapter 3.

6.1 Caveats and Further work

As with any model evaluation study, there are a few caveats and assumptions and these should be taken into consideration when interpreting the results. The first of these is the uncertainty in both observational data sets used in validating the models, especially as only eight years were available and this is unfortunately one of the limitations of the study. The fact that only two RCMs were used to downscale the GCMs is the second limitation. As Giorgi and Coppola (2010) noted, at least four to five models should be used to obtain a robust regional precipitation change estimates. The use of more RCMs will allow a more complete sampling of the uncertainty space introduced by the downscaling. Also, the use of statistical downscaling would be beneficial to determine the credibility of both downscaling methods (Daron et al., 2014; Barsugli et al., 2013) and lead to a better understanding of the uncertainty contributed by each downscaling method. Furthermore, future changes in precipitation extremes need to be assessed in relation to soil moisture and vegetation (e.g., Eltahir, 1998; Seneviratne et al., 2006) for a comprehensive understanding of the future changes simulated over southern Africa. While the effect of the circulation patterns and model physics on precipitation over southern Africa has been identified, more quantitative methods may yield more certain results. There is therefore much scope to investigate further factors that contribute to current and projected changes of precipitation and extreme precipitation over southern Africa.

References

Aguilar, E., Barry, A., Brunet, M., Ekang, L., Fernandes, A., Massoukina, M., Mbah, J., Mhanda, A., do Nascimento, D., Peterson, T., et al. (2009). Changes in temperature and precipitation extremes in western central Africa, Guinea Conakry, and Zimbabwe, 1955–2006. *Journal of Geophysical Research*, 114(D2):D02115.

Alexander, L. and Arblaster, J. (2009). Assessing trends in observed and modelled climate extremes over Australia in relation to future projections. *International Journal of Climatology*, 29(3):417–435.

Alexandru, A., de Elia, R., and Laprise, R. (2007). Internal variability in regional climate downscaling at the seasonal scale. *Monthly Weather Review*, 135(9):3221–3238.

Arritt, R. W. and Rummukainen, M. (2011). Challenges in regional-scale climate modeling. *Bulletin of the American Meteorological Society*, 92(3):365–368.

Barsugli, J. J., Guentchev, G., Horton, R. M., Wood, A., Mearns, L. O., Liang, X.-Z., Winkler, J. A., Dixon, K., Hayhoe, K., Rood, R. B., et al. (2013). The Practitioner's Dilemma: How to assess the credibility of downscaled climate projections. *Eos, Transactions American Geophysical Union*, 94(46):424–425.

Bechtold, P., Bazile, E., Guichard, F., Mascart, P., and Richard, E. (2001). A mass-flux

convection scheme for regional and global models. *Quarterly Journal of the Royal Meteorological Society*, 127:869–886.

Bresson, R. and Laprise, R. (2011). Scale-decomposed atmospheric water budget over North America as simulated by the Canadian Regional Climate Model for current and future climates. *Climate Dynamics*, 36(1-2):365–384.

Brown, J. R., Jakob, C., and Haynes, J. M. (2010). An evaluation of rainfall frequency and intensity over the Australian region in a global climate model. *Journal of Climate*, 23(24):6504–6525.

Buishand, T. (1989). Statistics of extremes in climatology. *Statistica Neerlandica*, 43(1):1–30.

Buonomo, E., Jones, R., Huntingford, C., and Hannaford, J. (2007). On the robustness of changes in extreme precipitation over Europe from two high resolution climate change simulations. *Quarterly Journal of the Royal Meteorological Society*, 133:65–81.

Cassano, J. J., Uotila, P., and Lynch, A. (2006). Changes in synoptic weather patterns in the polar regions in the twentieth and twenty-first centuries, part 1: Arctic. *International Journal of Climatology*, 26(8):1027–1049.

Cazavos, T. (2000). Using self-organizing maps to investigate extreme climate events: An application to wintertime precipitation in the Balkans. *Journal of Climate*, 13:1718–1732.

Christensen, J., Carter, T. R., Rummukainen, M., and Amanatides, G. (2007). Evaluating the perfomance of regional climate models: The PRUDENCE project. *Climatic Change*, 81:1–6.

Coles, S. (2001). *An Introduction to Statistical Modeling of Extreme Values* . Springer Series in Statistics, London, UK.

Collins, W., Bellouin, N., Doutriaux-Boucher, M., Gedney, N., Halloran, P., Hinton, T., Hughes, J., Jones, C., Joshi, M., Liddicoat, S., et al. (2011). Development and evaluation of an Earth-system model–HadGEM2. *Geoscientific Model Development Discussions*, 4(2):997–1062.

Cook, C., Reason, C. J., and Hewitson, B. C. (2004). Wet and dry spells within particularly wet and dry summers in the South African summer rainfall region. *Climate Research*, 26(1):17–31.

Curry, J. A. and Lynch, A. H. (2002). Comparing Arctic regional climate models. *Eos, Transactions Amererican Geophysical Union*, 83:87.

D'Abreton, P. C. and Lindesay, J. A. (1993). Water vapour transport over Southern Africa during wet and dry early and late summer months. *International Journal of Climatology*, 13:151–170.

Daron, J. D., Sutherland, K., Jack, C., and Hewitson, B. C. (2014). The role of regional climate projections in managing complex socio-ecological systems. *Regional Environmental Change*, 15(1):1–12.

Dee, D., Uppala, S., Simmons, A., Berrisford, P., Poli, P., Kobayashi, S., Andrae, U., Balmaseda, M., Balsamo, G., Bauer, P., et al. (2011). The ERA-Interim reanalysis: Configuration and performance of the data assimilation system. *Quarterly Journal of the Royal Meteorological Society*, 137(656):553–597.

Di Luca, A., de Elía, R., and Laprise, R. (2012). Potential for added value in precipitation simulated by high-resolution nested Regional Climate Models and observations. *Climate dynamics*, 38(5-6):1229–1247.

Di Luca, A., de Elía, R., and Laprise, R. (2013). Potential for small scale added value of RCMs downscaled climate change signal. *Climate Dynamics*, 40(3-4):601–618.

Dieterich, C., Schimanke, S., Wang, S., Väli, G., Liu, Y., Hordoir, R., Axell, L.,

Höglund, A., and Meier, H. (2013). Evaluation of the SMHI coupled atmosphere-ice-ocean model RCA4_NEMO. *Report Oceanography 47*, page 80.

Donat, M., Alexander, L., Yang, H., Durre, I., Vose, R., Dunn, R., Willett, K., Aguilar, E., Brunet, M., Caesar, J., et al. (2013). Updated analyses of temperature and precipitation extreme indices since the beginning of the twentieth century: The HadEX2 dataset. *Journal of Geophysical Research: Atmospheres*, 118(5):2098–2118.

Dosio, A., Panitz, H.-J., Schubert-Frisius, M., and Lüthi, D. (2015). Dynamical downscaling of CMIP5 global circulation models over CORDEX-Africa with COSMO-CLM: evaluation over the present climate and analysis of the added value. *Climate Dynamics*, 44:2637–2661.

Dupuis, D. and Tsao, M. (1998). A hybrid estimator for generalized Pareto and extreme-value distributions. *Communications in Statistics-Theory and Methods*, 27(4):925–941.

Durman, C. F., Gregory, J. M., Hassel, D. H., Jones, R. G., and Murphy, J. M. (2001). A comparison of extreme European daily precipitation simulated by a global and a regional climate model for present and future climates. *Quarterly Journal of the Royal Meteorological Society*, 127(573):1005–1015.

Dyson, L. and van Heerden J. (2001). The heavy rainfall and floods over the north-eastern interior of South Africa during February 2000. *South African Journal of Science*, (97):80–86.

Elguindi, N. and Grundstein, A. (2013). An integrated approach to assessing 21st century climate change over the contiguous US using the NARCCAP RCM output. *Climatic change*, 117(4):809–827.

Eltahir, E. A. (1998). A soil moisture–rainfall feedback mechanism: 1. Theory and observations. *Water Resources Research*, 34(4):765–776.

Embrechts, P., Klüppelberg, C., and Mikosch, T. (1997). *Modelling extremal events for insurance and finance*, volume 33. Springer Verlag.

Emori, S., Hasegawa, A., Suzuki, T., and Daikaru, K. (2005). Validation, parameterization dependence, and future projection of daily precipitation simulated with a high-resolution atmospheric GCM. *Geophysical Research Letters*, 32:L06708.

Endris, H. S., Omondi, P., Jain, S., Lennard, C., Hewitson, B., Chang'a, L., Awange, J., Dosio, A., Ketiem, P., Nikulin, G., et al. (2013). Assessment of the Performance of CORDEX Regional Climate Models in Simulating East African Rainfall. *Journal of Climate*, 26(21):8453–8475.

Engelbrecht, C., Engelbrecht, F., and Dyson, L. (2012). High-resolution model-projected changes in mid-tropospheric closed-lows and extreme rainfall events over southern Africa. *International Journal of Climatology*, 33(1):173–187.

Engelbrecht, F., McGregor, J., and Engelbrecht, C. (2009). Dynamics of the Conformal-Cubic Atmospheric Model projected climate-change signal over southern Africa. *International Journal of Climatology*, 29(7):1013–1033.

Fauchereau, N., Trzaska, S., Rouault, M., and Richard, Y. (2003). Rainfall Variability and Changes in Southern Africa during the 20th Century in the Global Warming Context . *Natural Hazards*, 29(2):139–154.

Favre, A., Bewitson, B., Lennard, C., Cerezo-Mota, R., and Tadross, M. (2013). Cut-off Lows in the South Africa region and their contribution to precipitation. *Climate Dynamics*, (41):2331–2351.

Feser, F. (2006). Enhanced detectability of added value in limited-area model results separated into different spatial scales. *Monthly weather review*, 134(8):2180–2190.

Feser, F., Rockel, B., von Storch, H., Winterfeldt, J., and Zahn, M. (2011). Regional climate models add value to global model data: a review and selected examples. *Bulletin of the American Meteorological Society*, 92(9):1181–1192.

Fischer, E., Beyerle, U., and Knutti, R. (2013). Robust spatially aggregated projections of climate extremes. *Nature Climate Change*, 3(12):1033–1038.

Fisher, R. and Tippett, L. (1928). Limiting forms of the frequency distribution of the largest or smallest member of a sample. In *Mathematical Proceedings of the Cambridge Philosophical Society*, volume 24, pages 180–190. Cambridge Univ Press.

Fowler, A. and Hennessy, K. (1995). Potential impacts of global warming on the frequency and magnitude of heavy precipitation. *Natural Hazards*, 11(3):283–303.

Frei, C., Christensen, J., Deque, M., Jacob, D., Jones, R., and Vidale, P. (2003). Daily precipitation statistics in Regional Climate Models: Evaluation and intercomparison for the European Alps. *Journal of Geophysical Research*, 108(D3):4124–4142.

Frei, C., Schöll, R., Fukutome, S., Schmidli, J., and Vidale, P. (2006). Future change of precipitation extremes in Europe: Intercomparison of scenarios from regional climate models. *Journal of Geophysical Research*, 111(6):D06105.

Fu, C., Wang, S., Xiong, Z., Gutowski, W., Lee, D., McGregor, J., Sato, Y., Kato, H., Kim, J., and Su, M. (2005). Regional climate model intercomparison project for Asia (RMIP). *Bulletin of the American Meteorological Society*, 86:257–266.

Gao, X., Shi, Y., Zhang, D., Wu, J., Giorgi, F., Ji, Z., and Wang, Y. (2012). Uncertainties in monsoon precipitation projections over China: results from two high-resolution RCM simulations. *Climate Research*, 2:213.

Gbobaniyi, E., Sarr, A., Sylla, M. B., Diallo, I., Lennard, C., Dosio, A., Dhiédiou, A., Kamga, A., Klutse, N. A. B., Hewitson, B., et al. (2013). Climatology, annual cycle and interannual variability of precipitation and temperature in CORDEX simulations over West Africa. *International Journal of Climatology*, 34(7):2241–2257.

Gilleland, E. and Katz, R. (2006). Analyzing seasonal to interannual extreme weather and climate variability with the extremes toolkit. In *18th Conference on Climate*

Variability and Change, 86th American Meteorological Society (AMS) Annual Meeting, volume 29.

Giorgi, F. (1990). Simulation of regional climate using a limited area model nested in a general circulation model. *Journal of Climate*, 3:941–964.

Giorgi, F. and Coppola, E. (2010). Does the model regional bias affect the projected regional climate change? An analysis of global model projections. *Climatic Change*, 100(3-4):787–795.

Giorgi, F., Coppola, E., Raffaele, F., Diro, G., Fuentes-Franco, R., Giuliani, G., Mamgain, A., Llopart, M., Mariotti, L., and Torma, C. (2014). Changes in extremes and hydroclimatic regimes in the CREMA ensemble projections. *Climatic Change*, 125(1):39–51.

Giorgi, F., Jones, C., and Asrar, G. (2009). Addressing climate information needs at the regional level: the CORDEX framework. *WMO Bulletin*, 58(3):175.

Gnedenko, B. (1943). Sur la distribution limite du terme maximum d'une serie aleatoire. *The Annals of Mathematics*, 44(3):423–453.

Groisman, P., Knight, R., Easterling, D., Karl, T., Hegerl, G., and Razuvaev, V. (2005). Trends in intense precipitation in the climate record. *Journal of Climate*, 18(9):1326–1350.

Gumbel, E. (1984). Statistics of extremes, 1958. *Columbia Univ. press, New York*.

Harangozo, S. and Harrison, M. S. J. (1983). On the use of synoptic data in indicating the presence of clould bands over southern Africa. *South Africa Journal of Science*, 79:413–414.

Hart, N., Reason, C., and Fauchereau, N. (2010). Tropical-extratropical interactions over southern Africa: three cases of heavy summer season rainfall. *Monthly Weather Review*, 138(7):2608–2623.

Hart, N., Reason, C., and Fauchereau, N. (2012). Cloud bands over southern Africa: Seasonality, contribution to rainfall variability and modulation by the MJO. *Climate Dynamics*, (41):1199–1212.

Hazeleger, W., Severijns, C., Semmler, T., Stefanescu, S., Yang, S., Wang, X., Wyser, K., Dutra, E., Baldasano, J. M., Bintanja, R., et al. (2010). EC-Earth: a seamless earth-system prediction approach in action. *Bulletin of the American Meteorological Society*, 91(10):1357–1363.

Hernández-Díaz, L., Laprise, R., Sushama, L., Martynov, A., Winger, K., and Dugas, B. (2013). Climate simulation over CORDEX Africa domain using the fifth-generation Canadian Regional Climate Model (CRCM5). *Climate Dynamics*, 40(5-6):1415–1433.

Hewitson, B. (2010). Enhancing regional climate change message through assessing multi-model regional circulation changes. In Stocker, T.F., D. Qin, G.-K. Plattner, M. Tignor, and P.M. Midgley, editor, *Meeting Report of the Intergovernmental Panel on Climate Change Expert Meeting on Assessing and Combining Multi Model Climate Projections*. IPCC Working Group I Technical Support Unit, University of Bern, Bern, Switzerland.

Hewitson, B., Daron, J., Crane, R., Zermoglio, M., and Jack, C. (2013). Interrogating empirical-statistical downscaling. *Climatic Change*, 122(4):539–554.

Hewitson, B. C. and Crane, R. G. (1996). Climate downscaling: Techniques and application. *Climate Research*, 7:85–95.

Hewitson, B. C. and Crane, R. G. (2002). Self-organizing maps: applications to synoptic climatology. *Climate Research*, 22:13–26.

Hewitt, C. (2005). The ENSEMBLES project: providing ensemble-based predictions of climate changes and their impacts. *EGU Newsletter*, 13:22–25.

Hope, P. K. (2006). Projected future changes in synoptic systems influencing southwest Western Australia. *Climate Dynamics*, 26(7-8):765–780.

Hope, P. K., Drosdowsky, W., and Nicholls, N. (2006). Shifts in the synoptic systems influencing southwest Western Australia. *Climate Dynamics*, 26(7-8):751–764.

Hosking, J. R. M. (1990). L-Moments: Analysis and Estimation of Distributions Using Linear Combinations of Order Statistics. *Journal of the Royal Statistical Society. Series B (Methodological)*, 52(1):pp. 105–124.

Hosking, J. R. M., Wallis, J. R., and Wood, E. F. (1985). Estimation of the Generalized Extreme-Value Distribution by the Method of Probability-Weighted Moments. *Technometrics*, 27(3):pp. 251–261.

Hudson, D. A. and Jones, R. G. (2002). Regional climate model simulations of present-day and future climates of southern Africa. Technical report, Hadley Centre Technical Note 39, Hadley Centre for Climate Prediction and Research, Met Office, Bracknell, U.K.

Huffman, G., Adler, R., Bolvin, D., Gu, G., Nelkin, E., Bowman, K., Hong, Y., Stocker, E., and Wolff, D. (2007). The TRMM multisatellite precipitation analysis (TMPA): quasi-global, multiyear, combined-sensor precipitation estimates at fine scales. *Journal of Hydrometeorology*, 8(1):38–55.

Huffman, G. J., Adler, R. F., Morrissey, M. M., Bolvin, D. T., Curtis, S., Joyce, R., McGavock, B., and Joel Susskind (2001). Global precipitation at one-degree daily resolution from multisatellite observations. *Journal of Hydrometeor*, 2:36–50.

Huntingford, C., Jones, R. G., Prudhomme, C., Lamb, R., Gash, J. H., and Jones, D. A. (2003). Regional climate-model predictions of extreme rainfall for a changing climate. *Quarterly Journal of the Royal Meteorological Society*, 129:1607–1621.

Hurry, L. and Van Heerden, J. (1982). *Southern Africa's weather patterns: a guide to the interpretation of synoptic maps*. Via Afrika.

IPCC (2001). *Climate Change: The Scientific Basis. Contribution of Working Group 1 to the Third Assesment Report of the Intergornmental Panel on Climate Change*. Cambridge University Press, Cambridge, United Kingdom and New York.

IPCC (2007). *Climate Change 2007: The Physical Science Basis. Contribution of Working Group I to the Fourth Assessment Report of the Intergovernmental Panel on Climate Change*. [Solomon, S., D. Qin, M. Manning, Z. Chen, M. Marquis, K.B. Averyt, M. Tignor and H.L. Miller (eds.)], Cambridge University Press, Cambridge, United Kingdom and New York, NY, USA.

IPCC (2012). *Summary for policymakers. In: Managing the Risks of Extreme Events and Disasters to Advance Climate Change Adaptation*. [Field, C.B., V. Barros, T.F. Stocker, D. Qin, D.J. Dokken, K.L. Ebi, M.D. Mastrandrea, K.J. Mach, G.-K. Plattner, S.K. Allen, M. Tignor, and P.M. Midgley (eds.)]. A Special Report of Working Groups I and II of the Intergovernmental Panel on Climate Change. Cambridge University Press, Cambridge, UK, and New York, NY, USA, pp. 1-19.

Jones, R., Noguer, M., Hassell, D., Hudson, D., Wilson, S., Jenkins, G., and Mitchell, J. (2004). *Generating high resolution climate change scenarios using PRECIS*. Met Office Hadley Centre, Exeter, UK.

Joubert, A. M., Katzfey, J. J., McGregor, J. L., and Nguyen, K. C. (1999). Simulating midsummer climate over southern Africa using a nested regional climate model. *Journal of geophysical research*, 104(D16).

Jury, M., White, W., and Reason, C. (2004). Modelling the dominant climate signals around southern Africa. *Climate dynamics*, 23(7):717–726.

Kalnay, E., Kanamitsu, M., Kistler, R., Collins, W., Deaven, D., Gandin, L., Iredell, M., Saha, S., White, G., Woollen, J., et al. (1996). The NCEP/NCAR 40-year reanalysis project. *Bulletin of the American meteorological Society*, 77(3):437–471.

Kalognomou, E.-A., Lennard, C., Shongwe, M., Pinto, I., Favre, A., Kent, M., Hewitson, B., Dosio, A., Nikulin, G., Panitz, H.-J., and Büchner, M. (2013). A diagnostic evaluation of precipitation in CORDEX models over southern Africa. *Journal of climate*.

Katz, R., Parlange, M., and Naveau, P. (2002). Statistics of extremes in hydrology. *Advances in water resources*, 25(8-12):1287–1304.

Katz, R. W. and Brown, B. G. (1992). Extreme events in a changing climate: Variability is more important than averages. *Climatic Change*, 21:289–302.

Kawazoe, S. and Gutowski Jr, W. J. (2013). Regional, very heavy daily precipitation in NARCCAP simulations. *Journal of Hydrometeorology*, 14(4):1212–1227.

Kharin, V., Zwiers, F., and Zhang, X. (2005). Intercomparison of near-surface temperature and precipitation extremes in AMIP-2 simulations, reanalyses, and observations. *Journal of climate*, 18(24):5201–5223.

Kharin, V. V. and Zwiers, F. W. (2000). Changes in the Extremes in an Ensemble of Transient Climate Simulations with a Coupled Atmosphere-Ocean GCM. *Journal of Climate*, 13(21):3760–3788.

Kharin, V. V. and Zwiers, F. W. (2005). Estimating Extremes in Transient Climate Change Simulations. *Journal of Climate*, 18(8):1156–1173.

Kiktev, D., Sexton, D. M. H., Alexander, L., and Folland, C. K. (2003). Comparison of Modeled and Observed Trends in Indices of Daily Climate Extremes. *Journal of Climate*, 16:3560–3571.

Kim, J., Waliser, D. E., Mattmann, C. A., Goodale, C. E., Hart, A. F., Zimdars, P. A., Crichton, D. J., Jones, C., Nikulin, G., Hewitson, B., et al. (2013). Evaluation of the CORDEX-Africa multi-RCM hindcast: systematic model errors. *Climate Dynamics*, pages 1–14.

Klein Tank, A. M., Zwiers, F. W., and Zhang, X. (2009). Guidelines on analysis of extremes in a changing climate in support of informed decisions for adaptation. *WCDMP-72, WMO-TD*, 1500.

Kohonen, T. (2001). *Self-organizing maps*. Springer.

Kruger, A. (2006). Observed trends in daily precipitation indices in South Africa: 1910–2004. *International Journal of Climatology*, 26(15):2275–2285.

Laprise, R., Hernández-Díaz, L., Tete, K., Sushama, L., Šeparović, L., Martynov, A., Winger, K., and Valin, M. (2013). Climate projections over CORDEX Africa domain using the fifth-generation Canadian Regional Climate Model (CRCM5). *Climate Dynamics*, pages 1–28.

Lennard, C., Coop, L., Morison, D., and Grandin, R. (2013). Extreme events: Past and future changes in the attributes of extreme rainfall and the dynamics of their driving processes. Water Research Commission.

Lennard, C. and Hegerl, G. (2014). Relating changes in synoptic circulation to the surface rainfall response using self-organising maps. *Climate Dynamics*, pages 1–19.

Liang, X.-Z., Kunkel, K. E., Meehl, G. A., Jones, R. G., and Wang, J. X. (2008). Regional climate models downscaling analysis of general circulation models present climate biases propagation into future change projections. *Geophysical research letters*, 35(8).

Lynch, A., Uotila, P., and Cassano, J. J. (2006). Changes in synoptic weather patterns in the polar regions in the twentieth and twenty-first centuries, part 2: Antarctic. *International Journal of Climatology*, 26(9):1181–1199.

MacKellar, N., Tadross, M., and Hewitson, B. (2010). Synoptic-based evaluation of climatic response to vegetation change over southern africa. *International Journal of Climatology*, 30(5):774–789.

Mason, S. (2001). El Niño, climate change, and Southern African climate. *Environmetrics*, 12(4):327–345.

Mason, S. and Joubert, A. (1997). Simulated changes in extreme rainfall over southern Africa. *International Journal of Climatology*, 17(3):291–301.

Mason, S. and Jury, M. (1997). Climatic variability and change over southern Africa: a reflection on underlying processes. *Progress in physical geography*, 21(1):23.

Mason, S. J., Waylen, P. R., Mimmack, G. M., Rajaratnam, B., and Harrison, J. M. (1999). Changes in Extreme Rainfall Events in South Africa. *Climatic Change*, 41:249–257. 10.1023/A:1005450924499.

McGregor, J. L. (1997). Regional Climate Modelling. *Meteorology and Atmospheric Physics*, 63:105–117.

McSweeney, C. F. and Jones, R. G. (2012). No consensus on consensus: the challenge of finding a universal approach to measuring and mapping ensemble consistency in GCM projections. *Climatic Change*, pages 1–13.

Mearns, L. O., Gutowski, W., Jones, R., Leung, R., McGinnis, S., A. Nunes, and Qian, Y. (2009). A Regional Climate Change Assessment Program for North America. *EOS, Transactions Amererican Geophysical Union*, 90(36):311.

Meehl, G. A., Arblaster, J. M., and Tebaldi, C. (2005). Understanding future patterns of increased precipitation intensity in climate model simulations. *Geophysical Research Letters*, 32(L18719).

Meehl, G. A., Karl, T., Easterling, D., Changnon, S., Pielke, R. J., et al. (2000). An introduction to trends in extreme weather and climate events: Observations, socioeconomic impacts, terrestrial ecological impacts, and model projections. *Bulletin of the American Meteorological Society*, 81:413–416.

Menéndez, C., de Castro, M., Sorensson, A., and Boulanger, J. (2010). CLARIS Project: towards climate downscaling in South America. *Meteorologische Zeitschrift*, 19(4):357–362.

Min, S.-K., Zhang, X., Zwiers, F. W., and Hegerl, G. C. (2011). Human contribution to more-intense precipitation extremes. *Nature*, 470(7334):378–381.

Moss, R., Edmonds, J., Hibbard, K., Manning, M., Rose, S., van Vuuren, D., Carter, T., Emori, S., Kainuma, M., Kram, T., et al. (2010). The next generation of scenarios for climate change research and assessment. *Nature*, 463(7282):747–756.

Nakicenovic, N., Alcamo, J., Davis, G., de Vries, B., Fenhann, J., Gaffin, S., Gregory, K., Grübler, A., Jung, T. Y., Kram, T., Rovere, E. L. L., Michaelis, L., Mori, S., Morita, T., Pepper, W., Pitcher, H., Price, L., Raihi, K., Roehrl, A., Rogner, H.-H., Sankovski, A., Schlesinger, M., Shukla, P., Smith, S., Swart, R., van Rooijen, S., Victor, N., and Dadi, Z. (2000). *IPCC Special Report on Emissions Scenarios*. Cambridge University Press, Cambridge, United Kingdom and New York, NY, USA.

Naveau, P., Nogaj, M., Ammann, C., Yiou, P., Cooley, D., and Jomelli, V. (2005). Statistical methods for the analysis of climate extremes. *Comptes Rendus Geoscience*, 337(10):1013–1022.

New, M. et al. (2006). Evidence of trends in daily climate extremes over southern and west Africa. *Journal of Geophysical Research*, 111:D14102.

Nicholson, S. (2000). The nature of rainfall variability over Africa on time scales of decades to millenia. *Global and Planetary Change*, 26(1-3):137–158.

Nicholson, S. (2003). Comments on " The South Indian Convergence Zone and Interannual Rainfall Variability over Southern Africa" and the Question of ENSO's Influence on Southern Africa. *Journal of Climate*, 16:555–562.

Nikulin, G., Jones, C., Giorgi, F., Asrar, G., Büchner, M., Cerezo-Mota, R., Christensen, O. B., Déqué, M., Fernandez, J., Hänsler, A., et al. (2012). Precipitation climatology

in an ensemble of CORDEX-Africa regional climate simulations. *Journal of Climate*, 25(18):6057–6078.

Nikulin, G., Kjellström, E., Hansson, U., Strandberg, G., and Ullerstig, A. (2011). Evaluation and future projections of temperature, precipitation and wind extremes over Europe in an ensemble of regional climate simulations. *Tellus A*, 63(1):41–55.

Noguer, M., Jones, R., and Murphy, J. M. (1998). Sources of systematic errors in the climatology of a regional climate model over Europe. *Climate Dynamics*, 14(10):691–712.

OCHA (2015). SOUTHERN AFRICA: Floods and Cyclones Update. http://reliefweb.int/map/malawi/southern-africa-floods-and-cyclones-update-17-jan-2015.

Oppenheimer, M., Campos, M., Warren, R., Birkmann, J., Luber, G., ONeill, B., and Takahashi, K. (2014). *Emergent risks and key vulnerabilities. In: Climate Change 2014: Impacts, Adaptation, and Vulnerability. Part A: Global and Sectoral Aspects. Contribution of Working Group II to the Fifth Assessment Report of the Intergovernmental Panel on Climate Change [Field, C.B., V.R. Barros, D.J. Dokken, K.J. Mach, M.D. Mastrandrea, T.E. Bilir, M. Chatterjee, K.L. Ebi, Y.O. Estrada, R.C. Genova, B. Girma, E.S. Kissel, A.N. Levy, S. MacCracken, P.R. Mastrandrea, and L.L. White (eds.)]*. Cambridge University Press, Cambridge, United Kingdom and New York, NY, USA, pp. 1039-1099.

Orlowsky, B. and Seneviratne, S. (2011). Global changes in extreme events: regional and seasonal dimension. *Climatic Change*, pages 1–28. 10.1007/s10584-011-0122-9.

Palutikof, J., Brabson, B., Lister, D., and Adcock, S. (1999). A review of methods to calculate extreme wind speeds. *Meteorological Applications*, 6(02):119–132.

Panitz, H.-J., Dosio, A., Büchner, M., Lüthi, D., and Keuler, K. (2014). COSMO-CLM

(CCLM) climate simulations over CORDEX-Africa domain: analysis of the ERA-Interim driven simulations at 0.44° and 0.22° resolution. *Climate Dynamics*, pages 1–24.

Pierce, D. W., Cayan, D. R., Das, T., Maurer, E. P., Miller, N. L., Bao, Y., Kanamitsu, M., Yoshimura, K., Snyder, M. A., Sloan, L. C., et al. (2013). The key role of heavy precipitation events in climate model disagreements of future annual precipitation changes in California. *Journal of Climate*, 26(16):5879–5896.

Pinto, I. S. D. S. (2011). Future changes in extreme events in Mozambique as simulated using the PRECIS regional climate modeling system. Master's thesis, University of Cape Town, Department of Environmental & Geographical Science.

Radic, V. and Clarke, G. K. C. (2011). Evaluation of IPCC models' performance in simulating late-Twentieth-Century climatologies and weather patterns over North America. *Journal of Climate*, 24:5257–5274.

Rauscher, S. A., Coppola, E., Piani, C., and Giorgi, F. (2010). Resolution effects on regional climate model simulations of seasonal precipitation over Europe. *Climate dynamics*, 35(4):685–711.

Reason, C. (2001). Subtropical Indian Ocean SST dipole events and southern African rainfall. *Geophysical Research Letters*, 28(11):2225–2227.

Reason, C. and Jagadheesha, D. (2005). A model investigation of recent ENSO impacts over southern Africa. *Meteorology and Atmospheric Physics*, 89(1):181–205.

Reason, C. and Keibel, A. (2004). Tropical Cyclone Eline and Its Unusual Penetration and Impacts over the Southern African Mainland. *Weather & Forecasting*, 19(5).

Reason, C., Landman, W., and Tennant, W. (2006). Seasonal to decadal prediction of southern African climate and its links with variability of the Atlantic Ocean. *Bulletin of the American Meteorological Society*, 87(7):941–955.

Rocha, A., Melo-Gonçalves, P., Marques, C., Ferreira, J., and Castanheira, J. M. (2008). High-frequency precipitation changes in southeastern Africa due to anthropogenic forcing. *International Journal of Climatology*, 28(9):1239–1253.

Rudolf, B., Becker, A., Schneider, U., Meyer-Christoffer, A., and Ziese, M. (2010). The new GPCC Full Data Reanalysis Version 5 providing high-quality gridded monthly precipitation data for the global land-surface is public available since December 2010. *GPCC status report December*.

Rummukainen, M. (2012). Changes in climate and weather extremes in the 21st century. *Wiley Interdisciplinary Reviews: Climate Change*.

Samuelsson, P., Jones, C. G., Willén, U., Ullerstig, A., Gollvik, S., Hansson, U., Jansson, C., Kjellström, E., Nikulin, G., and Wyser, K. (2011). The Rossby Centre Regional Climate model RCA3: model description and performance. *Tellus A*, 63(1):4–23.

Sang, H., Gelfand, A. E., Lennard, C., Hegerl, G., and Hewitson, B. (2008). Interpreting self-organizing maps through space-time data models. *The Annals of Applied Statistics*, pages 1194–1216.

Seneviratne, S. I., Lüthi, D., Litschi, M., and Schär, C. (2006). Land–atmosphere coupling and climate change in Europe. *Nature*, 443(7108):205–209.

Seneviratne, S. I., Nicholls, N., Easterling, D., Goodess, C., Kanae, S., Kossin, J., Luo, Y., Marengo, J., McInnes, K., Rahimi, M., et al. (2012). Changes in climate extremes and their impacts on the natural physical environment. *Managing the risks of extreme events and disasters to advance climate change adaptation*, pages 109–230.

Shongwe, M., Van Oldenborgh, G., Van Den Hurk, B., De Boer, B., Coelho, C., and Van Aalst, M. (2009). Projected changes in extreme precipitation in Africa under global warming. Part 1: Southern Africa. *Journal of Climate*, 22:3819–3837.

Sillmann, J., Kharin, V., Zhang, X., Zwiers, F., and Bronaugh, D. (2013a). Climate extremes indices in the CMIP5 multimodel ensemble: Part 1. Model evaluation in the present climate. *Journal of Geophysical Research: Atmospheres*, 118(4):1716–1733.

Sillmann, J., Kharin, V., Zwiers, F., Zhang, X., and Bronaugh, D. (2013b). Climate extremes indices in the CMIP5 multimodel ensemble: Part 2. Future climate projections. *Journal of Geophysical Research: Atmospheres*, 118(6):2473–2493.

Singleton, A. T. and Reason, C. J. C. (2006). Numerical Simulations of a Severe Rainfall event over the Eastern Cape coast of South Africa: Sensitivity to sea surface temperature and topography. *Tellus A*, (58):355–367.

Singleton, A. T. and Reason, C. J. C. (2007). A numerical model study of an intense cut-off low pressure system over South Africa. *Monthly Weather Review*, (135):1128–1150.

Stephenson, D. (2008). *Definition, diagnosis, and origin of extreme weather and climate events*. In: Climate Extremes and Society. R. Murnane and H. Diaz (Eds). Cambridge University Press.

Stevens, B., Giorgetta, M., Esch, M., Mauritsen, T., Crueger, T., Rast, S., Salzmann, M., Schmidt, H., Bader, J., Block, K., et al. (2013). The atmospheric component of the MPI-M earth system model: ECHAM6. *Journal of Advances in Modeling Earth Systems*.

Sun, Y., Solomon, S., Dai, A., and Portmann, R. W. (2006). How often does it rain? *Journal of Climate*, 19(6):916–934.

Sylla, M., Giorgi, F., Coppola, E., and Mariotti, L. (2013). Uncertainties in daily rainfall over Africa: assessment of gridded observation products and evaluation of a regional climate model simulation. *International Journal of Climatology*.

Tadross, M., Hewitson, B., and Usman, M. (2005). The interannual variability of the onset of the maize growing season over South Africa and Zimbabwe. *Journal of climate*, 18(16):3356–3372.

Tadross, M., Suarez, P., Lotsch, A., Hachigonta, S., Mdoka, M., Unganai, L., Lucio, F., Kamdonyo, D., and Muchinda, M. (2009). Growing-season rainfall and scenarios of future change in southeast Africa: implications for cultivating maize. *Climate Research*, 40:147–161.

Taljaard, J. (1995). Atmospheric circulation systems, synoptic climatology and weather phenomena of South Africa. Part2: Atmospheric circulation systems in the South African region. Technical Paper No. 28, Weather Bureau.

Taljaard, J. J. (1986). Change of rainfall distribution and circulation patterns over Southern Africa in summer. *Journal of Climatology*, 6(6):579–592. Paper copy.

Tebaldi, C., Hayhoe, K., Arblaster, J., and Meehl, G. (2006). Going to the Extremes; An Intercomparison of Model-Simulated Historical and Future Changes in Extreme Events. *Climatic Change*, 79:185–211.

Tennant, W. J. and Hewitson, B. C. (2002). Intra-seasonal rainfall characteristics and their importance to the seasonal prediction problem. *International Journal of Climatology*, 22(9):1033–1048.

Tiedtke, M. (1989). A comprehensive mass flux scheme for cumulus parameterization in large-scale models. *Monthly Weather Review*, 117:1779–1800.

Todd, M. and Washington, R. (1999). Circulation anomalies associated with tropical-temperate troughs in southern Africa and the south west Indian Ocean. *Climate dynamics*, 15(12):937–951.

Todd, M., Washington, R., and Palmer, P. (2004). Water vapour transport associated with tropical-temperate trough systems over southern Africa and the southwest Indian Ocean. *International journal of climatology*, 24(5):555–568.

Tyson, P., Garstang, M., and Swap, R. (1996a). Large-scale recirculation of air over southern Africa. *Journal of applied meteorology*, 35(12):2218–2236.

Tyson, P., Garstang, M., Swap, R., Kallberg, P., and Edwards, M. (1996b). An air transport climatology for subtropical southern Africa. *International journal of climatology*, 16(3):265–291.

Tyson, P. D., Cooper, G. R. J., and McCarthy, T. S. (2002). Millennial to multi-decadal variability in the climate of southern Africa. *International Journal of Climatology*, 22(9):1105–1117.

Tyson, P. D. and Preston-White, R. A. (2000). *The weather and climate of southern Africa*. Oxford University Press, Cape Town.

Voldoire, A., Sanchez-Gomez, E., y Mélia, D. S., Decharme, B., Cassou, C., Sénési, S., Valcke, S., Beau, I., Alias, A., Chevallier, M., et al. (2011). The CNRM-CM5. 1 global climate model: description and basic evaluation. *Climate Dynamics*, pages 1–31.

von Storch, H. and Zwiers, F. W. (1999). *Statistical Analysis in Climate Research*, volume 95. Cambridge University Press.

Washington, R., Harrison, M., Conway, D., and Black, E. (2004). *African climate report: a report commissioned by the UK Government to review African climate science, policy and options for action*. Department for Environment, Food and Rural Affairs.

Washington, R. and Preston, A. (2006). Extreme wet years over southern Africa: Role of Indian Ocean sea surface temperatures. *Journal of geophysical research*, 111(D15):D15104.

Wehner, M. F. (2004). Predicted twenty-first-century changes in seasonal extreme precipitation events in the parallel climate model. *Journal of Climate*, 17:4281 – 4290.

Wilby, R. L., Charles, S. P., Zorita, E., Timbal, B., Whetton, P., and Mearns, L. O. (2004). *Guidelines for Use of Climate Scenarios Developed from Statistical Downscaling Methods*, page 27pp. IPCC Data Distribution Centre, University of East Anglia, U.K.

Wilby, R. L. and Wigley, T. (1997). Downscaling general circulation model output: a review of methods and limitations. *Progress in Physical Geography*, 21:530–548.

Willett, K. M., Jones, P. D., Thorne, P. W., and Gillett, N. P. (2010). A comparison of large scale changes in surface humidity over land in observations and CMIP3 general circulation models. *Environmental Research Letters*, 5(2):025210.

WMO (2014). Atlas of Mortality and Economic Losses from Weather, Climate and Water Extremes 1970-2012.

Yarnal, B. (1993). *Synoptic Climatology in Environmental Analysis: A Primer*. Belhaven Press: London.

Zwiers, F. W. and Kharin, V. V. (1998). Changes in the Extremes of the Climate Simulated by CCC GCM2 under CO2 Doubling. *Journal of Climate*, 11(9):2200–2222.